



## UNIVERSITY OF CALGARY

The author of this thesis has granted the University of Calgary a non-exclusive license to reproduce and distribute copies of this thesis to users of the University of Calgary Archives.

Copyright remains with the author.

Theses and dissertations available in the University of Calgary Institutional Repository are solely for the purpose of private study and research. They may not be copied or reproduced, except as permitted by copyright laws, without written authority of the copyright owner. Any commercial use or publication is strictly prohibited.

The original Partial Copyright License attesting to these terms and signed by the author of this thesis may be found in the original print version of the thesis, held by the University of Calgary Archives.

The thesis approval page signed by the examining committee may also be found in the original print version of the thesis held in the University of Calgary Archives.

Please contact the University of Calgary Archives for further information,

E-mail: [uarc@ucalgary.ca](mailto:uarc@ucalgary.ca)

Telephone: (403) 220-7271

Website: <http://www.ucalgary.ca/archives/>

UNIVERSITY OF CALGARY

Use of the Boundary Element Method in Electrostatic Modeling of the Interaction  
Between Two Blockers in Sodium Ion Channels

By

Tatiana Britvina

A THESIS

SUBMITTED TO THE FACULTY OF GRADUATE STUDIES  
IN PARTIAL FULFILMENT OF THE REQUIREMENTS OF THE  
DEGREE OF MASTER OF SCIENCE

DEPARTMENT OF PHYSICS AND ASTRONOMY

CALGARY, ALBERTA

OCTOBER, 2001

© Tatiana Britvina 2001

## ABSTRACT

The presence of positively-charged DEA molecules in the solution bathing the intracellular side of a sodium channel in a lipid bilayer, blocks the current through the channel. This blocking is inhibited by adding the positively-charged  $\mu$ -conotoxin GIIIA derivative, R13Q, to the extracellular solution. The hypothesis that this inhibitory effect can be explained by electrostatic repulsion between two molecules is tested in this thesis.

For this purpose, the potential inside the channel due to the toxin molecule was calculated. Calculations were performed using a cylindrical geometry for the channel and spherical model of the R13Q-molecule under the mean field approximation for ionic solution. The Boundary Element Method was chosen, as it is more efficient for this problem than the typical finite difference methods. To implement the method, a program was written and tested on a variety of simple geometries.

Experiment shows that the probability for the DEA to be unbound increases when R13Q is bound at the extracellular end of the channel. Based on the experimental data and our calculated potential, an estimate of the position DEA adsorption site in the channel was obtained. This estimate is in reasonable agreement with the present understanding of the sodium channel structure, demonstrating that the method produces plausible results.

## ACKNOWLEDGEMENTS

Deep appreciation goes to all who made this work possible.

It is a pleasure to acknowledge the excellent opportunities I have received for research and study in the laboratory of Dr. R.J. French. I would like to thank Dr. R.J. French for formulating a multidisciplinary problem that challenged me in different areas of physics, both experimental and theoretical. He also educated me in principles of ion channel theory and introduced me to the latest investigations in this field. His revealing analysis of biophysical matters and his patience in answering my endless questions was crucial for my progress in solving the problem.

I gratefully acknowledge and appreciate the interest and advice of Dr. R.B. Hicks. Going from chapter to chapter through every detail of the work he taught me to write and logically communicate scientific ideas. I wish to thank Dr. R.B. Hicks for challenging and thoughtful discussions related to theory and methods of physical measurements and data analysis.

I also wish to thank my both supervisors, Dr. R.J. French and Dr. R.B. Hicks, for their continued support, encouragements and understanding, without which this work would definitely not be possible.

I would like to thank Dr. H. Laue for the opportunity to have deep discussions of "Stochastic processes in physics" course. The principles and ideas of this course gave me a new level of understanding of the physical processes in the ion channels.

I wish to express great thanks to Dr. S.I. Kryuchkov, my husband, for his support and patience. He introduced me to the Boundary Element Method and clarified physical

and mathematical concepts of this relatively new area. I also wish to say thanks to him for fruitful and critical discussions of physical aspects related to this work.

I sincerely appreciate the help and kindness of the Administrative Support Staff of the Department of Physics and Astronomy, especially Leslie Holmes and Tracy Korsgaard, and the secretary of the Department of Physiology and Biophysics, Ellen Wong.

Great thanks I would like to give my daughters, Alexandra and Anastasia, for their sharing of my problems, and, especially, Alexandra for her open and real help in figures, printing, and other difficult technical work.

Finally, I would like to say "Thank you" to my "old" friends living in Moscow for their love – without this the present work would not be finished.

## TABLE OF CONTENTS

<b>ABSTRACT</b>	<b>iii</b>
<b>ACKNOWLEDGEMENTS</b>	<b>iv</b>
<b>TABLE OF CONTENTS</b>	<b>vi</b>
<b>LIST OF FIGURES AND ILLUSTRATIONS</b>	<b>ix</b>
<b>LIST OF TABLES</b>	<b>xiii</b>
<b>Introduction</b>	<b>1</b>
<b>Chapter 1. Basic properties of biological membrane channels.....</b>	<b>3</b>
<b><i>1.1. Gating</i></b>	<b>4</b>
1.1.1. Stochastic nature of gating	4
1.1.2. Voltage dependence of gating	6
<b><i>1.2. Blocking</i></b>	<b>8</b>
1.2.1. Slow and fast blockers	9
1.2.2. Calculation of the probability for the channel to be unblocked	12
1.2.3. Voltage dependence of blocking	14
<b>Chapter 2. Interaction between internal and external blockers of sodium channel</b>	<b>18</b>
<b><i>2.1. Experiment with two blockers, R13Q and DEA</i></b>	<b>18</b>
<b><i>2.2. Electrostatic interaction of two blockers. Estimation of location of DEA binding site from electrostatic potential due to R13Q</i></b>	<b>23</b>

<b>Chapter 3. Physical models of the system (Ionic solution-R13Q-molecule-Channel)</b>	<b>26</b>
<b>3.1. Models of ionic solution</b>	<b>26</b>
<b>3.2. Structure of an ion channel</b>	<b>30</b>
<b>3.3. Channel as a continuous medium</b>	<b>34</b>
<b>3.4. Advantages of BEM</b>	<b>34</b>
<b>3.5. Our Model</b>	<b>35</b>
<b>Chapter 4. Boundary element method (BEM). Theory</b>	<b>37</b>
<b>4.1. BEM applied to the Laplace and Poisson equations</b>	<b>37</b>
4.1.1. Integral representation for potential	37
4.1.2. Integral equations for potential on the surface	39
4.1.3. Discretization of equations (Implementation of BEM)	47
<b>4.2. Boundary element method applied to the Laplace and Poisson-Boltzmann equations</b>	<b>50</b>
<b>Chapter 5. BEM applied to the Laplace and Poisson-Boltzmann equations</b>	<b>54</b>
<b>5.1. Point Charge near membrane with finite cylindrical channel in the absence of ionic solution in the surrounding space (<math>k=0</math>)</b>	<b>54</b>
<b>5.2. Point Charge near membrane with finite cylindrical channel in the presence of ionic solution in the surrounding space (<math>k \neq 0</math>)</b>	<b>58</b>
<b>5.3. Charged sphere near membrane with finite cylindrical channel in the presence of ionic solution in the surrounding space (<math>k \neq 0</math>)</b>	<b>60</b>
<b>Chapter 6. Testing the program</b>	<b>63</b>
<b>6.1. Infinite cylindrical hole</b>	<b>63</b>

6.1.1. Formulation and solution of the problem.....	63
6.1.2. Results and analysis.....	64
6.1.3. Comparison with results obtained by numerical method.....	69
<i>6.2. Behavior of the potential and the electric field in the membrane with the finite channel. Comparison with the infinite cylinder.</i> .....	71
<b>Chapter 7. Results and discussion</b> .....	76
<i>7.1. Influence of parameters on the basic model on the behavior of the potential inside the channel</i> .....	76
<i>7.2. Estimation of location of DEA binding site</i> .....	83
<i>7.3. Conclusion</i> .....	85
<b>Bibliography</b> .....	87
<b>APPENDIX A. Infinite cylindrical hole</b> .....	91
<b>APPENDIX B. Point charge near membrane of the finite width surrounded by ionic solution</b> .....	95

## LIST OF FIGURES AND ILLUSTRATIONS

<b>Figure 1.1.</b> Structure of a bacterial potassium channel(ribbon representation of protein backbone)_____	<b>3</b>
<b>Figure 1.2.</b> Single-sodium-channel current fluctuations, taken at $-95$ mV_____	<b>4</b>
<b>Figure 1.3.</b> Cumulative open-time distribution with a single exponential fit (smooth curve) to data superimposed_____	<b>6</b>
<b>Figure 1.4.</b> Fractional open time (or the probability for the channel to be open) as a function of membrane voltage for single sodium channel_____	<b>7</b>
<b>Figure 1.5.</b> Records from single rat skeletal muscle sodium channels showing discrete blocking events produced by various derivatives of conotoxin GIIIA (slow blocker)...	<b>10</b>
<b>Figure 1.6.</b> Current traces recorded from single sodium channel from rat skeletal muscle in absence and presence of procainamide (fast blocker) on the intracellular side_____	<b>11</b>
<b>Figure 1.7.</b> Calculation of probability $P^B_0$ for the channel to be unblocked from experimental data in the case of a fast blocker_____	<b>13</b>
<b>Figure 1.8.</b> Voltage dependence of procainamide block of bovine cardiac and skeletal muscle sodium channels. _____	<b>14</b>
<b>Figure 1.9.</b> Energy profile for the molecule in the membrane and in the solution without (left) and with (right) an applied potential $\Phi$ which is shown as a dashed line_____	<b>15</b>
<b>Figure 2.1.</b> Structures of native $\mu$ -Conotoxin ( $\mu$ CTX, MW= $2.5 \cdot 10^3$ amu.) and diethylammonium (DEA, MW=74 amu)_____	<b>19</b>

<b>Figure 2.2.</b> Current recordings from the single rat skeletal muscle sodium channel in the presence of R13Q at the extracellular side (+60 mV)	21
<b>Figure 2.3.</b> Voltage dependence of probability $P_0$ for the channel to be unblocked by DEA for two cases: R13Q is not bound to the channel(black squares) and R13Q is bound to the channel (circles)	22
<b>Figure 2.4.</b> Graphical solution of equation (2.8)	25
<b>Figure 3.1.</b> 3-Dimensional representation of the Ksc	32
<b>Figure 3.2.</b> Possible geometry of $\text{Na}^+$ channel	33
<b>Figure 3.3.</b> Geometry of the cylindrically symmetric model of Na channel and electrolyte system, from [M.Cai and P.Gordan, 1990]	34
<b>Figure 3.4.</b> Our model	36
<b>Figure 4.1.</b> Geometry of the system	37
<b>Figure 4.2.</b> Local geometry in the vicinity of point $\xi_0$ on the surface $\Gamma$	42
<b>Figure 4.3.</b> Local geometry in the vicinity of point $\xi_0$ in the case when $\xi$ approaches $\xi_0$ along the w axis	45
<b>Figure 4.4.</b> Representation of the boundary by finite elements	48
<b>Figure 4.5.</b> Geometry of the system	50
<b>Figure 5.1.</b> Cross-section of infinite membrane (region II) with a finite cylindrical channel	54
<b>Figure 5.2.</b> Representation of the surface by the symmetrical rings	55
<b>Figure 5.3.</b> An example of local position of point $\xi$ and $r$ on the surface: the figure shows the case of $r \in \Gamma_2, \xi \in \Gamma_3$	56

<b>Figure 5.4.</b> Charged sphere near membrane with finite cylindrical channel in the presence of ionic solution in the channel and surrounding space ( $k \neq 0$ )	60
<b>Figure 6.1.</b> A cylindrical hole of radius $R$ and infinite length is filled with ionic solution with dielectric constant $\epsilon_1$ and Debye radius $\lambda=1/\kappa$	64
<b>Figure 6.2.</b> The normal derivative of the potential in region I on the channel surface as a function of coordinate $z$ for the case shown in Fig. 6.1	65
<b>Figure 6.3.</b> Same as Fig. 6.2., but for the case $k=0$ (no ionic solution in channel)	66
<b>Figure 6.4.</b> The potential inside the cylinder at point $z=5 \text{ \AA}$ as a function of radial coordinate $\rho$ for four different channel radii when the two dielectric constants are the same ( $\epsilon_1=\epsilon_2$ )	67
<b>Figure 6.5.</b> Graph representing the potential at a fixed point ( $z=5 \text{ \AA}$ , $\rho=0.2 \text{ \AA}$ ) inside the channel as a function of the channel radius $R$ for four different values of $\lambda$	68
<b>Figure 6.6.</b> Polarized surface charge as a function of coordinate $z$ for the case when $R=7 \text{ \AA}$ , $\epsilon_1=80$ , $\epsilon_2=10$	69
<b>Figure 6.7.</b> Potential at the channel surface as a function of $z$ coordinate (both graphs)	70
<b>Figure 6.8.</b> Normal derivative of the potential on the surface of the cylindrical channel as a function of $z$ coordinate ( $k=0$ , $k \neq 0$ )	70
<b>Figure 6.9.</b> Equipotential maps inside the channel ( $R=5 \text{ \AA}$ ) and membrane for three cases: $\lambda=21 \text{ \AA}$ ( $\lambda > R$ ), $\lambda=7 \text{ \AA}$ ( $R \approx \lambda$ ), $\lambda=2.3 \text{ \AA}$ ( $\lambda \ll R$ )	72
<b>Figure 6.10.</b> Equipotential lines (in the plane containing $z$ axes) inside the channel ( $R=5 \text{ \AA}$ ) and membrane for the case: $\lambda = 7 \text{ \AA}$ ( $R \approx \lambda$ ), $d=7 \text{ \AA}$ , $\epsilon_1 = 80$ , $\epsilon_2 = 10$	73

<b>Figure 6.11.</b> Potential as a function of z coordinate for three different radii of the channel: R=15 Å (bottom), R=3 Å, R=1 Å	75
<b>Figure 7.1.</b> Potential as a function of z coordinate ( $\rho=0$ ) for different models	77
<b>Figure 7.2.</b> Potential as a function of z coordinate ( $\rho=0$ ) for different width of the channel	78
<b>Figure 7.3.</b> Potential as a function of z coordinate ( $\rho=0$ ) for different values of dielectric constants	79
<b>Figure 7.4.</b> Potential as a function of z coordinate ( $\rho=0$ ) for different radii of the channel	80
<b>Figure 7.5.</b> Potential as a function of z coordinate ( $\rho=0$ ) for different radii R of the charged sphere	81
<b>Figure 7.6.</b> Simple modeling of nonuniform charge distribution in R13Q-molecule....	82
<b>Figure 7.7.</b> Potential as a function of z coordinate ( $\rho=0$ ) for different diameters of surface charge nonuniformity of the sphere	83
<b>Figure 7.8.</b> Final graph for estimation of location of DEA binding site	84
<b>Figure A.1.</b> Geometry of the system: point charge near membrane with finite width surrounded by ionic solution	95

## LIST OF TABLES

<b>Table 1.1.</b> Four possible conformational states of a channel for the case when a blocker is present in ionic solution	<b>2</b>
<b>Table 2.1.</b> Amino acids of $\mu$ -Conotoxin	<b>20</b>

## INTRODUCTION

Biophysical properties of cellular membranes have been a subject of research for a substantial period of time. Experiments with voltage-dependent ion membrane channels [Hille, 1992] have shown significant influence of added toxins and drugs on electrical properties of these channels. The study of these effects is extremely important for medical research. Certain toxins or drugs applied to cells can change the electric current through the membrane channels. This can result in suppression of the transmission of nerve impulses, which is based on the sodium channel activity.

Investigation of this phenomenon poses the question of the nature of the contribution to the electric potential inside the channel due to toxin molecules. A related field of research, leading to the same type of problem, is the study of the charge transport through the channel. To calculate the potential, it is necessary to adopt an appropriate model of the ionic solution around the ion channel and of the complex molecular structure of ion channel itself.

The first work in this area was done by Stillinger [1961]. He obtained an analytical solution for the potential due to a point charge placed at some distance from the infinite planar boundary between an ionic solution and a uniform dielectric substrate, utilizing the linearized Poisson-Boltzmann equation for the ionic solution. Biophysical application of this result means that the membrane is modeled by a continuous dielectric semi-infinite medium.

Other authors [Mathias et al., 1992] derived an exact expression for the potential due to a single charge placed between the interface of a semi-infinite ionic solution and a semi-infinite dielectric substrate, based on the linearized Poisson-Boltzmann equation. They also numerically calculated the potential for a substrate (membrane) with finite width. The mathematical method used in this work was different from that of Stillinger [1961]. An analytical solution of a more general problem (for an arbitrary distance between the charge and the membrane with the finite width) can also be found.

More sophisticated models of the channel were studied with the aid of numerical methods. The main efforts were concentrated on the study of cylindrical model of the channel [Jordan, 1983]. Later, bi-conical or combined channels came into play (see, for

example, Cai and Jordan [1990], Hoyles et al.,1996). These studies utilized the Poisson equation and the linearized or nonlinear Poisson-Boltzmann equations.

Kuyucak et al. [1998] found the analytical solution of the Poisson equation for a point charge near a toroidal channel. This solution was used to calculate the potential inside the channel using Brownian Dynamics simulation [Li et al, 1998].

In spite of the fact that many different complicated models have been utilized, no specific calculations were performed on the electric potential created by large toxin molecules within the channel. The purpose of our work is to solve this problem and attempt to explain experimental data [French et al., 1996] for the two charged molecules, R13Q and DEA, in the ion channel based on the hypothesis of their electrostatic interaction.

We found that the Boundary Element Method (BEM) was the most appropriate mathematical tool for solution of this problem. This method has been developed recently (in the 1980s) mostly for engineering applications (for example, elasticity, fluid dynamics, heat transfer etc.). In biophysics it was applied to calculations of properties of macromolecules (see Juffer et al., 1997 and references therein). BEM is very powerful for systems with complicated geometry and is easily adjustable to the changes of geometrical shape. This is an advantage in the case of ion channels, which have complicated geometrical structure. We have solved the problem on the electric potential inside the cylindrical channel with the aid of this method and applied this solution to interpret experimental data.

The structure of the thesis is as follows. In Chapter 1 we discuss the main properties of the ion channels. Experimental measurements in such channels are described in Chapter 2. In Chapter 3 we analyze possible models of the ion channel, the ionic solution surrounding the membrane, and toxin molecule. Since BEM is a recent numerical technique, in Chapters 4 and 5 we present the details of the method and its application to particular models of the channel. In Chapter 6 we present the results of testing the program in a variety of ways, for example, by comparing its performance on problems for which analytical solutions are known. In Chapter 7 we investigate the sensitivity of the potential calculation to variations in model parameters to allow us to assign an error range to the results.

## CHAPTER 1. BASIC PROPERTIES OF BIOLOGICAL MEMBRANE CHANNELS

Ion channels are large protein molecules incorporated into the cellular membrane [Hiller, 1992], which consists of a bimolecular layer (bilayer) of lipid molecules (Fig.1.1, [Doyle et al., 1998]).

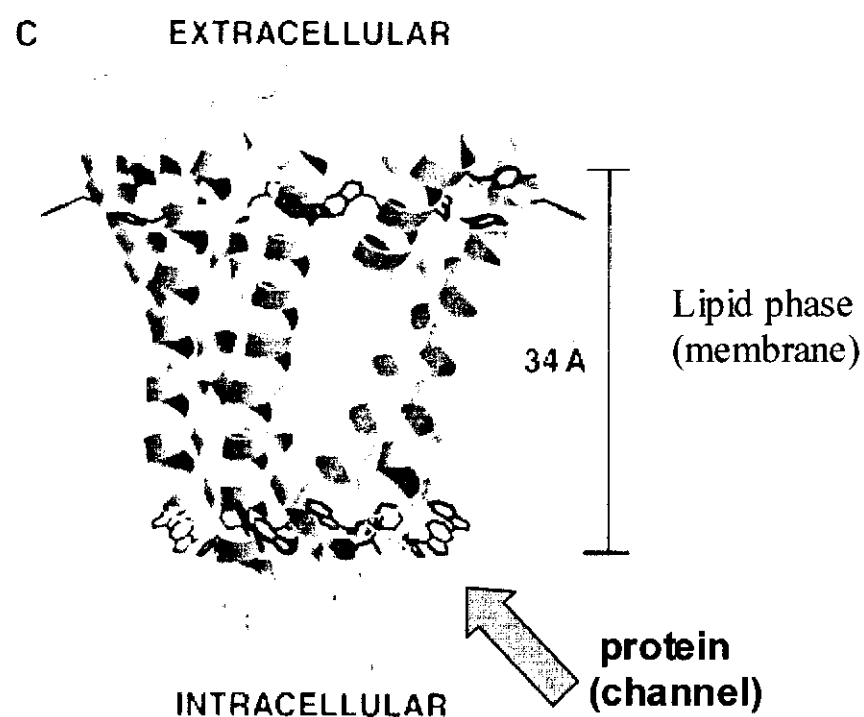


**Fig.1.1. Structure of a bacterial potassium channel (ribbon representation of protein backbone).**

The membrane is surrounded by a water solution of different ions,  $\text{Na}^+$ ,  $\text{K}^+$ ,  $\text{Ca}^+$ ,  $\text{Mg}^+$  etc. Ion channels are highly permeable to some but not to all ions. Thus sodium channels are very permeable to  $\text{Na}^+$  ions and less permeable to  $\text{K}^+$ , while potassium channels are very permeable to  $\text{K}^+$  ions but not to  $\text{Na}^+$ . Ions from the surrounding solutions (intracellular or extracellular) flow through the central narrow part of the protein, or pore, carrying an electric current through the channel, the magnitude and the direction of which depends on the applied external voltage across the membrane and the concentrations of the ions in the solution. By measuring the channel current in different

physical conditions it is possible to investigate the properties of the channel and obtain some information about its structure. In this chapter we will discuss two key properties of the channel, gating and blocking.

## 1.1. Gating

### 1.1.1. Stochastic nature of gating

For most ion channels the current  $I$  fluctuates with time between two discrete levels, the open level ( $I \neq 0$ ) and the closed level ( $I = 0$ ). This stochastic process of opening and closing is called gating. Fig.1.2 [French et al., 1986] shows an example of a current recording from a single ion channel. One notes that current fluctuations are essentially rectangular in shape (  $\sim$ several ms ) with extremely small transition times between open (O) and closed (C) states. The transitions are so rapid ( $< 1$  ns) that the observed transition times are limited by the response time recording instruments. According to a common physiological convention, voltage  $V$  is defined as voltage inside the cell with respect to outside.

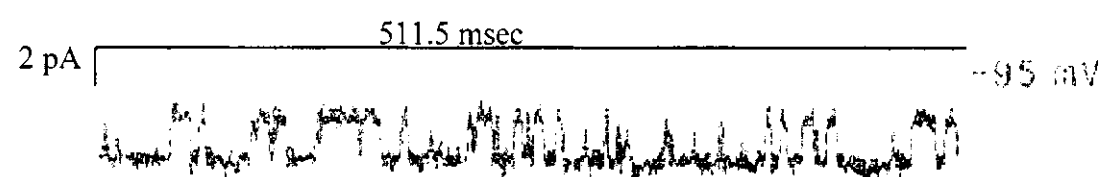


Fig.1.2. Single-sodium-channel current fluctuations, taken at  $-95$  mV. Upper level is closed in this trace. Vertical scale, 2 pA; horizontal scale, 511.5 msec. From [French et al., 1986]

Gating results from changes in the conformation or structure of the channel protein, but the detailed mechanism, on the molecular level, is unknown. Gating can be treated within statistical mechanics as a stochastic Markov process (Horn, 1984). In essence, the channel has no memory, such that the probability of a transition between conformational states does not depend on the sequence of previous states of the channel.

The probability function that governs the gating process is analogous to that for a radioactive decay. Let the channel made a C→O transition at t=0. If  $\tau_0$  is the average lifetime of the open state ( $1/\tau_0$  is the probability of the decay of the open state per unit time) then the probability  $p(t, \tau_0)dt$  that the open state will decay (close) during the time interval (t, t+dt) is

$$p(t, \tau_0)dt = \frac{1}{\tau_0} e^{-t/\tau_0} dt \quad (1.1)$$

This formula describes the probability density function  $p(t, \tau_0)$  for channel open lifetimes.

The probability  $P(t, \tau_0)$  that the open state will remain open at the time t is given by:

$$P(t, \tau_0) = e^{-t/\tau_0} \quad (1.2)$$

This function defines the cumulative distribution of channel open times.

Experiments (see, for example, [French et. al., 1986; Sigworth, 1980]) confirm that the probabilities (1.1) and (1.2) do describe the gating mechanism. To illustrate this we give the experimental data from French et al. [1986].

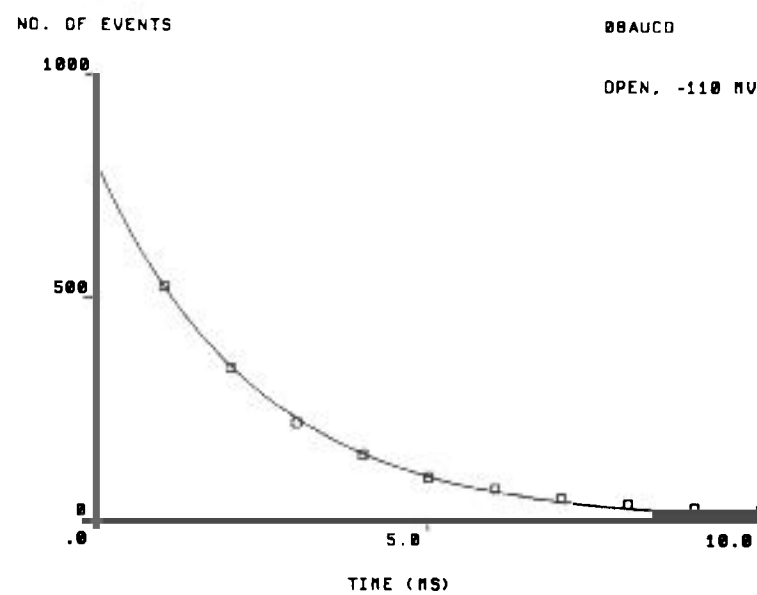


Fig.1.3. Cumulative open-time distribution with a single exponential fit (smooth curves) to data superimposed. The ordinate represents the number of events lasting at least as long as the time on the abscissa. The average life time  $\tau_0$  of open state is 2.4 msec. From [French et al., 1986]

Fig.1.3 shows the number of open states  $N_t$  which survived till the time  $t$ , starting from the instant of channel opening, as a function of this time. The smooth curve is the theoretical curve  $N_t = N \cdot P(t, \tau_0)$ , where  $N$  is the total number of open states and  $P(t, \tau_0)$  is a fit of (1.2) to the data with  $\tau_0$  as an adjustable parameter. One sees that the probability (1.2) fits the data points reasonably. The average life time  $\tau_c$  of the closed state can be obtained the same manner. Experiments (see, for example, [French et. al., 1986]) show that both  $\tau_0$  and  $\tau_c$  change with applied external voltage.

### 1.1.2.Voltage dependence of gating

One can also ask, what is the steady state probability  $P(V)$  for the channel to be open as a function of voltage? (In the steady state at any particular voltage, the open probability  $P(V)$  is invariant in time). The answer is straightforward:

$$P(V) = \frac{\sum_i t_o^i(V)}{\sum_i t_o^i(V) + \sum_i t_c^i(V)} = \frac{\tau_o(V)}{\tau_o(V) + \tau_c(V)} \quad (1.3)$$

where index  $i$  numerates individual open and closed events and  $t^i$  is the lifetime of the  $i^{\text{th}}$  event. The recording time during which the lifetimes of individual events are measured should be, of course, much large than the  $\tau_o$  and  $\tau_c$ .

If values  $\tau_o$  and  $\tau_c$  are known for each voltage applied across the membrane we can calculate the open probability  $P(V)$  as a function of the applied voltage. Fig 1.4 [French et al., 1986] shows experimental data for the estimated probability  $P(V)$  (or fractional open time) versus applied voltage. Note again, that voltage  $V$  is defined as voltage inside the cell with respect to outside.

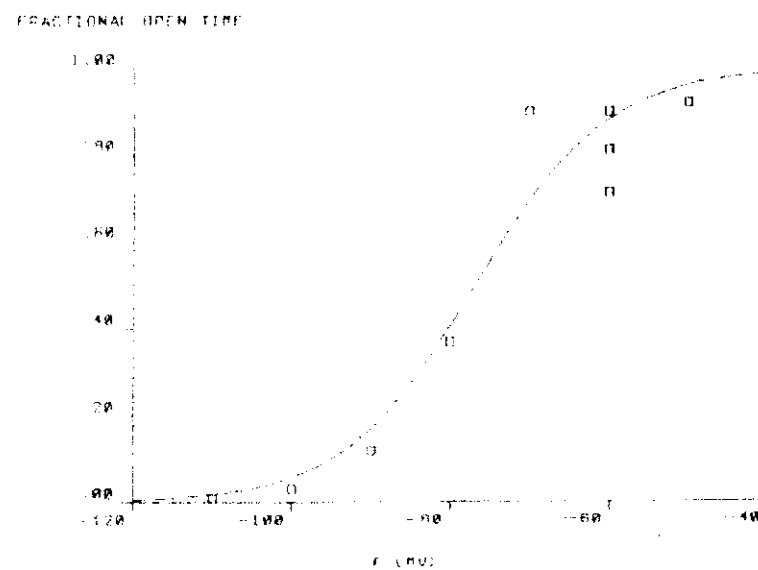


Fig.1.4. Fractional open time (or the probability for the channel to be open) as a function of membrane voltage for single sodium channel. The smooth curve is drawn according to equation (1.4) of the text. From [French et al., 1986].

This experiment, as do many others, shows that the experimental data can be well fit with the following formula:

$$P(V) = \frac{1}{1 + C \exp[qV/kT]} \quad (1.4)$$

where  $V$  is the applied voltage and parameters  $C$  and  $q$  are found by fitting the data. The physical meaning of relationship (1.4) can be understood on the basis of statistical physics. If, at zero voltage, the energies of open and closed states are  $\varepsilon_0$  and  $\varepsilon_c$  respectively, then the probability for the channel to be open at some voltage is given by the following formula

$$P(V) = \frac{1}{1 + C \exp[(\varepsilon_0 - \varepsilon_c) + \Delta U] / kT} \quad (1.5)$$

where  $C$  is constant,  $T$  is the temperature,  $k$  is the Boltzmann constant, and term  $\Delta U$  is the change of the energy difference between open and close state due to the presence of an external voltage. The exponential term in this formula represents the Boltzmann factor for the ratio of probabilities for the system to be in each of the two states. If we assume that some effective charge  $q$ , inside the channel, is responsible for the voltage dependence of gating, we can rewrite (1.5) in the following way:

$$P(V) = \frac{1}{1 + C^* \exp[qV / k / T]} \quad (1.6)$$

where  $C^* = C \exp(\varepsilon_0 - \varepsilon_c) / kT$ .

Recent investigations of molecular structure of the sodium channel protein [W. Stühmer et al., 1989] reveal charged helical chains of amino acids, called S4, that are involved in the process of opening and closing the channel. A detailed discussion of this question is beyond the scope of this thesis.

Now we will consider another important property of the channel - blocking of channel by a drug molecule or a toxin added to one side of the membrane.

## 1.2. Blocking

There are some classes of molecules that can partially or completely block the channel, i.e. decrease or eliminate the current through the channel. These molecules are

called blockers. Typically, blockers are charged molecules and have the same sign as the permeant ion. When present in intracellular or extracellular aqueous solution, these molecules undergo Brownian motion. They may stochastically surmount the energy barrier near the surface of the channel protein, bind to this protein, and then, after some period of time, leave the binding site and move to the salt solution again. Mean lifetime in the bound state  $\tau_b$  depends on the type of the molecule, the shape of the intrinsic potential profile within the channel, and on the voltage applied. This stochastic process could be described in terms of the Fokker-Planck equation (or, strictly speaking, in terms of the Kramer's equation [Van Kampen, 1984] for a Brownian particle in an external potential field). However, experimentally observable properties that the channel exhibits when the blocker is present in the ionic solution adjacent to membrane can be described satisfactorily in terms of kinetics of chemical reactions or thermodynamic theory. At the end of this section we will discuss briefly the thermodynamic approach to this problem.

### 1.2.1. Slow and fast blockers

The blockers can be divided operationally into at least two classes: a) fast blockers, which oscillate very rapidly between bound and unbound states with a period much less than  $\tau_o$  and  $\tau_c$ , and b) slow blockers, for which the time of binding to the channel protein is much larger than  $\tau_o$  and  $\tau_c$ . Below, we give examples of current recordings for both types of blockers: (Fig 1.5 [Becker, et al., 1992] illustrates the action of slow blockers, and Fig 1.6 [Zamponi, et al., 1993] shows a fast blocker).

Fig. 1.5 shows records from single rat skeletal muscle sodium channel in the presence of slow blockers,  $\mu$ -conotoxin GIIIA and its derivatives on the extracellular side of the channel.  $\mu$ -Conotoxin is a toxin from the venom of the piscivorous sea snail; it is a small peptide which consists of 22 amino acid residues and has a known 3-dimensional structure.

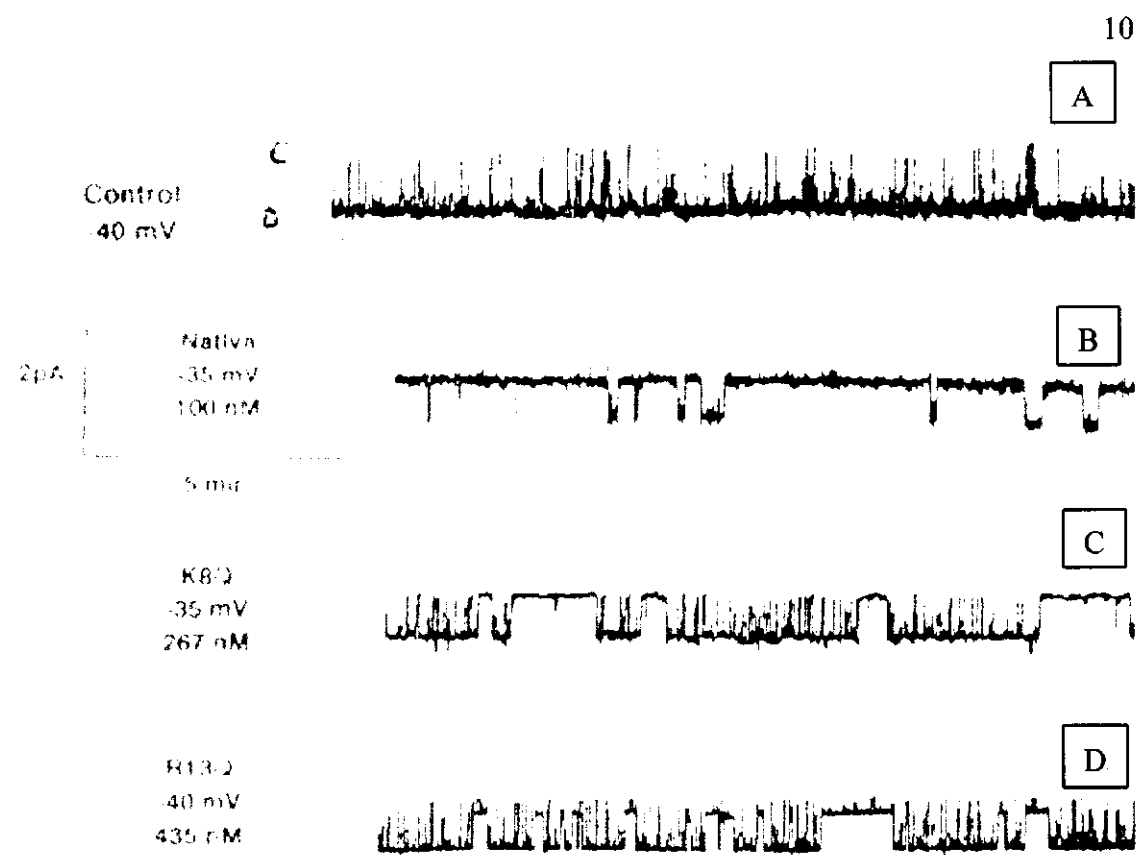


**Fig. 1.5.** Records from single rat skeletal muscle sodium channels showing discrete blocking events produced by various derivatives of conotoxin GIIIA (slow blocker). In all traces openings are in the downward direction. In control records, taken in the absence of toxin, the channel spent > 98% of the time in the open state. Addition of  $\mu$ -conotoxin or its derivatives to the extracellular side of the channel induced long lived blocking events. The peptide concentration used, and the voltage, are indicated alongside each record. From [S.Becker, et al., 1992].

One sees that the addition of the  $\mu$ -conotoxin GIII or its derivatives to the extracellular side of the channel induces long-lived blocking events. Control records (Fig. 1.5 A) show only occasional brief gating closures; the channel spent > 98% of the time in the open, conducting state. Native conotoxin (Fig. 1.5 B) blocks the channel almost all of the time. During individual blocking events no current flows through the channel. The derivative K16Q (Fig. 1.5 C) closes and opens the channel with some period of time of the order of a minute, not changing the amplitude of current fluctuations. The derivative R13Q exhibits a different behavior: seconds-long interruptions in current flow induced by R13Q do not result in complete occlusion of current flow through the channel but, rather, appear as abrupt steps to a reduced, but nonzero current.

Fig. 1.6 shows current recordings from a single sodium channel of rat skeletal muscle in the presence of a fast blocker, the local anaesthetic procainamide, in the intracellular side of the membrane.

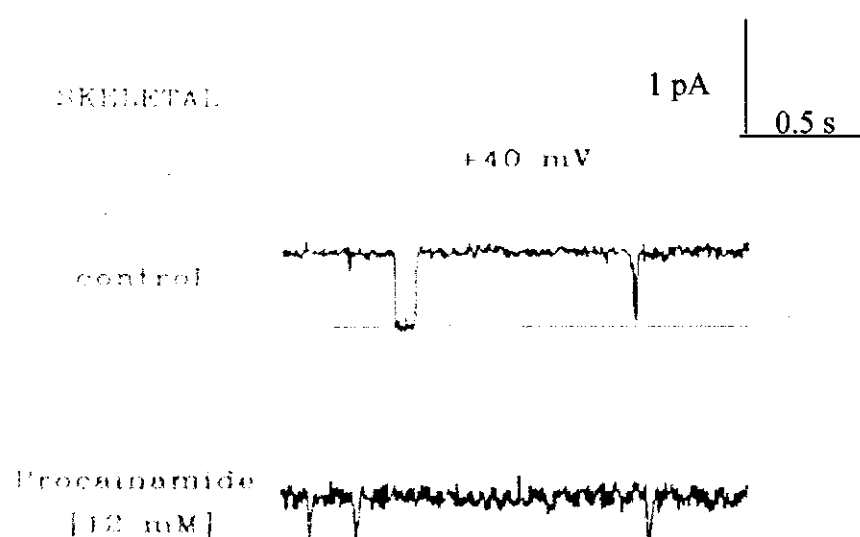


**Fig.1.6. Current traces recorded from single sodium channel from rat skeletal muscle in absence and presence of procainamide (fast blocker) on the intracellular side. The solid lines indicate the closed level. Blocking events appear as an increase in open channel noise with a concomitant decrease in the apparent single channel current amplitude. From [Zamponi, et al., 1993].**

In the absence of the drug, the channel is open most of the time. Procainamide, applied to the intracellular side, acts by inducing rapid blocking events, which were not resolved as discrete rectangular steps, but rather appear as an increase in open channel noise with a concomitant decrease in the apparent single channel current amplitude.

From the above analysis of current recordings for fast and slow blockers, one sees that it is possible also to investigate the behavior of the channel when both slow and fast blockers are present; the slow blocker may bind to the channel for seconds or minutes, while the fast blocker oscillates with period much less than a millisecond. We will return to this question in Chapter 3, in which we will discuss an experiment that demonstrates interaction between such a pair of blockers.

### 1.2.2. Calculation of the probability for the channel to be unblocked

It is natural to ask the question, what is the probability for the channel to be unblocked at some arbitrary moment of time? It is easy to obtain this probability from the current recordings, described above. With a blocker in the ionic solution the channel has four possible conformational states. For the purpose of our calculation we only need to know that these states differ with respect to the probability for the channel to be in each of these states, and by the magnitude of channel state current. Characteristics of each state are given in Table 1.1.

Conformational state (Gating, Blocking)	Open, Unblocked OO	Open, Blocked OB	Closed, Unblocked CO	Closed, Blocked CB
Probability (P)	$P_{oo}$	$P_{ob}$	$P_{co}$	$P_{cb}$
Current (I)	$I_{oo}$	$I_{ob}$ ( $I_{ob} < I_{oo}$ )	$I_{co}$	$I_{cb}$
Conductance of the state	Nonzero	Nonzero ( $I_{ob} < I_{oo}$ ) or Zero (depending on the type of blocker)	Zero	Zero

**Table 1.1.** Four possible conformational states of a channel for the case when a blocker is present in ionic solution.

The expression for the average current  $\langle I \rangle^{\text{with blocker}}$  flowing through the channel when the blocker is present in the solution can be written in a standard way, using the ergodic theorem:

$$\begin{aligned} \langle I \rangle^{\text{with blocker}}_{\text{time}} &= \langle I \rangle^{\text{with blocker}}_{\text{ensemble}} \\ &= P_{oo}I_{oo} + P_{ob}I_{ob}. \end{aligned} \quad (1.7)$$

The other two terms are omitted since there is no current through the closed channel.

In the case of molecules that totally block the channel  $I_{ob}=0$ . For this type of blocking molecules the expression (1.7) for an average current becomes

$$\langle I \rangle^{\text{with blocker}} = P_{oo}I_{oo} \quad (1.8)$$

If we assume that the processes of gating and of blocking are independent then we can rewrite (1.8) in the following way:

$$\langle I \rangle^{\text{with blocker}} = P_{oo} I_{oo} = P_o^G P_o^B I_{oo}, \quad (1.9)$$

where  $P_o^G$  and  $P_o^B$  are probabilities for the channel to be open due to gating and unblocked respectively.

For the ratio of average currents  $\langle I \rangle^{\text{with blocker}}$  and  $\langle I \rangle^{\text{without blocker}}$  through the channel with and without the blocking molecules in the surrounding solution we have

$$\frac{\langle I \rangle^{\text{with blocker}}}{\langle I \rangle^{\text{without blocker}}} = \frac{\langle I \rangle^{\text{without blocker}}}{\langle I \rangle^{\text{Gating}}} = \frac{P_o^G P_o^B I_{oo}}{P_o^G I_{oo}} = P_o^B \quad (1.10)$$

Finally,

$$P_o^B = \frac{\langle I \rangle^{\text{with blocker}}}{\langle I \rangle^{\text{without blocker}}} \quad (1.11)$$

This formula is valid for slow and for fast blockers (provided blocking is complete). Fig.1.7 illustrates the calculation of  $P_o^B$  for experimental data in the case of a fast blocker.

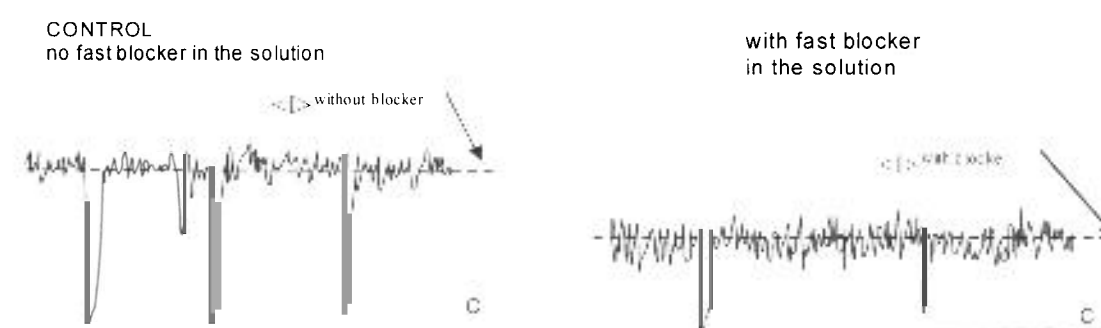


Figure 1.7. Calculation of probability  $P_o^B$  for the channel to be unblocked from experimental data in the case of a fast blocker (See equation (1.12)). The ratio of the two average currents is the desired probability.

So, according to (1.11), the probability for the channel to be unblocked (by a blocker that blocks the channel completely) is equal simply to the ratio of average currents in the presence and absence of blocker respectively and can be found easily from experimental data.

### 1.2.3. Voltage dependence of blocking

Experiments show [Zamponi et al., 1993, Zamponi and French, 1993] that probability  $P_o^B$  for the channel not to be blocked by a cationic blocker present on the cytoplasmic side (inside) depends on the applied voltage as shown in Fig.1.8 [Zamponi et al., 1993]

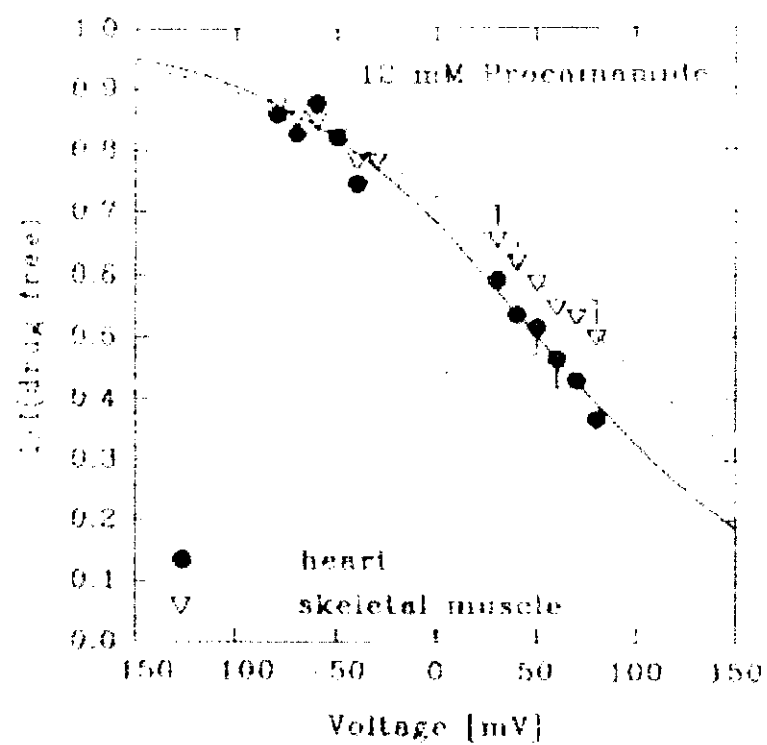


Fig.1.8. Voltage dependence of procainamide block of bovine cardiac and rat skeletal muscle sodium channels. The data were fitted with the formula (1.12). From [Zamponi et al., 1993].

Experimental data are usually fitted with the following formula:

$$P_a^h = \frac{1}{1 + P_a^b / P_a^s} = \frac{1}{1 + C^* \exp(z\Phi / kT)} \quad (1.12)$$

where  $C^*$  and  $z$  are constants, found from the experimental data, and  $\Phi$  is the potential difference across the membrane, previously denoted by  $V$ .

This formula can be naturally explained in terms of adsorption theory. Let us consider two systems: membrane with or without molecule A (system I) and solution with a known concentration of A (system II). Systems I and II are in thermodynamic equilibrium and can exchange a molecule A. There is exactly one adsorption site in the membrane. Molecule A is a charged particle with charge  $z$ . Fig. 1. 9 shows the energy profile for the molecule in the membrane and in the solution without and with an applied potential  $\Phi$ .

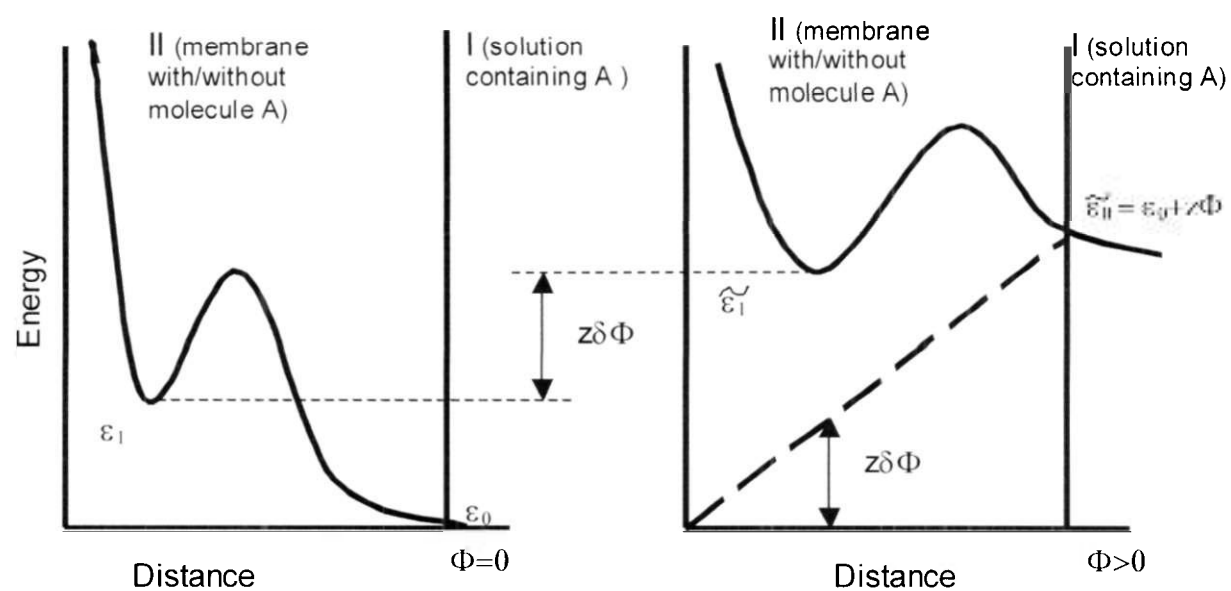


Fig. 1.9. Energy profile for the molecule in the membrane and in the solution without (left) and with (right) an applied potential  $\Phi$  which is shown as a dashed line. When  $\Phi=0$  energy of molecule A in a bound state is  $\varepsilon_1$ , the energy of molecule A in solution is  $\varepsilon_0$ . Symbol  $\tilde{\varepsilon}$  indicates new energy levels for  $\Phi \neq 0$ .  $\delta$  is some number ( $0 < \delta < 1$ ) which characterizes the value of potential on the binding site

When  $\Phi=0$ , the energy of molecule A in a bound state is  $\varepsilon_1$ , and the energy of molecule A in solution is  $\varepsilon_0$ . The energy profile changes when external voltage  $\Phi$  is applied. Let new energies of molecule A in the bound state and in the solution be  $\tilde{\varepsilon}_1$  and  $\tilde{\varepsilon}_0$  respectively. Let  $P_1$  and  $P_0$  denote the probabilities that the channel (system II) contains or does not contain molecule A, respectively. Assuming a single energy state

at the adsorption site we get for the ratio of these probabilities when system II is brought to thermodynamic equilibrium with system I:

$$\frac{P_1}{P_0} = C \cdot \exp(-(\mathcal{E}_1 - \mathcal{E}_0)/kT) \quad (1.13a)$$

$$\frac{\tilde{P}_1}{\tilde{P}_0} = C \cdot \exp(-(\tilde{\mathcal{E}}_1 - \tilde{\mathcal{E}}_0)/kT) \quad (1.13b)$$

The symbol  $\sim$  in (1.13b) indicates that this formula is written for the case when  $\Phi \neq 0$ . The constant  $C$ , as can be shown from more detailed analysis of adsorption theory, for low concentration  $n_A$  of molecules A in the water, has the form:

$$C = n_A \exp(\mu_{sA}/kT) \quad (1.13c)$$

where  $\mu_{sA}$  is the standard chemical potential of molecule A in solution.

Now we will assume that the change of energy levels is caused only by the change of electrostatic energy due to the external field. Then the energy of molecule in the solution changes by  $\Delta_0(\Phi) = z\Phi$ , and the energy of the molecule in a bound state changes by  $\Delta_1(\Phi) = z \cdot \delta \cdot \Phi$ , where  $\delta$  is some number ( $0 \leq \delta \leq 1$ ) which characterizes the magnitude of the potential at the binding site. So, for new energy levels of molecule we have:

$$\tilde{\mathcal{E}}_1 = \mathcal{E}_1 + \Delta_1(\Phi) = \mathcal{E}_1 + z \cdot \delta \cdot \Phi \quad (1.14a)$$

$$\tilde{\mathcal{E}}_0 = \mathcal{E}_0 + \Delta_0(\Phi) = \mathcal{E}_0 + z \cdot \Phi. \quad (1.14b)$$

With (1.14) expression (1.13b) becomes:

$$\begin{aligned} \frac{\tilde{P}_1}{\tilde{P}_0} &= C \cdot \exp(-(\tilde{\mathcal{E}}_1 - \tilde{\mathcal{E}}_0)/kT) = C \cdot \exp(-(\mathcal{E}_1 - \mathcal{E}_0)/kT) \exp(-(\Delta_1(\Phi) - \Delta_0(\Phi))/kT) \\ &= C^* \cdot \exp(z \cdot (1 - \delta) \cdot \Phi / kT) \end{aligned} \quad (1.15)$$

$$\text{where } C^* = C \cdot \exp(-(\mathcal{E}_1 - \mathcal{E}_0)/kT) \quad (1.15a)$$

Finally, by rearranging terms in (1.15) we get for the probability  $\tilde{P}_0$  for the channel to be unblocked when external voltage is applied across membrane:

$$\tilde{P}_0 = \frac{1}{1 + \tilde{P}_1 / \tilde{P}_0} = \frac{1}{1 + C^* \cdot \exp(z \cdot (1 - \delta) \cdot \Phi / kT)}. \quad (1.16)$$

Comparing this expression with (1.12) we note that  $\bar{z} = z \cdot (1 - \delta)$

So, based on an adsorption theory, and the assumption that the energy of molecule A in the presence of an external potential is influenced only by the electrostatic effects, we have derived the basic formula (1.12) for voltage dependent blocking.

## CHAPTER 2. INTERACTION BETWEEN INTERNAL AND EXTERNAL BLOCKERS OF SODIUM CHANNEL

In Section 1.2.3 we described the blocking action of a series of derivatives of  $\mu$ -conotoxin GIIIA on rat skeletal muscle sodium channels. We noticed that derivative R13Q is unusual in that it only partially blocks the single-channel current and remains in a bound state long enough for that state be easily distinguished from periods of gating closure or fast blocking. These two principal properties of R13Q provide a unique opportunity to study, for example, voltage-dependent channel gating during both free and peptide bound states. Such an experiment was performed [French et al. 1996] and it was shown that R13Q, when bound to the channel, decreases the probability for the channel to be open. R13Q, being a slow extracellular blocker, also gives a possibility to investigate and compare the behavior of fast intracellular blockers during both free and R13Q bound states. Such experiments [French et al. 1996] show that the probability for the channel to be blocked by fast blocker decreases when R13Q is bound to the channel. Both R13Q and fast blockers in these experiments are positively charged molecules; the probability for the channel to be blocked by fast blocker depends on the external voltage; this probability decreases at each external voltage when R13Q is bound to the channel – these three facts lead to the idea that the experimental result may be explained by simple electrostatic repulsion between two positively charged blockers [French et al. 1996]. An estimate of the distance between two molecules, based on the hypothesis of electrostatic interaction between the two blockers, was made by French et al. [1996] and it was shown that the distance obtained was consistent with the present understanding of the channel size and structure.

### Section 2.1. Experiment with two blockers, R13Q and DEA

The experiment was performed with single sodium rat skeletal muscle channels to investigate the interaction between R13Q, a slow extracellular blocker, and diethylammonium (DEA), a fast internal blocker. Both blockers are positively charged molecules. The total charge of R13Q is +5; the charge of DEA is +1.

The structures of the molecules, native conotoxin (net charge +6) and DEA (net charge +1), are shown in Fig. 2.1. The sequence of symbols represents the sequence of amino acids of which peptide consists. Positively charged amino acids are shown blue colored, and negatively charged amino acids are shown red colored. The net charge of native conotoxin is +6. The derivative R13Q with net charge +5 can be obtained by substitution of the positively charged (+1) residue R13 of native conotoxin by the neutral residue Q.

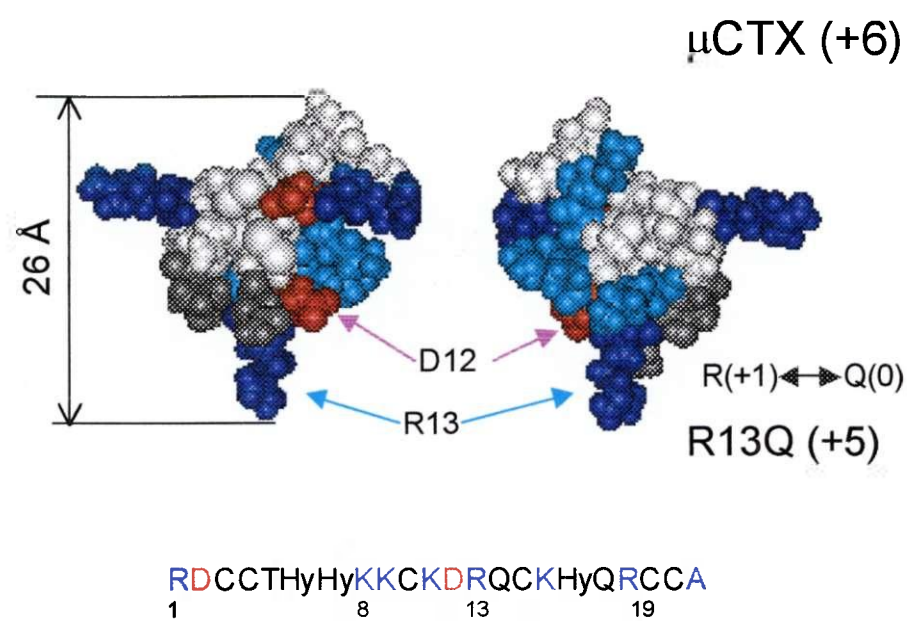


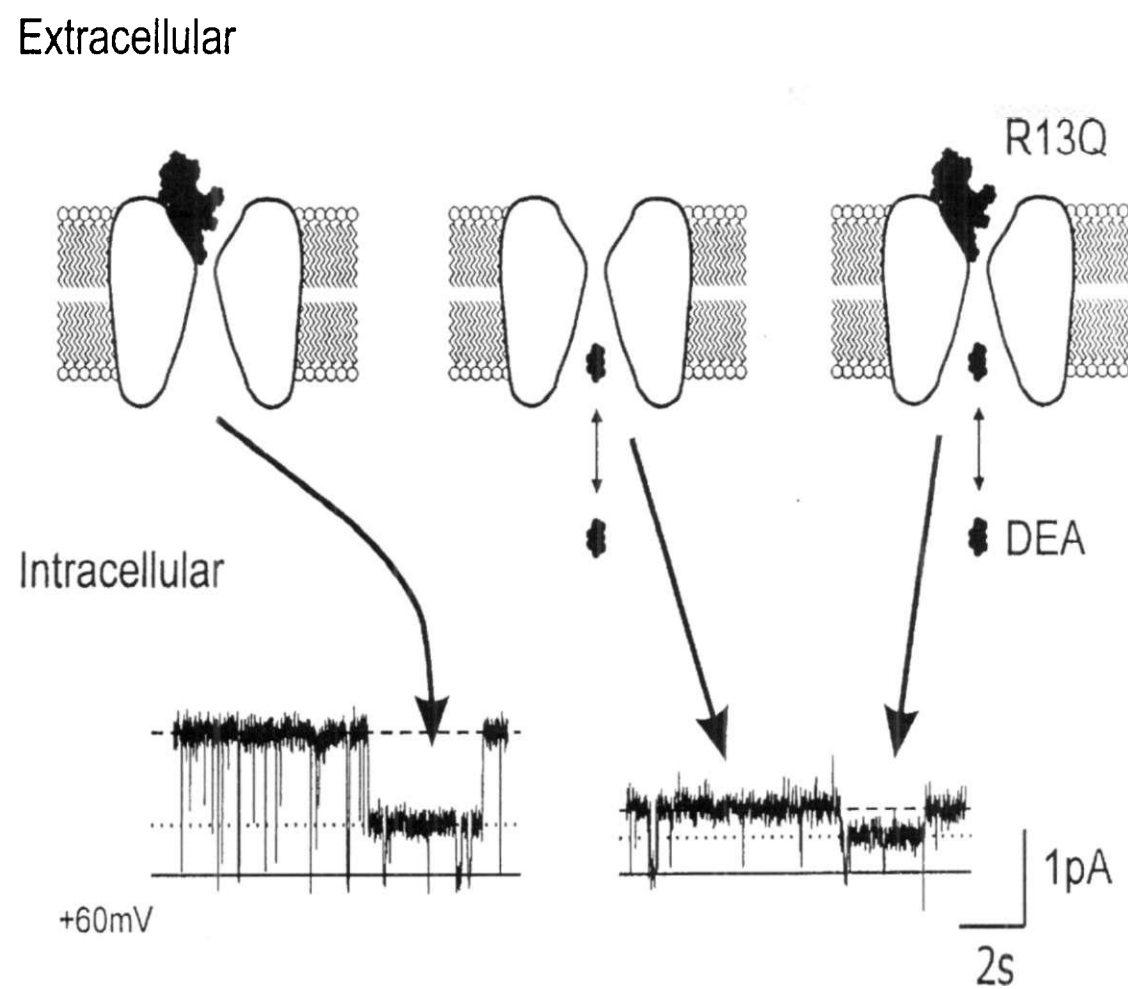
Fig. 2.1. Structures of native  $\mu$  Conotoxin ( $\mu\text{CTX}$ ,  $\text{MW}=2.5 \cdot 10^3$  amu) and diethylammonium (DEA,  $\text{MW}=74$  amu). For clarity, DEA is shown on a large scale. Two views of the 3-dimensional structure ( $\mu\text{CTX}$ ) are shown. The complete linear sequence of amino acids in  $\mu\text{CTX}$  is shown below the 3 dimensional representation, using standard single-letter codes, except for Hy, 4-trans-hydroxyproline. Positively charged amino acids are shown blue colored, and negatively charged amino acids are shown red colored. The net charge of ( $\mu\text{CTX}$ ) is +6. Substitution of neutral residue Q instead of positively charged (+1) residue R13 will give the derivative called R13Q, with net charge +5.

Table 2.1 lists the name of amino acids of  $\mu$ -Conotoxin with their symbols and individual charges.

Amino Acids	Symbol	Charge
Arginine	R	+1
Aspartate	D	-1
Cysteine	C	0
Threonine	T	0
4-trans-hydroxyproline	Hy	0
Lysine	K	+1
Glutamine	Q	0
Alanine amide	A-NH <sub>2</sub>	+1

**Table 2.1. Amino acids of  $\mu$ -Conotoxin**

The objective of the experiment was to obtain the voltage dependence of the probability for the channel to be unblocked by the DEA for two cases, when R13Q was bound, and when it was not bound to the channel. Single-channel recordings were made in the presence and absence of DEA in the intracellular solution for 8 voltages in the range -80mV – 80 mV. R13Q was permanently present on the extracellular side of membrane. The concentration of NaCl was the same in both internal and external solutions and was equal to 200 mM. The experiment was performed at the room temperature, T=25° C. Examples of current recordings obtained at +60mV are presented in Fig. 2.2 ( from [French et al., 1998 ]).



**Fig. 2.2.** Current recordings from the single rat skeletal muscle sodium channel in the presence of R13Q at the extracellular side (+60 mV). Left recording – no DEA in the intracellular solution. Right recording – DEA present. The dashed line indicates open level for unbound state of R13Q, the dotted line shows open level for R13Q bound state. From [French et al., 1998 ].

Fig.2.2 shows that the individual slow block events by R13Q are easily identified. Thus, the fast block by DEA can be analyzed separately for the R13Q-bound and -unbound states. In Sections 1.2.1 we discussed such types of recordings, and in Section 1.2.2 (see formula (1.11) and Fig. 1.7) we analyzed the way of calculation of the probability  $P^B$  for the channel to be unblocked by the internal fast blocker from the similar experimental data. When the slow blocker binds the channel, the method of

calculation of  $P_0^B$  is the same, but the time of averaging the currents will be equal to the total time of slow blocker binding.

The probability  $P_0^B$  was calculated by using formula (1.11) for each experimental voltage, for R13Q-bound and R13Q-unbound states. The results are presented on Fig.2.3.

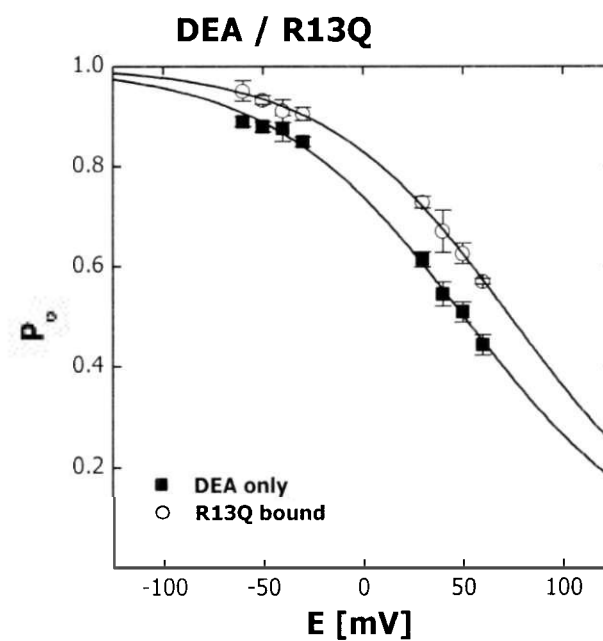


Fig.2.3. Voltage dependence of probability  $P$  for the channel to be unblocked by DEA for two cases: R13Q is not bound to the channel (black squares) and R13Q is bound to the channel (circles). DEA block is shifted to more positive voltages by R13Q binding.

One sees that the probability for the channel to be unblocked by DEA is greater, for each experimental voltage, when R13Q is bound to the channel.

Two voltage-dependent curves for  $P_0^B$  were obtained by fitting data with the formula  $P_0^B = \frac{1}{1 + C^* \exp(\bar{z}\Phi/kT)}$  (see (1.12), (1.16)), which was discussed in Section

1.2.3. The values obtained for parameters,  $C^*$  and  $\bar{z}$ , are the following:

$$\text{without R13Q} \quad \bar{z} = 0.514 \pm 0.018 \quad (2.1a)$$

$$\begin{aligned}
 & C^* = 0.358 \pm 0.011 \\
 \text{with R13Q} & \quad \bar{z}' = 0.560 \pm 0.023 \\
 & C^* = 0.203 \pm 0.010
 \end{aligned} \tag{2.1b}$$

The indicated errors are the estimated standard deviations for the parameters.

To find fitting parameters and their errors we first linearized the expression for  $P_c^b$  and then performed data analysis by using "maximum likelihood method" for the case when error is known in one variable only.

In Section 2.2 we will give an explanation of the experimental results based on the hypothesis of electrostatic repulsion of two positively charged blockers.

## 2.2. Electrostatic interaction of two blockers. Estimation of location of DEA binding site from electrostatic potential due to R13Q.

In Section 1.2.3 we analyzed the relationship between the probability for the channel to be unblocked and applied external voltage (See Fig 1.9, formulas (1.12)-(1.16)). We will now continue this analysis for the case when R13Q is bound to the channel.

If, in addition, the R13Q molecule is present on the binding site at the external side of the membrane the energy of molecule A (DEA) will experience an additional change. Let new energies of DEA in the R13Q-bound state and in the solution be  $\tilde{\mathcal{E}}_1$  and  $\tilde{\mathcal{E}}_0$  respectively. Then we can write:

$$\tilde{\mathcal{E}}_0 = \mathcal{E}_0 + z \cdot \Phi, \quad \tilde{\mathcal{E}}_1 = \mathcal{E}_1 + z \cdot \delta' \cdot \Phi + \Delta \mathcal{E}_{R13Q} \tag{2.2}$$

where  $\Delta \mathcal{E}_{R13Q}$  is the change of energy of DEA on the binding site. The energy of DEA at infinity in the solution does not change.

Then for the ratio of probabilities for the channel to be unblocked by DEA when R13Q is bound to the channel from external side of membrane we have from (1.13):

$$\begin{aligned} \left( \frac{P_1}{P_0} \right)_{R13Q} &= C \cdot \exp(-(\tilde{\varepsilon}_1 - \tilde{\varepsilon}_0)/kT) \\ &= C^* \cdot \exp(z \cdot (1 - \delta') \Phi / kT - \Delta \mathcal{E}_{R13Q} / kT) \end{aligned} \quad (2.3)$$

Finally, the probability for the channel to be unblocked by DEA in R13Q-bound state is:

$$\begin{aligned} (P_0)_{R13Q} &= \frac{1}{1 + C^* \cdot \exp(-\Delta \mathcal{E}_{R13Q} / kT) \exp(z \cdot (1 - \delta') \cdot \Phi / kT)} \\ &= \frac{1}{1 + C^* \cdot \exp(-\Delta \mathcal{E}_{R13Q} / kT) \exp(\bar{z}' \cdot \Phi / kT)} \end{aligned} \quad (2.4)$$

For convenience we will write again the analogous formula for  $P_0^B$  in the case of R13Q-unbound state of the channel (see (1.16)):

$$P_0 = \frac{1}{1 + C^* \cdot \exp(z \cdot (1 - \delta) \cdot \Phi / kT)} = \frac{1}{1 + C^* \cdot \exp(\bar{z} \cdot \Phi / kT)} \quad (2.5)$$

According to relationships (1.15a) and (1.13c), constant  $C^*$  is the same in formula (2.4) for  $(P_0)_{R13Q}$  and formula (2.5) for  $P_0$ . Hence, value of  $\Delta \mathcal{E}_{R13Q}$  can be found from the fitting parameters (1.17a, 1.17b) :

$$\Delta \mathcal{E}_{R13Q} = kT \ln \frac{C^{*'}}{C^*} = (14.6 \pm 1.5) \text{ meV} \quad (2.6)$$

We will assume now that the energy change of DEA due to R13Q,  $\Delta \mathcal{E}_{R13Q}$ , is related only to electrostatic interaction between DEA and R13Q. Then we can write:

$$\Delta \mathcal{E}_{R13Q} = z \cdot \Phi_{R13Q}(R^*) \quad (2.7)$$

where  $R^*$  is the distance between R13Q and DEA.

We see that if we knew the potential due to R13Q, as a function of distance we could estimate the distance between R13Q and the binding site of DEA by solving equation

$$\Delta\varepsilon_{\text{DEA}} = z \cdot \Phi_{\text{R13Q}}(R) \quad (2.8)$$

for  $R^*$ . Fig 2.4. illustrates this idea.

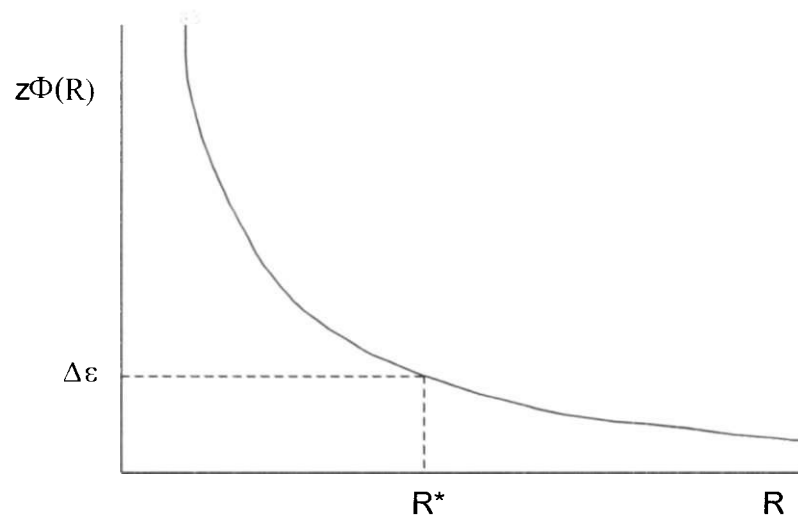


**Fig. 2.4. Graphical solution of equation (2.8).  $R^*$  is the distance between R13Q and DEA binding site.**

To calculate the potential inside the channel due to R13Q we have to create an appropriate model of the channel itself, the R13Q molecule and the ionic solution surrounding the membrane. We will do this in the following chapter.

### **CHAPTER 3. PHYSICAL MODELS OF THE SYSTEM (IONIC SOLUTION- R13Q MOLECULE- CHANNEL)**

We want to estimate the location of the DEA binding site by solving equation (2.8). This equation was obtained with the assumption that the external potential and potential due to R13Q do not cause conformational changes inside the channel protein and, hence, do not disturb the intrinsic potential of the channel. In other words, we assume that the potential inside the channel is a linear combination of intrinsic channel, external and R13Q potentials. Although we do not need to know the intrinsic potential of the channel in this approach, channel geometry and dielectric properties influence the potential due to R13Q inside and outside the membrane. This potential also depends on the structure of the R13Q-molecule and on the properties of the ionic solution that surrounds the membrane. We now consider possible physical models of the system consisting of ionic solution-R13Q molecule and channel. For a detailed review of present models for similar systems that allow calculation of potential distribution inside the channel see [Partenskii and Jordan, 1992]. In more recent studies, other workers have continued to test the ability of continuum electrostatic theories to predict ion channel properties [e.g. Corry et al., 2000; Moy et al., 2000; Nonner et al., 2000].

#### **3.1. Models of ionic solution**

If we consider the water as a continuous dielectric medium with dielectric constant  $\epsilon$  then the distribution of the potential inside the solution due to free external charges, i.e. ions of solution and other arbitrary ions, is determined by Maxwell equation:

$$-\epsilon \nabla^2 \varphi = 4\pi \rho_{free} \quad (3.1)$$

where  $\rho_{free}$  is the density of free charges in the solution. This equation is often called the Poisson equation.

Two approaches can be used to solve (3.1), as detailed below.

**1. Mean field approximation.** The solution is considered as a continuous charged medium with a continuous charge density  $\rho_{free}$ :

$$\rho_{free} = \sum z_i n_i \quad (3.2)$$

where  $n_i$  is a continuous number-density of specific charged particles. In this case potential  $\varphi$  and density  $\rho$  are values averaged over physically infinitesimal volume. Physically infinitesimal volume ( $V_{inf}$ ) is the volume that on one hand is big enough to contain many particles (in order to exclude microfield fluctuations), and on the other hand is small enough in order to have a small difference in macrofields (averaged over the volume) with respect to adjacent volumes.

For this description to be applicable, the following condition should be satisfied: inside the volume with characteristic scale  $\lambda$  of the potential change the number of particles  $N_\lambda$  should be sufficiently large, i.e.

$$N_\lambda = n(4\pi/3)\lambda^3 \gg 1 \quad (3.3)$$

Otherwise, it is not possible to talk about the average (mean) potential, and fluctuations of the potential will dominate. We will show further that the characteristic length  $\lambda$  of the potential change is:

$$\lambda = \left( \frac{kT\epsilon}{8\pi z^2} \right)^{1/2} \quad (3.4)$$

where  $k$  is the Boltzmann constant.  $T$  is temperature,  $n$  is concentration of ions, and  $z$  is the charge of an individual ion.

From (3.3) and (3.4) we get the following estimate for an upper limit of concentration:

$$\sqrt[3]{n} \ll (4\pi/3)^{2/3} \left( \frac{kT\epsilon}{8\pi z^2} \right) \quad (3.5)$$

The numerical value for this upper limit of concentration (for particles with  $z=1$ ) is:  $n \ll 3 \cdot 10^{18} \text{ cm}^{-3}$  ( $n \ll 5 \text{ mM}$ )

In order to write an appropriate expression for the average charge density  $\rho_{free}$  we will recall that this continuous charged medium consists of charged particles, which are in random thermal motion. The energy of each particle consists of two parts: 1) energy of the ion in the average field and 2) correlation energy [J.Mayer and M.Goeppert Mayer, 1977]. If correlation energy is negligible, then for singly charged positive and negative ions in the solution we can write:

$$\begin{aligned}\rho_{free}(r) &= qn^+(r) - qn^-(r) + \rho_{ext} \\ &= qn \left[ \text{Exp}\left(\frac{q\phi(r)}{kT}\right) - \text{Exp}\left(-\frac{q\phi(r)}{kT}\right) \right] + \rho_{ext}\end{aligned}\quad (3.6)$$

where  $q$  is the elementary charge,  $\rho_{ext}$  is the density of external charges, and  $\phi$  is the average potential. To justify neglecting the correlation energy we should have:

$$\frac{q^2}{\epsilon r} \ll kT \quad (3.7)$$

i.e. the energy of interaction between charges has to be small compared to their thermal energy. With relation  $r \sim \frac{1}{n^{1/3}}$  we get from (3.7):

$$\sqrt[3]{n} \ll \frac{kT\epsilon}{q^2} \quad (3.8)$$

We see that this condition coincides with (3.5) up to a numerical multiplier.

Maxwell equation (3.1) with expression (3.6) for  $\rho_{free}$ ,

$$-\epsilon \nabla^2 \phi = n4\pi q \left[ \exp\left(\frac{q\phi(r)}{kT}\right) - \exp\left(-\frac{q\phi(r)}{kT}\right) \right] + \rho_{ext}, \quad (3.9)$$

is a nonlinear Poisson-Boltzmann equation. The approach described above is called the mean field approximation.

Analytical solution of (3.9) is possible in a few very restricted cases. To linearize this equation we should have  $q\phi(r)/kT \ll \sqrt{6}$ . Then from (3.9) we obtain:

$$-\nabla^2 \phi + \kappa^2 \phi = 4\pi\rho_{ext} \quad (3.10)$$

where  $\kappa = 1/\lambda$  ( $\lambda$  is defined in (3.4)). This equation is called the linear Poisson-Boltzmann equation, and the parameter  $\lambda$  is the Debye length. For a point charge placed in infinite space with dielectric constant  $\epsilon$  the solution of the linear Poisson-Boltzmann equation is:

$$\varphi(r) = \frac{qe^{-\kappa r}}{\epsilon r} \quad (3.11)$$

From this expression we see that parameter  $\lambda = 1/\kappa$  characterizes the scale of the potential change. The ions of the solution create “a cloud of oppositely charged particles” around the external charge and partially screen its field.

We will check now the validity of the mean field approximation for parameters of our biophysical system.

The concentration of  $\text{Na}^+$  ions in the solution for our experiment is  $n = 1.2 \cdot 10^{20} \text{ cm}^{-3}$ . For this concentration the value of the Debye length is  $\lambda = 6.8 \text{ \AA}$ .

If we model the R13Q-molecule as a sphere with uniform surface charge and solve the boundary value problem with the linear Poisson-Boltzmann equation (3.10) in the infinite space and the Laplace equation inside the sphere, then for the potential  $\varphi(r)$  at any point  $r$  outside the sphere we obtain:

$$\varphi(r) = \frac{Qe^{-r/\lambda}}{r} \cdot \frac{e^{R/\lambda}}{1 + R/\lambda} \quad (3.11)$$

where  $R$  is the radius of the sphere and  $Q$  is the charge of the sphere.

It is worthwhile to note that the potential outside a uniformly charged ball (charge distributed throughout volume) is expressed by the same relationship (3.11). The radius of the R13Q-molecule is about 10-12  $\text{\AA}$ , the charge  $Q$  is  $+5q$ . Then for the number of particles  $N_\lambda$  in the spherical layer of thickness  $\lambda = 6.8 \text{ \AA}$  around a ball of radius  $R=10 \text{ \AA}$  we get  $N_\lambda \cong 2 > 1$ . So, we are at the margin of application of the mean field approximation. In such cases it is common to use the approximation to obtain a reasonable estimate for the solution of a problem.

Now we will check the possibility of linearizing the Poisson-Boltzmann equation for our physical parameters. Condition  $q\phi(r) \ll kT\sqrt{6}$  for the room temperature and potential (3.11) is valid. Also if we substitute potential (3.11) due to the charged sphere, obtained as a solution of the linear Poisson Boltzmann equation, into the nonlinear equation (3.9) and compare the values of the left and the right side of this equation for any point  $r$ , we will find that the relative difference for  $R=12 \text{ \AA}$  at  $r=R$  is 20%. This number diminishes rapidly with the increase of  $r$ : at  $r=15 \text{ \AA}$  the relative difference is 5%.

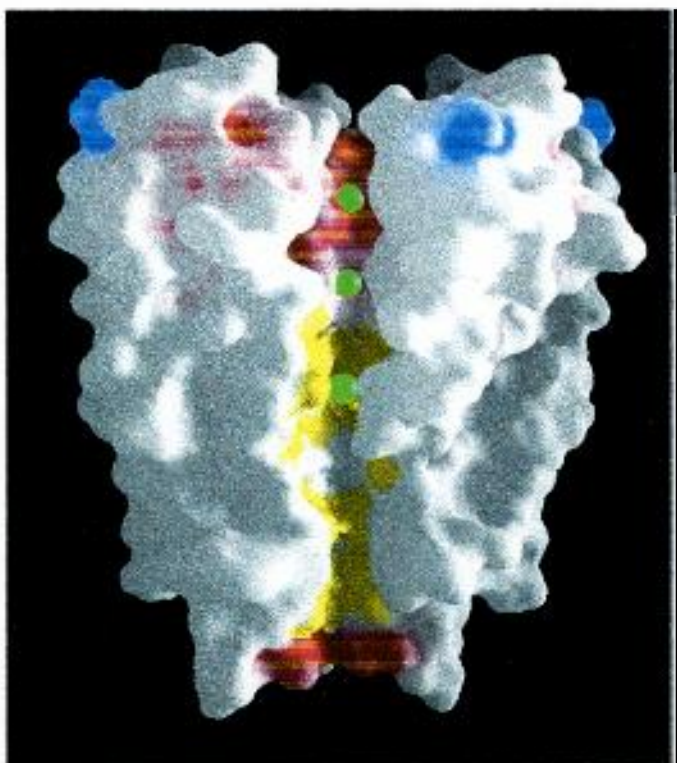
Based on the above estimates it is reasonable to use the mean field approximation for our system, and under this approximation solve the linear Poisson-Boltzmann equation.

**2. Brownian Dynamics (BD) simulation.** For another limiting case, when  $N_i \ll 1$ , the mean field approximation cannot be used. The electric field inside the ionic solution fluctuates with time and is determined by the motion of individual ions in the solution. To find the electric field at some point  $r$  at time  $t$ , one needs to compute the electric forces acting on each of the ions due to the other charges and couple these results with Brownian dynamics simulations, i.e solve the Langevin equation. This computation has to be repeated at every step (in some time interval). Such calculations became available only in the last few years because of their huge computational intensity and are not employed in this thesis. This approach is often called Brownian Dynamics (BD) simulation. For solution of a particular problem utilizing this approach see [Kuyucak et al., 1998, Li et. al., 1998].

### 3.2. Structure of an ion channel

We will consider now the general architecture of the channel and take the bacterial  $K^+$  (KcsA) channel as an example. The detailed structure of the KcsA channel crystals was obtained by X-ray analysis with resolution  $3 \text{ \AA}$  [Doyle et al., 1998]. This channel is not voltage dependent and has relatively small size ( $\sim 45 \text{ \AA}$  in length and

diameter). Eight long helices (transmembrane helices) that constitute the channel protein cross the membrane forming a narrow pore (on the axis of the channel), through which the ions flow [see Figs.1.1, 3.1]. Short helices that form part of the connection between the two transmembrane helices from the extracellular side of the membrane form the vestibule, or mouth, of the channel. The overall length of the pore is about 45 Å. The diameter of the pore varies along its length (see Fig.3.1A). From inside the cell (bottom) the pore begins as a tunnel 18 Å in length and ~ 5-6 Å in diameter, and then opens into a wide cavity ~ 10 Å across near the middle of the membrane. This cavity is filled with water. Then follows the narrowest part of the pore, ~12 Å in length and ~ 3 Å in diameter, representing a selectivity filter, which “recognizes” and selects ions. The rest of the upper part of the pore (~ 5 Å in length) has a conical form with vestibule (mouth) of 6 Å diameter. The distribution of the charge inside the channel can be seen from Fig.3.1 A. The channel is mainly neutral, except for the ends of the pore, which are negatively charged.

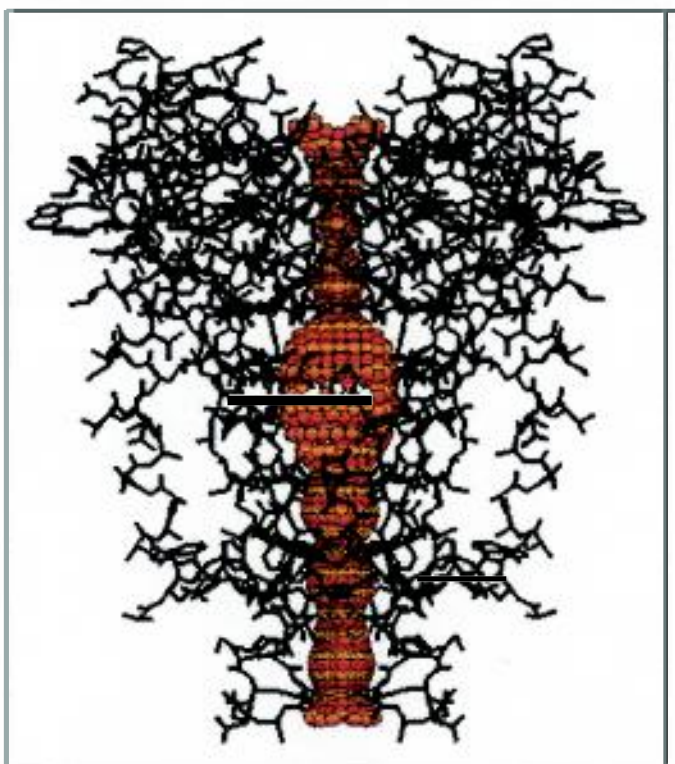


B

**Fig.3.1. 3-Dimensional representation of the Ksc.**

**A (bottom). Pore (red) and pore former (stick representation, black)**

**B (top) Distribution of the charge in the channel. Positive charges are blue colored, negative charges are red colored. White colour is for neutral area. The green spheres represent Na ions position in the conduction pathway.**



A

It is unlikely that such a detailed examination will be available soon for voltage dependent Na channels, because of their size ( $\sim 80 - 100 \text{ \AA}$  in length and diameter) and less symmetrical structure. However, biophysical and mutational information suggests that the structural framework of KcsA may also be found in  $\text{Na}^+$  channels [Lipkind and Fozzard, 2000].

Voltage dependent  $\text{Na}^+$  channel has 24 transmembrane helices. Based on the data from various investigations [Lipkind and Fozzard, 2000] one can think that the selectivity filter of this channel is shorter than that of KcsA and at its narrowest part is larger,  $\sim 4-6 \text{ \AA}$  in diameter. The extracellular vestibule is essentially wider,  $\sim 12 \text{ \AA}$  in diameter [Lipkind and Fozzard, 2000]. Being inserted into the lipid bilayer, an  $\text{Na}^+$  channel will extend into the surrounding solution for at least  $20 \text{ \AA}$  from each sides of the membrane. Although the chemical composition of the  $\text{Na}^+$  channel is known, information about its geometry is uncertain. The following drawing is a possible representation of the geometry of  $\text{Na}^+$  channel:

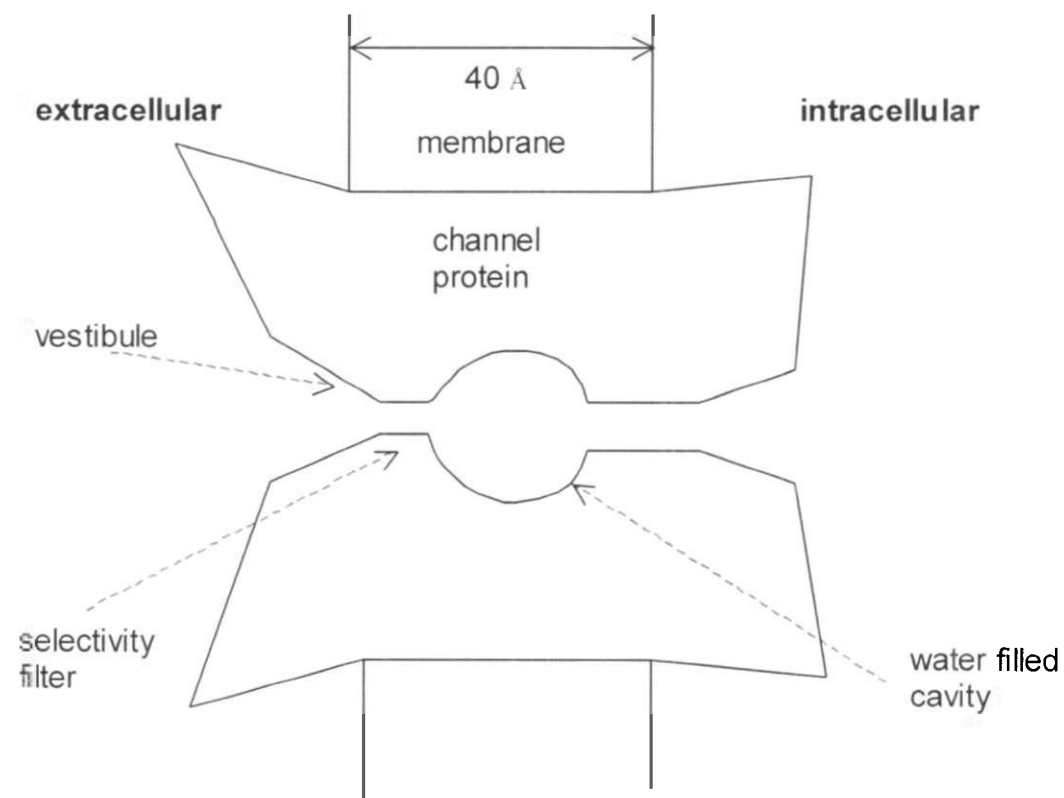


Fig.3.2. Possible geometry of  $\text{Na}^+$  channel.

### 3.3. Channel as a continuous medium

Usually the membrane and the channel proteins are modeled as continuous and uniform dielectrical media. The molecular structure of the channel is ignored in this approach. The membrane and the pore former are considered to be one unit with average dielectric constant  $\epsilon_m$  between 2 and 10. For the narrow pore, the dielectric constant  $\epsilon_p$  depends on the diameter of the pore. In the wide channel cavity the water structure should be essentially that of bulk water with  $\epsilon_p=80$ . In the narrow part of the pore, where water molecules behave as individual particles, it is difficult to assign a particular value to the dielectric constant. Probably it should be taken to be much less than 80. Because of their computational complexity, models with nonuniform distribution of  $\epsilon$  inside the pore former and the pore itself were not considered. For detailed analysis of this problem see [Partenskii and Jordan, 1992].

### 3.4. Advantages of BEM

Cai and Jordan [1990] considered the following realistic model

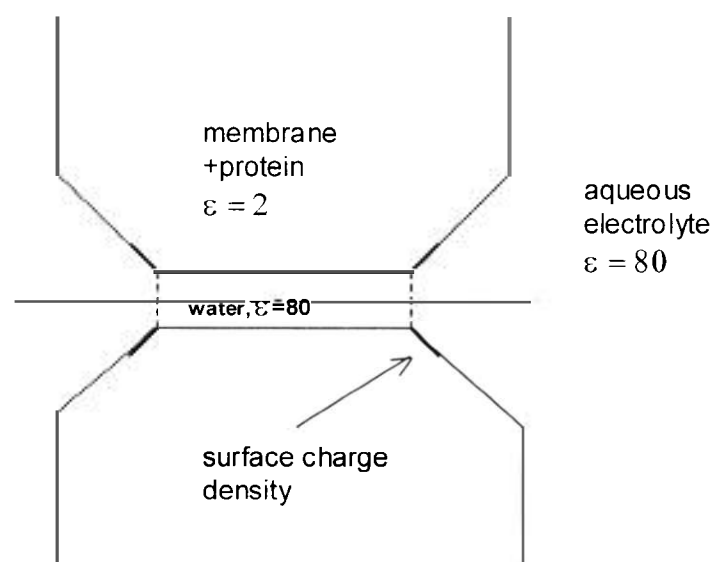


Fig.3.3. Geometry of the cylindrically symmetric model Na channel and electrolyte system, from [Cai and Jordan, 1990]. The regions to the right and to the left of the membrane contain aqueous electrolyte. The vestibule contains electrolyte, and  $\epsilon$  for the vestibule is the same as for bulk solution. Concentration of ions in the narrow pore is zero and  $\epsilon$  is the same as the bulk water. The black regions represent the vestibule charges.

The potential inside the channel due to the surface charge located on the channel was calculated. Application of the finite difference method in this work was causing a number of difficulties when applied to this complex geometry as discussed by the authors of the paper. Disadvantages of finite difference methods, most commonly used in numerical calculations of this type, lie in the difficulty of representing the complex geometry of the boundaries and in describing singularities. Also any change in geometry requires rebuilding the numerical grid. The computational cost of such changes is very high.

Boundary Element Method is perfectly suited to overcome all the above problems for the following reasons:

- 1) No grid is needed;
- 2) Singularities are described with analytical accuracy;
- 3) Any changes in the boundary geometry are easily implemented, which is especially important for examining systems whose geometry is uncertain.

### **3.5. Our Model**

We use the mean field approximation for the ionic solution, and treat the membrane and the channel as continuous and uniform dielectric mediums. The pore is represented as a cylinder containing ionic solution (see Fig. 3.4), and the toxin molecule R13Q is modeled as a sphere with uniform charge density. The nonuniform charge distribution of R13Q is also considered. For calculation of the potential due to the R13Q-molecule inside the channel we apply BEM. Using the advantages of this method, we examine the influence of various physical parameters (for example, the width and radius of the channel, the radius of the toxin, dielectric constant, nonuniform charge distribution of R13Q) on the behaviour of the potential in the channel. Mathematical details of these procedures are given in Chapters 4-6, and results are discussed in Chapter 7.

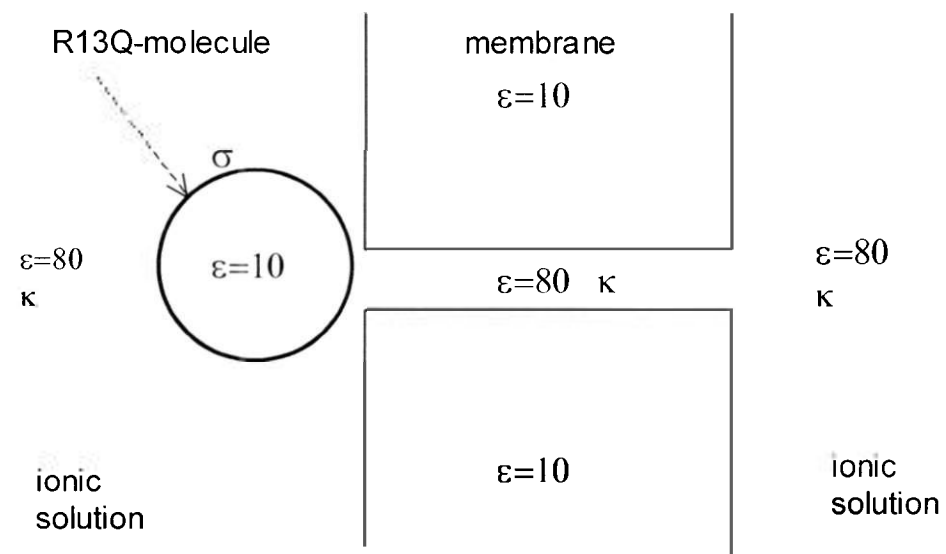


Fig 3.4. Our model. Geometry of the cylindrically symmetric model Na channel. The regions to the right and to the left of the membrane contain ionic solution, the pore is also filled with ionic solution.  $1/\kappa = \lambda = 7 \text{ \AA}$ .  $\epsilon$  of the pore is the same as the bulk water.

## CHAPTER 4. BOUNDARY ELEMENT METHOD (BEM). THEORY.

### 4.1. BEM applied to the Laplace and Poisson equations

#### 4.1.1. Integral representation for potential

Let us consider the following problem (see Fig.4.1). Two regions (I and II) with a separating smooth surface  $\Gamma$  are filled with uniform dielectrics that have dielectric constants  $\varepsilon_1$  and  $\varepsilon_2$  respectively. The space charge  $q$  is placed in the first region. This charge  $q$  may be a point charge or distributed charge. We want to find the electric potential  $\varphi$  in both regions. Charge density distribution is described by  $f(\mathbf{r})\varepsilon_1/4\pi$ , where  $f(\mathbf{r})$  is some arbitrary function of position,  $\mathbf{r}$ .

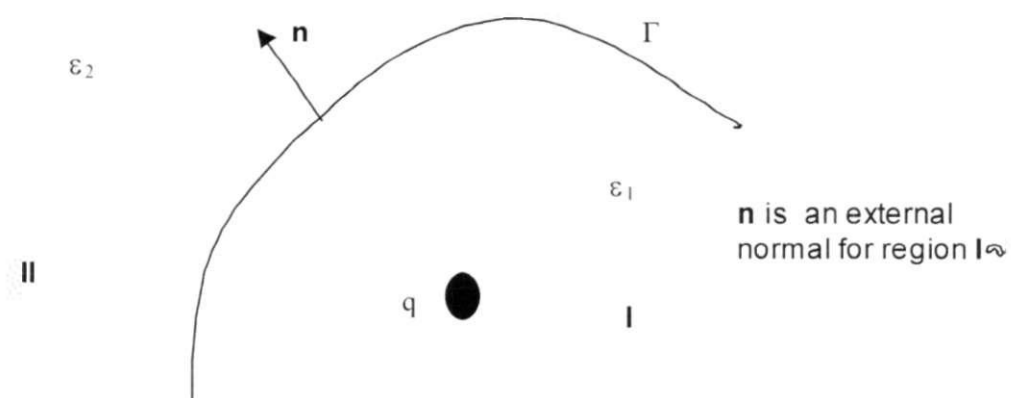


**Figure 4.1.** Geometry of the system. Two regions, I and II, with dielectric constants  $\varepsilon_1$  and  $\varepsilon_2$  respectively are separated by surface  $\Gamma$ . Charge  $q$  is in region I.

This problem is governed by the following system of equations:

$$\text{For region I. } -\nabla^2 \varphi_I = f(\mathbf{r}) \quad \text{Poisson equation} \quad (4.1)$$

$$\text{For region II. } -\nabla^2 \varphi_{II} = 0 \quad \text{Laplace equation} \quad (4.2)$$

These equations have to be accompanied by the usual boundary conditions on the surface  $\Gamma$ :

$$\varphi_I|_{\Gamma} = \varphi_{II}|_{\Gamma} \quad (4.3a)$$

$$\varepsilon_1 (\mathbf{n} \cdot \bar{\nabla})\varphi_I|_{\Gamma} = \varepsilon_2 (\mathbf{n} \cdot \bar{\nabla})\varphi_{II}|_{\Gamma} \quad (4.3b)$$

$$\lim_{r \rightarrow \infty} \varphi(r) = 0 \quad (4.3c)$$

where  $(\mathbf{n} \cdot \bar{\nabla})$  is the derivative along the direction  $\mathbf{n}$ , normal to the surface. The condition (4.3c) is applied to potentials that contain infinity in their domain.

Equations (4.1)-(4.3) uniquely define the potential in the whole space.

Now we wish to write an integral representation for the potentials  $\varphi_I$  and  $\varphi_{II}$ . To do this we will introduce a Green function, which is a solution of the following equation:

$$-\nabla_r^2 G(\mathbf{r}, \xi) = \delta(\mathbf{r} - \xi) \quad (4.4)$$

where point  $\xi$  is an arbitrary point belonging to regions I or II, and symbol  $\delta(\mathbf{r} - \xi)$  represents the Dirac delta function. Here subscript r attached to the Laplacian means that differentiation is performed with respect to variable  $\mathbf{r}$ . Explicitly the Green function can be written as

$$G(\mathbf{r}, \xi) = \frac{1}{4\pi |\mathbf{r} - \xi|} + F(\mathbf{r}, \xi) \quad (4.5)$$

with the function  $F(\mathbf{r}, \xi)$  satisfying the Laplace equation inside regions I or II:

$$-\nabla_r^2 F(\mathbf{r}, \xi) = 0 \quad (4.6)$$

We will need Green's second identity or Green's theorem, which states that for any two differentiable functions  $\phi$  and  $\psi$  the following equation is valid:

$$\int_V (\phi \nabla^2 \psi - \psi \nabla^2 \phi) dV = \oint_{\Gamma} (\phi \nabla \psi - \psi \nabla \phi) \cdot d\mathbf{S} \quad (4.7)$$

where V is the volume enclosed by the surface  $\Gamma$ .

With Green's theorem (4.7),  $\phi = \varphi$ ,  $\psi = G(\mathbf{r}, \xi)$ , the specified properties of  $G$  (4.4), and equations (4.1), (4.2) it is simple to obtain the integral representation for potentials in regions I and II [Jackson, 1999; Morse and Feshbach, 1953]:

$$\varphi_I(\xi) = \int_{V_I} f(\mathbf{r})G(\mathbf{r}, \xi)dV_r - \int_{\Gamma} \varphi_I(\mathbf{r})\nabla_r G(\mathbf{r}, \xi) \cdot d\bar{S}_r + \int_{\Gamma} G(\mathbf{r}, \xi)\nabla_r \varphi_I(\mathbf{r}) \cdot d\bar{S}_r \quad (4.8a)$$

$$\varphi_{II}(\xi) = -\int_{V_{II}} \varphi_{II}(\mathbf{r})\nabla_r G(\mathbf{r}, \xi) \cdot d\bar{S}_r + \int_{\Gamma} G(\mathbf{r}, \xi)\nabla_r \varphi_{II}(\mathbf{r}) \cdot d\bar{S}_r \quad (4.8b)$$

Here  $\xi$  is an inner point (the observation point) of the corresponding region ( $\xi \in V$ ,  $\xi \notin \Gamma$ ),  $f(\mathbf{r})$  is the right hand side of (4.1), and subscript  $r$  in the symbols  $dV_r$  and  $d\bar{S}_r$  means that integration is performed with respect to variable  $\mathbf{r}$ . According to common convention one measures the gradient pointing outward from the surface (in other words, the surface element  $d\bar{S}$  points away from the interior of the volume, where the field is to be evaluated), so that the surface integrals are the usual normal outflow integrals.

It is worthwhile to emphasize that the above equations (4.8) are not a solution to a boundary value problem but only an integral statement since arbitrary specification of both the potential  $\varphi$  and its normal derivative  $\frac{\partial \varphi}{\partial n}$  (Cauchy boundary conditions) on the surface  $\Gamma$  is an over specification of the problem. But the above equations relate the value of the potential  $\varphi(\xi)$  anywhere inside the volume to the values of the potential and its normal derivative at the boundary surface  $\Gamma$ . If we knew the values of the potential and its normal derivative on the boundary  $\Gamma$  we could find the values of the potential in any point of the region by simple integration.

Now we will investigate the possibility of finding the potentials and their normal derivatives on the surface.

#### 4.1.2. Integral equations for potential on the surface

Equations (4.1a) and (4.1b) are valid only for inner points  $\xi$ , but since the potential is a continuous function we can get its values on the boundary by a limiting process.

Let  $\xi_0$  be a point on the boundary  $\Gamma$ . In the limit of  $\xi \rightarrow \xi_0$  we have

$$\begin{aligned} \varphi_I(\xi_0) &= \lim_{\xi \rightarrow \xi_0} \varphi_I(\xi) \\ &= \lim_{\xi \rightarrow \xi_0} \int_{V'} f(\mathbf{r}) G(\mathbf{r}, \xi) dV - \lim_{\xi \rightarrow \xi_0} \int_{\Gamma} \varphi_I(\mathbf{r}) \bar{\nabla}_r G(\mathbf{r}, \xi) \cdot d\bar{S}_r \\ &\quad + \lim_{\xi \rightarrow \xi_0} \int_{\Gamma} G(\mathbf{r}, \xi) \bar{\nabla} \varphi_I(\mathbf{r}) \cdot d\bar{S}_r \end{aligned} \quad (4.9a)$$

$$\varphi_{II}(\xi_0) = \lim_{\xi \rightarrow \xi_0} \varphi_{II}(\xi) = - \lim_{\xi \rightarrow \xi_0} \int_{\Gamma} \varphi_{II}(\mathbf{r}) \bar{\nabla}_r G(\mathbf{r}, \xi) \cdot d\bar{S}_r + \lim_{\xi \rightarrow \xi_0} \int_{\Gamma} G(\mathbf{r}, \xi) \bar{\nabla} \varphi_{II}(\mathbf{r}) \cdot d\bar{S}_r \quad (4.9b)$$

These equations are still very general. Using the freedom of choice of Green function (via the function  $F(\mathbf{r}, \xi)$ ) we will take its simplest form, namely, the free space Green function:

$$G(\mathbf{r}, \xi) = \frac{1}{4\pi |\mathbf{r} - \xi|} \quad (4.10)$$

In this case equations (4.9a) and (4.9b) become:

$$\begin{aligned} \varphi_I(\xi_0) &= \lim_{\xi \rightarrow \xi_0} \varphi_I(\xi) \\ &= \int_{V'} f(\mathbf{r}) \frac{1}{4\pi |\mathbf{r} - \xi_0|} dV - \lim_{\xi \rightarrow \xi_0} \int_{\Gamma} \varphi_I(\mathbf{r}) \bar{\nabla}_r \frac{1}{4\pi |\mathbf{r} - \xi|} \cdot d\bar{S}_r \\ &\quad + \lim_{\xi \rightarrow \xi_0} \int_{\Gamma} \frac{1}{4\pi |\mathbf{r} - \xi|} \bar{\nabla} \varphi_I(\mathbf{r}) \cdot d\bar{S}_r \end{aligned} \quad (4.10a)$$

$$\begin{aligned} \varphi_{II}(\xi_0) &= \lim_{\xi \rightarrow \xi_0} \varphi_{II}(\xi) \\ &= - \lim_{\xi \rightarrow \xi_0} \int_{\Gamma} \varphi_{II}(\mathbf{r}) \bar{\nabla}_r \frac{1}{4\pi |\mathbf{r} - \xi|} \cdot d\bar{S}_r + \lim_{\xi \rightarrow \xi_0} \int_{\Gamma} \frac{1}{4\pi |\mathbf{r} - \xi|} \bar{\nabla} \varphi_{II}(\mathbf{r}) \cdot d\bar{S}_r \end{aligned} \quad (4.10b)$$

To do the next step and obtain particular expressions for  $\varphi(\xi_0)$  we have to investigate the integrals on the right hand side of the above equations. We will perform this analysis the way it is done in [Stakgold, 1979]. We shall investigate the behavior of integrals in the vicinity of a fixed point  $\xi_0$  on  $\Gamma$ .

Let us consider integrals that determine, say,  $\varphi_I$ :

$$\begin{aligned} \varphi_l(\xi) = & \int_V f(\mathbf{r}) \frac{1}{4\pi|\mathbf{r}-\xi_0|} dV - \int_\Gamma \varphi_l(\mathbf{r}) \nabla_r \frac{1}{4\pi|\mathbf{r}-\xi|} \cdot d\vec{S}_r \\ & + \int_\Gamma \frac{1}{4\pi|\mathbf{r}-\xi|} \nabla \varphi_l(\mathbf{r}) \cdot d\vec{S}_r \end{aligned} \quad (4.11)$$

We first analyze the second integral in (4.11). Let

$$I_2 = g(\xi) = \int_\Gamma \frac{1}{4\pi|\mathbf{r}-\xi|} \nabla \varphi_l(\mathbf{r}) \cdot d\vec{S}_r, \quad \xi \notin \Gamma \quad (4.12)$$

This integral is well defined when  $\xi$  is outside  $\Gamma$ . Further, it is also well defined when  $\xi$  is on  $\Gamma$ . To see this, we need only prove that for  $\forall \xi_0 \in \Gamma$  and any well-defined vector function  $\nabla \varphi(\mathbf{r})$

$$\lim_{\xi \rightarrow \xi_0} g(\xi) = g(\xi_0) = \int_\Gamma G(\mathbf{r}, \xi_0) \nabla \varphi_l(\mathbf{r}) \cdot d\vec{S}_r \quad (4.13)$$

where the last integral is understood as an improper integral. Let us take a point  $\xi_0 \in \Gamma$  and calculate the limit of function  $g(\xi)$  for  $\xi \rightarrow \xi_0$ . First we divide  $\Gamma$  into the complementary parts  $\Gamma_\varepsilon$  and  $\Gamma - \Gamma_\varepsilon$ , where  $\Gamma_\varepsilon$  is the portion of  $\Gamma$  within a sphere of radius  $\varepsilon$  centered at point  $\xi_0$ . Since integral (4.12) converges for any  $\xi \notin \Gamma$  it can be represented as the sum of two integrals:

$$g(\xi) = \int_{\Gamma - \Gamma_\varepsilon} G(\mathbf{r}, \xi) \nabla \varphi_l(\mathbf{r}) \cdot d\vec{S}_r + \int_{\Gamma_\varepsilon} G(\mathbf{r}, \xi) \nabla \varphi_l(\mathbf{r}) \cdot d\vec{S}_r \quad (4.14)$$

Let us introduce the following notation:

$$g^{\Gamma - \Gamma_\varepsilon}(\xi) = \int_{\Gamma - \Gamma_\varepsilon} G(\mathbf{r}, \xi) \nabla \varphi_l(\mathbf{r}) \cdot d\vec{S}_r \quad (4.15a)$$

$$g^{\Gamma_\varepsilon}(\xi) = \int_{\Gamma_\varepsilon} G(\mathbf{r}, \xi) \nabla \varphi_l(\mathbf{r}) \cdot d\vec{S}_r \quad (4.15b)$$

So that  $g(\xi) = g^{\Gamma - \Gamma_\varepsilon}(\xi) + g^{\Gamma_\varepsilon}(\xi)$ .

We calculate limits of functions  $g^{\Gamma-\Gamma_\varepsilon}(\xi)$  and  $g^{\Gamma_\varepsilon}(\xi)$  for  $\xi \rightarrow \xi_0$  separately. If these limits exist and are finite then the limit of function  $g(\xi)$  for  $\xi \rightarrow \xi_0$  exists and is equal to the sum of these two limits.

Consider first the integral over  $\Gamma-\Gamma_\varepsilon$ . Since  $\xi_0$  does not belong to the region of integration ( $\xi_0 \notin \Gamma-\Gamma_\varepsilon$ ) the integral does not have any singularity, and hence

$$\lim_{\xi \rightarrow \xi_0} g^{\Gamma-\Gamma_\varepsilon}(\xi) = \int_{\Gamma-\Gamma_\varepsilon} G(\mathbf{r}, \xi_0) \vec{\nabla} \varphi_l(\mathbf{r}) \cdot d\vec{S}_r \equiv g^{\Gamma-\Gamma_\varepsilon}(\xi_0) \quad (4.16)$$

Now consider the second integral, over  $\Gamma_\varepsilon$ . For  $\varepsilon$  sufficiently small,  $\Gamma_\varepsilon$  is nearly a flat surface and we can regard  $\Gamma_\varepsilon$  as lying in the plane tangent to  $\Gamma$  at  $\xi_0$ . We introduce a Cartesian coordinate system  $(u, v, w)$  with origin at  $\xi_0$ ;  $u, v$  lie in the tangent plane and the positive  $w$  axis is in the direction of the normal  $\mathbf{n}$ . Then we can write

$$g^{\Gamma_\varepsilon}(\xi) = \frac{1}{4\pi} \int_{\Gamma_\varepsilon} \frac{\psi(\xi_0 + \tilde{\mathbf{r}}) d\tilde{r}}{|\tilde{\mathbf{r}} - \tilde{\xi}|} + o(\varepsilon) \quad (4.17)$$

where  $\tilde{\mathbf{r}}$  is a point on the tangent plane (see Fig.4.2).

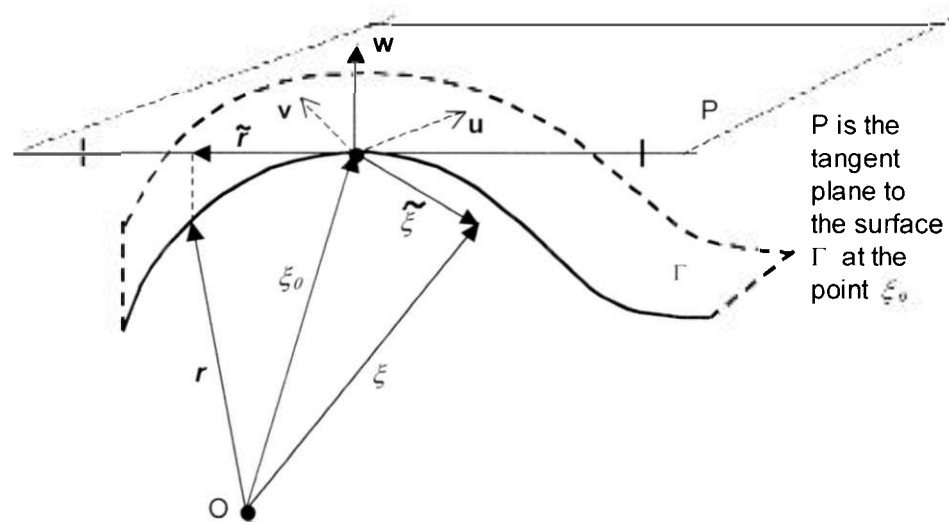


Figure 4.2. Local geometry in the vicinity of point  $\xi_0$  on the surface  $\Gamma$ .  $(u, v, w)$  is a local Cartesian coordinate system with origin at  $\xi_0$ .

Since  $\psi(\xi_0 + \tilde{\mathbf{r}})$  is continuous function we can rewrite equation using the mean value theorem:

$$g^{\Gamma_\varepsilon}(\xi) = \frac{\psi(\xi_0 + \tilde{\mathbf{r}}^*)}{4\pi} \int_{\Gamma_\varepsilon} \frac{dudv}{|\tilde{\mathbf{r}} - \tilde{\xi}|} + o(\varepsilon) \quad (4.18)$$

where  $\xi_0 + \tilde{\mathbf{r}}^*$  is some appropriate point on the plane in  $\Gamma_\varepsilon$ . If we let  $\xi$  lie on the normal to  $\Gamma$  at  $\xi_0$ , then we can write (this does not restrict the generality of the proof, see [Mikhlin, 1970; Paris and Canas, 1997])

$$\begin{aligned} g^{\Gamma_\varepsilon}(\xi) &= \frac{\psi(\xi_0 + \tilde{\mathbf{r}}^*)}{4\pi} \int_{\Gamma_\varepsilon} \frac{dudv}{(\xi_w^2 + u^2 + v^2)^{1/2}} + o(\varepsilon) \\ &= \frac{\psi(\xi_0 + \tilde{\mathbf{r}}^*)}{4\pi} \int_{\Gamma_\varepsilon} \frac{2\pi\rho d\rho}{(\xi_w^2 + \rho^2)^{1/2}} + o(\varepsilon) \\ &= \frac{\psi(\xi_0 + \tilde{\mathbf{r}}^*)}{2} ((\xi_w^2 + \varepsilon^2)^{1/2} - \xi_w) + o(\varepsilon) \end{aligned} \quad (4.19)$$

Now we can take the limit of  $g^{\Gamma_\varepsilon}(\xi)$  for  $\xi \rightarrow \xi_0$  using the last expression in (19):

$$\lim_{\xi \rightarrow \xi_0} g^{\Gamma_\varepsilon}(\xi) = \frac{\psi(\xi_0 + \tilde{\mathbf{r}}^*)}{2} \varepsilon + o(\varepsilon). \quad (4.20)$$

So, the limit of  $g(\xi)$  for  $\xi \rightarrow \xi_0$  exists and equals the following:

$$A = \lim_{\xi \rightarrow \xi_0} g(\xi) = \lim_{\xi \rightarrow \xi_0} g^{\Gamma-\Gamma_\varepsilon}(\xi) + \lim_{\xi \rightarrow \xi_0} g^{\Gamma_\varepsilon}(\xi) = g^{\Gamma-\Gamma_\varepsilon}(\xi_0) + \frac{\psi(\xi_0 + \tilde{\mathbf{r}}^*)}{2} \varepsilon + o(\varepsilon) \quad (4.21)$$

Since  $\lim_{\xi \rightarrow \xi_0} g(\xi)$  exists it is unique and therefore it does not depend on the way of dividing the region of integration  $\Gamma$  into two parts  $\Gamma_\varepsilon$  and  $\Gamma-\Gamma_\varepsilon$  and, hence, does not depend on  $\varepsilon$ . Then the following is valid:

$$\begin{aligned}
A &= \lim_{\varepsilon \rightarrow 0} \left( g^{\Gamma-\Gamma_\varepsilon}(\xi_0) - \frac{\psi(\xi_0 + \tilde{\mathbf{r}}^*)}{2} \varepsilon + o(\varepsilon) \right) \\
&= \lim_{\varepsilon \rightarrow 0} g^{\Gamma-\Gamma_\varepsilon}(\xi_0) + \lim_{\varepsilon \rightarrow 0} \left( \frac{\psi(\xi_0 + \tilde{\mathbf{r}}^*)}{2} \varepsilon + o(\varepsilon) \right) \\
&= \lim_{\varepsilon \rightarrow 0} g^{\Gamma-\Gamma_\varepsilon}(\xi_0) \\
&= \lim_{\varepsilon \rightarrow 0} \int_{\Gamma-\Gamma_\varepsilon} G(\mathbf{r}, \xi_0) \bar{\nabla} \varphi_l(\mathbf{r}) \cdot d\bar{S}_r
\end{aligned} \tag{4.22}$$

The last expression is the definition of integral  $\int G(\mathbf{r}, \xi_0) \bar{\nabla} \varphi_l(\mathbf{r}) \cdot d\bar{S}_r$  as an improper integral, i.e. we have

$$A = \lim_{\varepsilon \rightarrow 0} g^{\Gamma-\Gamma_\varepsilon}(\xi_0) = \lim_{\varepsilon \rightarrow 0} \int_{\Gamma-\Gamma_\varepsilon} G(\mathbf{r}, \xi_0) \bar{\nabla} \varphi_l(\mathbf{r}) \cdot d\bar{S}_r = g(\xi_0) \tag{4.23}$$

So, we have proven that  $\forall \xi_0 \in \Gamma \quad g(\xi_0) = \int G(\mathbf{r}, \xi_0) \bar{\nabla} \varphi_l(\mathbf{r}) \cdot d\bar{S}_r$  and the limit of the integral in question taken from appropriate side of the surface coincide with the value of  $g(\xi)$  right on the surface.

Let us now consider the first integral in the integral representation (4.11).

$$I_1(\xi) = \frac{1}{4\pi} \int_{\Gamma} \varphi(\mathbf{r}) \bar{\nabla}_r \frac{1}{|\mathbf{r} - \xi|} \cdot d\bar{S}_r \tag{4.24a}$$

This integral reduces to

$$I_1(\xi) = \frac{(-1)}{4\pi} \int_{\Gamma} \varphi(\mathbf{r}) \frac{\bar{\nu} \cdot \bar{n}}{|\mathbf{r} - \xi|^2} dS_r \tag{4.24b}$$

where  $\bar{\nu}(\mathbf{r})$  is a normal to the element of the surface  $dS_r$  and  $\bar{n}$  is the unit vector in the direction of gradient of  $|\mathbf{r} - \xi|$ .

This integral is well defined for any  $\xi$  not lying on the surface  $\Gamma$ . To analyze the behavior of integral  $I_1$ , we, as in the previous discussion, divide  $\Gamma$  into the complementary parts  $\Gamma_\varepsilon$  and  $\Gamma-\Gamma_\varepsilon$  ( $\xi_0$  is the center of  $\Gamma_\varepsilon$ ) and write:

$$I_1(\xi) = \frac{(-1)}{4\pi} \int_{\Gamma_\varepsilon} \varphi(r) \frac{\vec{v} \cdot \vec{n}}{|\mathbf{r} - \xi|^2} d\bar{S}_r + \frac{(-1)}{4\pi} \int_{\Gamma_\varepsilon} \varphi(r) \frac{\vec{v} \cdot \vec{n}}{|\mathbf{r} - \xi|^2} d\bar{S}_r \quad (4.25)$$

$$I_1(\xi) = I_1(\xi)^{\Gamma-\Gamma_\varepsilon} + I_1(\xi)^{\Gamma_\varepsilon}$$

The first integral is clearly continuous at any point  $\xi$  not lying on  $\Gamma-\Gamma_\varepsilon$ , and will therefore be continuous as  $\xi \rightarrow \xi_0$ . The second integral is over a nearly flat surface if  $\varepsilon$  is sufficiently small. Using the same Cartesian coordinate system that was introduced earlier we get:

$$\begin{aligned} I_1(\xi)^{\Gamma_\varepsilon} &= \frac{(-1)}{4\pi} \int_{\Gamma_\varepsilon} \frac{\varphi(\xi_0 + \tilde{\mathbf{r}}) \cos[\tilde{\mathbf{r}} - \tilde{\xi}, \vec{v}(\xi_0 + \tilde{\mathbf{r}})]}{|\tilde{\mathbf{r}} - \tilde{\xi}|^2} dudv + o(\varepsilon) \\ &= \frac{1}{2} \varphi(\xi_0 + \tilde{\mathbf{r}}) \int_{\Gamma_\varepsilon} \frac{\cos[\tilde{\mathbf{r}} - \tilde{\xi}, \vec{v}(\xi_0 + \tilde{\mathbf{r}})]}{|\tilde{\mathbf{r}} - \tilde{\xi}|^2} dudv + o(\varepsilon) \end{aligned} \quad (4.26a)$$

With  $\xi$  lying on the normal  $\vec{v}$  ( $\vec{v} = \vec{w}$ ) to  $\Gamma_\varepsilon$  at  $\xi_0$  (see Fig.4.3) the functions in the integrand can be written as

$$|\tilde{\xi} - \tilde{\mathbf{r}}|^2 = (\xi_w^2 + u^2 + v^2)$$

and

$$\cos[\tilde{\mathbf{r}} - \tilde{\xi}, \vec{v}(\xi_0 + \tilde{\mathbf{r}})] = \frac{-\xi_w}{(\xi_w^2 + u^2 + v^2)^{1/2}} \quad (4.26b)$$

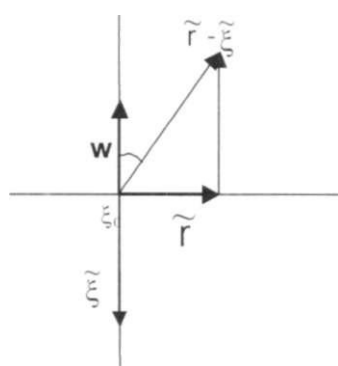


Figure 4.3. Local geometry in the vicinity of point  $\xi_0$  in the case when  $\xi$  approaches  $\xi_0$  along the  $w$  axis.

After this an expression for integral  $I^{\Gamma_\varepsilon}(\xi)$  becomes:

$$\begin{aligned}
 I_1(\xi)^{\Gamma_\varepsilon} &= \frac{(-1)}{4\pi} \varphi(\xi_0 + \tilde{\mathbf{r}}^*) \int_{\Gamma_\varepsilon} \frac{-\xi_w}{(\xi_w^2 + u^2 + v^2)^{3/2}} dudv + o(\varepsilon) = \\
 &= \frac{(-1)}{4\pi} \varphi(\xi_0 + \tilde{\mathbf{r}}^*) \int_{\Gamma_\varepsilon} \frac{-\xi_w 2\pi \rho d\rho}{(\xi_w^2 + \rho^2)^{3/2}} + o(\varepsilon) = \\
 &= \frac{1}{2} \varphi(\xi_0 + \tilde{\mathbf{r}}^*) \left( \frac{\xi_w}{(\xi_w^2 + \varepsilon^2)^{1/2}} - \frac{\xi_w}{|\xi_w|} \right) + o(\varepsilon)
 \end{aligned} \tag{4.27}$$

Now using the last expression in (4.27) we can take the limit of  $I_1^{\Gamma_\varepsilon}(\xi)$  at  $\xi \rightarrow \xi_0$  ( $\xi_w \rightarrow 0, \xi_w < 0$ ):

$$\lim_{\xi \rightarrow \xi_0} I_1^{\Gamma_\varepsilon}(\xi) = \frac{\varphi_1(\xi_0 + \tilde{\mathbf{r}}^*)}{2} + o(\varepsilon). \tag{4.28}$$

We note here that the limit of  $I_1^{\Gamma_\varepsilon}(\xi)$  is equal to one-half the value of potential at some point close to  $\xi_0$  on the plane up to the first order of radius  $\varepsilon$ . This limit does not depend on  $\varepsilon$  and will not disappear if we take radius  $\varepsilon$  smaller and smaller. In the analysis of the previous integral a similar contribution was proportional to  $\varepsilon$  and was disappearing in the limit of small  $\varepsilon$ .

If we imitate the argument that led to (4.22, 4.23), we can write that

$$\begin{aligned}
 \lim_{\xi \rightarrow \xi_0} I(\xi) &= \lim_{\varepsilon \rightarrow 0} \left( \frac{\varphi_1(\xi_0 + \tilde{\mathbf{r}}^*)}{2} + o(\varepsilon) \right) + \lim_{\varepsilon \rightarrow 0} \frac{(-1)}{4\pi} \int_{\Gamma_\varepsilon} \varphi(r) \frac{\vec{v} \cdot \vec{n}}{|\mathbf{r} - \xi_0|^2} d\vec{S}_r \\
 &= \frac{\varphi_1(\xi_0)}{2} + \frac{(-1)}{4\pi} \int_{\Gamma} \varphi(r) \frac{\vec{v} \cdot \vec{n}}{|\mathbf{r} - \xi_0|^2} d\vec{S}_r
 \end{aligned} \tag{4.29}$$

Now after this analysis of the behavior of integrals in the vicinity of a point lying on the surface from (4.10a, 4.10b) we can easily obtain a particular expression for the potential at an arbitrary point on the surface:

$$\begin{aligned} \frac{1}{2} \varphi_I(\xi_0) = & \int_V f(\mathbf{r}) \frac{1}{4\pi |\mathbf{r} - \xi_0|} dV - \int_S \varphi_I(r) \bar{\nabla} \frac{1}{4\pi |\mathbf{r} - \xi_0|} d\bar{S}_r \\ & + \int_S \frac{1}{4\pi |\mathbf{r} - \xi_0|} \bar{\nabla} \varphi_I(r) d\bar{S}_r \end{aligned} \quad (4.30a)$$

$$\frac{1}{2} \varphi_{II}(\xi_0) = - \int_S \varphi_{II}(r) \bar{\nabla} \frac{1}{4\pi |\mathbf{r} - \xi_0|} d\bar{S}_r - \int_S \frac{1}{4\pi |\mathbf{r} - \xi_0|} \bar{\nabla} \varphi_{II}(r) d\bar{S}_r \quad (4.30b)$$

With addition of conditions (4.3) on the surface for functions  $\varphi_I$  and  $\varphi_{II}$  these integral equations form a closed system. Analytical solution of these equations is possible only in very specific cases. In order to be able to solve them in general situation we have to develop a numerical method of solution.

#### 4.1.3 Discretization of equations ( Implementation of BEM).

One of the possible approaches to this problem is to subdivide the surface into elements within which the functions  $\varphi$  and  $\frac{\partial \varphi}{\partial n}$  do not change much, use some approximation for those functions within these elements (the simplest of which is constant value within the element) and discretize equations (4.30) based on this description. As a result a linear system of equations will be obtained, solution of which will be the values of functions  $\varphi$  and  $\frac{\partial \varphi}{\partial n}$  on each boundary element. Finally, substitution of these boundary values of potentials and their normal derivatives into the equations (4.10), discretized in the same manner, will give us the value of potential at any point of space. The above comments explain why this numeric method got the name Boundary Element Method (BEM).

Let us describe this approach in some detail.

We subdivide surface into  $N$  elements and number them with an index  $i = 1, \dots, N$  (see Fig.4.4).

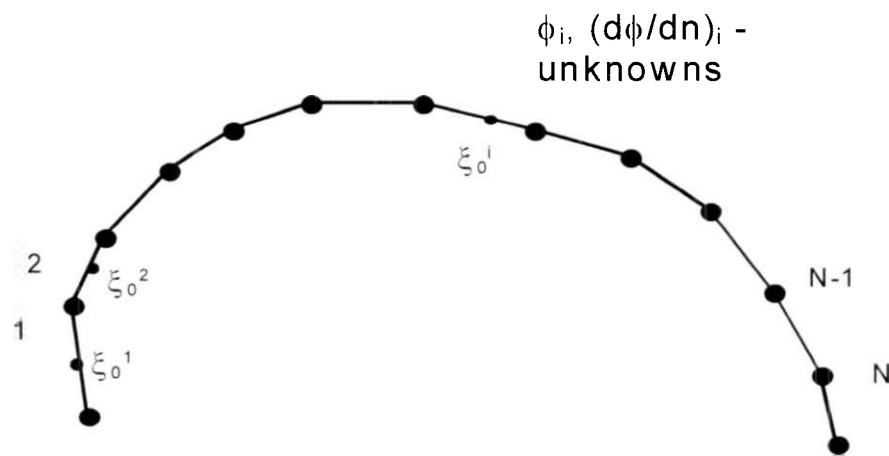


Figure 4.4. Representation of the boundary by finite elements.

At some point of each element we write two equations: one coming from the region I and the other coming from the region II in accordance with (4.30a)-(4.30b). This gives  $2N$  equations. We also have  $2N$  unknowns in this system of equations:  $N$  values of potential  $\varphi(\xi_0^i)$  and  $N$  values of normal derivative  $\frac{\partial \varphi}{\partial n}(\xi_0^i)$  on the surface  $\Gamma$ .

To keep the appearance of the formulas the same we will use notation  $\nabla_n$  instead of  $\frac{\partial}{\partial n}$  for the component of the gradient along the normal to the surface.

So, the system of equations (4.30a) and (4.30b) can be transformed to a linear system of equations as follows:

$$\frac{1}{2} \varphi_i(\xi_0^i) = \int_{V_i} f(\mathbf{r}) \frac{1}{4\pi |\mathbf{r} - \xi_0^i|} dV + \sum_j (-\varphi_j(\mathbf{r}_j) \int_{\Gamma_j} \nabla_n \frac{1}{4\pi |\mathbf{r} - \xi_0^i|} dS_r + (\nabla_n \varphi_j(\mathbf{r}_j)) \int_{\Gamma_j} \frac{1}{4\pi |\mathbf{r} - \xi_0^i|} dS_r) \quad (4.31a)$$

$$\frac{1}{2} \varphi_i(\xi_0^i) = \sum_j (-\varphi_j(\mathbf{r}_j) \int_{\Gamma_j} \nabla_n \frac{1}{4\pi |\mathbf{r} - \xi_0^i|} dS_r + \frac{-\varepsilon_1}{\varepsilon_2} (\nabla_n \varphi_j(\mathbf{r}_j)) \int_{\Gamma_j} \frac{1}{4\pi |\mathbf{r} - \xi_0^i|} dS_r) \quad (4.31b)$$

Note that in this system we substituted functions  $\varphi_{II}$  and  $\nabla_n \varphi_{II}$  from the region II by the corresponding functions from the region I based on boundary relations (4.3) and with the notion that the directions of the vector normal to the surface are opposite for regions I and II. After introducing the following notations

$$\begin{aligned} K_{ij} &= \int_{\Gamma_j} \nabla_n \frac{1}{4\pi |\mathbf{r} - \xi_0^i|} dS_r, \\ M_{ij} &= \int_{\Gamma_j} \frac{1}{4\pi |\mathbf{r} - \xi_0^i|} dS_r, \\ X_i &= \varphi_i(\xi_0^i), \quad Y_i = \nabla_n \varphi_i(\xi_0^i) \end{aligned} \quad (4.32'')$$

the above system of equations become:

$$\frac{1}{2} X_i = \int_{V_i} f(\mathbf{r}) \frac{1}{4\pi |\mathbf{r} - \xi_0^i|} dV + \sum_j (-K_{ij} X_j + M_{ij} Y_j) \quad (4.32a)$$

$$\frac{1}{2} X_i = \sum_j (-K_{ij} X_j + \frac{-\varepsilon_1}{\varepsilon_2} M_{ij} Y_j) \quad (4.32b)$$

Once we find a solution of this system of equations we can find the potential at any point of regions I and II using equations (4.8a), (4.8b) and the approximation employed in this method. For a point  $\xi$  of region I we have:

$$\varphi_I(\xi) = \int_{V_i} f(\mathbf{r}) \frac{1}{4\pi |\mathbf{r} - \xi|} dV + \sum_j (-X_j \int_{\Gamma_j} \nabla_n \frac{1}{4\pi |\mathbf{r} - \xi|} dS_r + Y_j \int_{\Gamma_j} \frac{1}{4\pi |\mathbf{r} - \xi|} dS_r) \quad (4.33a)$$

and for a point  $\xi$  of region II we have:

$$\varphi_{II}(\xi) = \sum_j (-X_j \int_{\Gamma_j} \nabla_n \frac{1}{4\pi |\mathbf{r} - \xi|} dS_r + Y_j \frac{-\varepsilon_1}{\varepsilon_2} \int_{\Gamma_j} \frac{1}{4\pi |\mathbf{r} - \xi|} dS_r) \quad (4.33b)$$

which is a quadrature that can be calculated by any standard method of numerical (sometimes, in symmetrical cases, analytical) integration.

## 4.2. Boundary element method applied to the Laplace and Poisson-Boltzmann equations.

We now consider a problem similar to that described in section 4.1. Again two regions (I and II) are separated by smooth surface  $\Gamma$  and region II is a uniform dielectric with dielectric constant  $\epsilon_2$ . In contrast to the previous case, region I is uniformly filled with dielectric constant  $\epsilon_1$  and the with ionic solution with dielectric constant  $\epsilon_1$  and Debye radius  $\lambda = 1/k$ . As before, the space charge  $q$  is located in the first region. The electric potential in both regions is to be found.

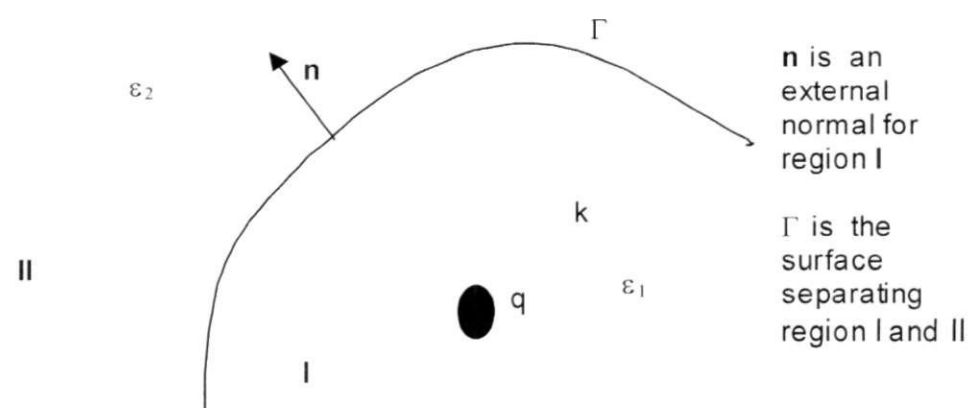


Figure 4.5. Geometry of the system. Ionic solution with Debye radius  $\lambda = 1/k$  is present in region I. The space charge  $q$  is located in the first region.

Since the idea of the method is treated in detail in section 4.1 and all main equations are analogous we will only point out the basic steps.

The problem is governed by the following equations:

$$\text{For region I. } -\nabla^2 \varphi_I + \kappa^2 \varphi_I = f(r) \quad \text{Poisson - Boltzmann equation} \quad (4.34)$$

$$\text{For region II. } -\nabla^2 \varphi_{II} = 0 \quad \text{Laplace equation} \quad (4.35)$$

Boundary conditions on the surface  $\Gamma$  are the same as in previous case (See (4.3a)-(4.3c)).

Equations for the Green function are:

$$\text{For region } I. \quad -\nabla^2 G_I + \kappa^2 G_I = \delta(\mathbf{r} - \xi) \quad (4.36)$$

$$\text{For region } II. \quad -\nabla^2 G_{II} = \delta(\mathbf{r} - \xi) \quad (4.37)$$

We see that in this problem the Green functions in the two regions are different.

The integral representation for potentials  $\varphi_I$  and  $\varphi_{II}$  (analogous to 4.8a-4.8b) now takes the form:

$$\varphi_I(\xi) = \int_{V_I} f(\mathbf{r}) G_I(\mathbf{r}, \xi) dV_r - \int_{\Gamma} \varphi_I(\mathbf{r}) \bar{\nabla}_r G_I(\mathbf{r}, \xi) \cdot d\bar{S}_r + \int_{\Gamma} G_I(\mathbf{r}, \xi) \bar{\nabla}_r \varphi_I(\mathbf{r}) \cdot d\bar{S}_r \quad (4.38a)$$

$$\varphi_{II}(\xi) = - \int_{\Gamma} \varphi_{II}(\mathbf{r}) \bar{\nabla}_r G_{II}(\mathbf{r}, \xi) \cdot d\bar{S}_r + \int_{\Gamma} G_{II}(\mathbf{r}, \xi) \bar{\nabla}_r \varphi_{II}(\mathbf{r}) \cdot d\bar{S}_r, \quad (4.38b)$$

With the simplest forms of Green functions

$$G_I(\mathbf{r}, \xi) = \frac{e^{-\kappa |\mathbf{r} - \xi|}}{4\pi |\mathbf{r} - \xi|} \quad (4.40)$$

$$G_{II}(\mathbf{r}, \xi) = \frac{1}{4\pi |\mathbf{r} - \xi|}$$

and in the limit of  $\xi \rightarrow \xi_0$ , where  $\xi_0$  is a point on the boundary  $\Gamma$ , the above equations become:

$$\begin{aligned} \varphi_I(\xi_0) &= \lim_{\xi \rightarrow \xi_0} \varphi_I(\xi) \\ &= \int_{V_I} f(\mathbf{r}) \frac{e^{-\kappa |\mathbf{r} - \xi_0|}}{4\pi |\mathbf{r} - \xi_0|} dV_r - \lim_{\xi \rightarrow \xi_0} \int_{\Gamma} \varphi_I(\mathbf{r}) \bar{\nabla}_r \frac{e^{-\kappa |\mathbf{r} - \xi_0|}}{4\pi |\mathbf{r} - \xi_0|} \cdot d\bar{S}_r + \\ &\quad \lim_{\xi \rightarrow \xi_0} \int_{\Gamma} \frac{e^{-\kappa |\mathbf{r} - \xi_0|}}{4\pi |\mathbf{r} - \xi_0|} \bar{\nabla}_r \varphi_I(\mathbf{r}) \cdot d\bar{S}_r \end{aligned} \quad (4.41a)$$

$$\begin{aligned} \varphi_{II}(\xi_0) &= \lim_{\xi \rightarrow \xi_0} \varphi_{II}(\xi) \\ &= - \lim_{\xi \rightarrow \xi_0} \int_{\Gamma_\varepsilon} \varphi_{II}(\mathbf{r}) \bar{\nabla}_r \frac{1}{4\pi |\mathbf{r} - \xi|} \cdot d\bar{S}_r + \lim_{\xi \rightarrow \xi_0} \int_{\Gamma_\varepsilon} \frac{1}{4\pi |\mathbf{r} - \xi|} \bar{\nabla} \varphi_{II}(\mathbf{r}) \cdot d\bar{S}_r \end{aligned} \quad (4.41b)$$

These equations are analogous to (4.10a)-(4.10b).

Both limits in the second equation were investigated in great detail in the previous section and it was proven that these limits exist and their values were obtained. Now we need to analyze the behavior of integrals of equation (4.41a) in the vicinity of a fixed point  $\xi_0$  on the boundary.

Let us first consider the second integral in (4.41a). Following the same logic as in the case of integral  $I_2$  (see (4.12)) we will come up with the function  $\tilde{g}^{\Gamma_\varepsilon}(\xi)$ :

$$\tilde{g}^{\Gamma_\varepsilon}(\xi) = \frac{1}{4\pi} \int_{\Gamma_\varepsilon} \frac{\psi(\xi_0 + \bar{\mathbf{r}}) e^{-k|\mathbf{r}-\xi|} dndv}{|\bar{\mathbf{r}} - \xi|} + o(\varepsilon) \quad (4.42)$$

which is similar to function  $g^{\Gamma_\varepsilon}(\xi)$  defined in (4.17).

It is easy to show that

$$\lim_{\xi \rightarrow \xi_0} \tilde{g}^{\Gamma_\varepsilon}(\xi) = \lim_{\xi \rightarrow \xi_0} g^{\Gamma_\varepsilon}(\xi) = \frac{\psi(\xi_0 + \bar{\mathbf{r}}^\varepsilon)}{2} \varepsilon + o(\varepsilon) \quad (4.43)$$

and hence this limit vanishes for  $\varepsilon \rightarrow 0$ . From the proof analogous to (4.22) it follows that

$$\begin{aligned} \lim_{\xi \rightarrow \xi_0} \int_{\Gamma_\varepsilon} \frac{e^{-k|\mathbf{r}-\xi|}}{4\pi |\mathbf{r} - \xi|} \bar{\nabla} \varphi_I(\mathbf{r}) \cdot d\bar{S}_r &= \lim_{\varepsilon \rightarrow 0} \int_{\Gamma_\varepsilon} \frac{e^{-k|\mathbf{r}-\xi_0|}}{4\pi |\mathbf{r} - \xi_0|} \bar{\nabla} \varphi_I(\mathbf{r}) \cdot d\bar{S}_r \\ &= \lim_{\varepsilon \rightarrow 0} \int_{\Gamma_\varepsilon} G_I(\mathbf{r}, \xi_0) \bar{\nabla} \varphi_I(\mathbf{r}) \cdot d\bar{S}_r = \int G_I(\mathbf{r}, \xi_0) \bar{\nabla} \varphi_I(\mathbf{r}) \cdot (\mathbf{r}) d\bar{S}_r \end{aligned} \quad (4.44)$$

and the limit under consideration is again a convergent improper surface integral.

Without detailed analysis of the first integral in (4.41a) we will write the final answer

$$\begin{aligned}
\lim_{\varepsilon \rightarrow 0} \int_{\Gamma_\varepsilon} \varphi_I(\mathbf{r}) \bar{\nabla}_r \frac{e^{-k|\mathbf{r}-\xi_0|}}{4\pi|\mathbf{r}-\xi_0|} \cdot d\mathbf{S}_r &= -\frac{\varphi_I(\xi_0)}{2} + \lim_{\varepsilon \rightarrow 0} \int_{\Gamma_\varepsilon} \varphi_I(\mathbf{r}) \bar{\nabla}_r \frac{e^{-k|\mathbf{r}-\xi_0|}}{4\pi|\mathbf{r}-\xi_0|} \cdot d\bar{\mathbf{S}}_r \\
&= -\frac{\varphi_I(\xi_0)}{2} + \lim_{\varepsilon \rightarrow 0} \int_{\Gamma_\varepsilon} \varphi_I(\mathbf{r}) \bar{\nabla}_r G_I(\mathbf{r}, \xi_0) \cdot d\bar{\mathbf{S}}_r \\
&= -\frac{\varphi_I(\xi_0)}{2} + \int \varphi_I(\mathbf{r}) \bar{\nabla}_r G_I(\mathbf{r}, \xi_0) \cdot d\bar{\mathbf{S}}_r
\end{aligned} \tag{4.45}$$

The similarity of this result to the result (4.29) obtained in the previous section can be understood by the notion that the exponent in the integral can be approximated by 1 on the plane tangent to the surface  $\Gamma_\varepsilon$ .

Finally, we use (4.44) and (4.45) in (4.41a) and (4.41b) to generate the following equations for the potential and its normal derivative on the boundary:

$$\begin{aligned}
\frac{1}{2} \varphi_I(\xi_0) &= \int_V f(\mathbf{r}) \frac{e^{-k|\mathbf{r}-\xi_0|}}{4\pi|\mathbf{r}-\xi_0|} dV_r - \int_{\Gamma} \varphi_I(\mathbf{r}) \bar{\nabla}_r \frac{e^{-k|\mathbf{r}-\xi_0|}}{4\pi|\mathbf{r}-\xi_0|} \cdot d\mathbf{S}_r + \\
&\quad \int_{\Gamma} \frac{e^{-k|\mathbf{r}-\xi_0|}}{4\pi|\mathbf{r}-\xi_0|} \bar{\nabla}_r \varphi_I(\mathbf{r}) \cdot d\bar{\mathbf{S}}_r
\end{aligned} \tag{4.42a}$$

$$\frac{1}{2} \varphi_{II}(\xi_0) = - \int_{\Gamma} \varphi_{II}(\mathbf{r}) \bar{\nabla}_r \frac{1}{4\pi|\mathbf{r}-\xi_0|} \cdot d\bar{\mathbf{S}}_r + \int_{\Gamma} \frac{1}{4\pi|\mathbf{r}-\xi_0|} \bar{\nabla}_r \varphi_{II}(\mathbf{r}) \cdot d\bar{\mathbf{S}}_r \tag{4.42b}$$

These equations are analogous to (4.30a) and (4.30b)).

As in section 4.1, we can numerically solve this system and then calculate the potential at any point of region I and II by using BEM. We discretize equations (4.42a)-(4.42b) and come up with the linear system analogous to (4.32a)-(4.32b), coefficients of which (see (4.32')) are to be calculated in accordance with integrals appearing in equations (4.42a)-(4.42b). Then we solve this linear system and substitute obtained values of potential and its normal derivative on the boundary elements into the discretized expressions (4.38a) - (4.38b). As a result we have equations analogous to (4.33a)-(4.33b) and can calculate potential at any point of regions I and II.

## CHAPTER 5. CHANNEL MODELS – APPLICATION OF THE BEM

### 5.1. Point charge near membrane with finite cylindrical channel in the absence of ionic solution in the surrounding space ( $k=0$ )

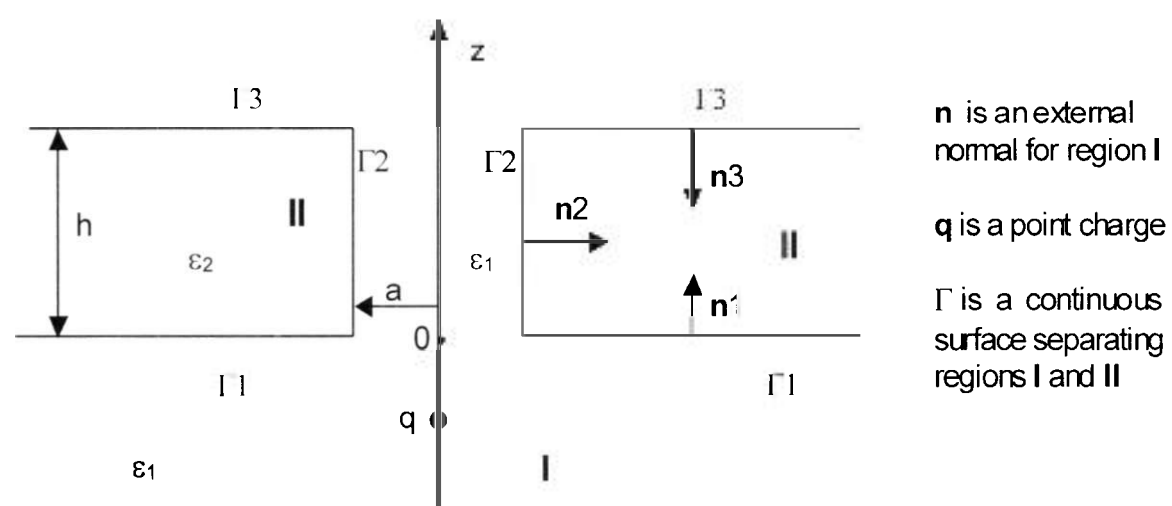


Figure 5.1 Cross-section of infinite membrane (region II) with a finite cylindrical channel. The arrangement is rotationally symmetric about the z-axis.

Fig.5.1 shows a simplified model of the membrane with a cylindrical channel of finite length. There is no ionic solution in this case. The dielectric constants of membrane and channel are  $\epsilon_2$  and  $\epsilon_1$  respectively. The surrounding space also has the same dielectric constant as the channel,  $\epsilon_1$ . The whole arrangement has cylindrical symmetry about the z-axis. The width of the membrane is  $h$  and the radius of the channel is  $a$ . A point charge  $q$  is placed on the z-axis at some distance from the channel. We wish to calculate the electric potential in all the space. The potential within the channel will be of special interest to us. The surface  $\Gamma$  between the regions I and II is piecewise smooth and we can apply the BEM for Laplace and Poisson equations, as described in section 4.1.

Let us write the basic equations for the potential and Green function (see section 4.1):

$$\text{For region } I. \quad -\nabla^2 \varphi_I = f(r), \quad -\nabla_r^2 G_I(r, \xi) = \delta(r - \xi) \quad (5.1)$$

$$\text{For region } II. \quad -\nabla^2 \varphi_{II} = 0, \quad -\nabla_r^2 G_{II}(r, \xi) = \delta(r - \xi), \quad (5.2)$$

$$G_I(r, \xi) = G_{II}(r, \xi) = \frac{1}{4\pi |r - \xi|}. \quad (5.3)$$

Given the cylindrical symmetry of the problem we choose cylindrical coordinates. Any point in space will be represented as  $\mathbf{r}=(z, \rho)$

Let us subdivide the membrane surface into N+P+S symmetrical rings of some width, which we can vary for the purpose of calculation (N, P, S correspond to the number of rings on the surfaces  $\Gamma_1$ ,  $\Gamma_2$ ,  $\Gamma_3$ ) (see Fig.5.2). The potential and its normal derivative are assumed to be constant within each ring.

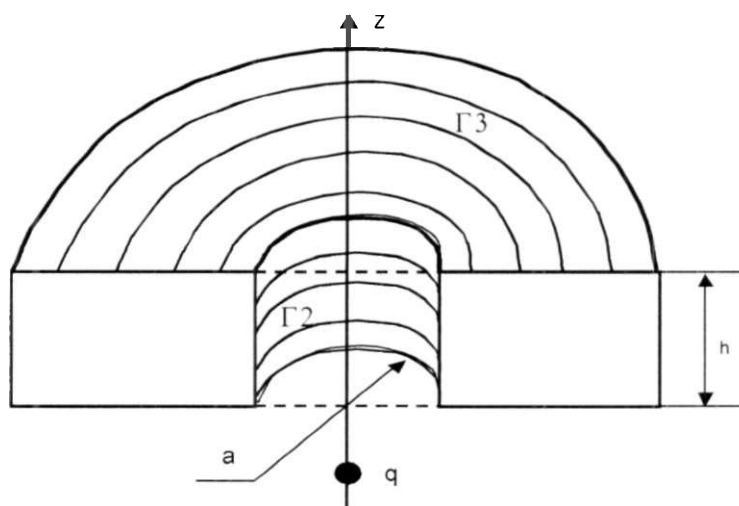


Figure 5.2. Representation of the surface by the symmetrical rings. A cross-section has been taken through the membrane in a plane containing the z-axes. A portion of the membrane lying behind this section is seen in perspective from above.  $\Gamma_1$ , the bottom surface of the membrane, is not shown.

The first step in solving this problem is to obtain the values of  $\varphi_k$  and  $\left(\frac{\partial \varphi}{\partial n}\right)_k$  on each ring, i.e. to solve the linear system (4.32a)-(4.32b). At first we have to obtain coefficients  $K_{ij}$  and  $M_{ij}$  of this system. To do this we write explicitly equation (4.31a) for

some point  $\xi'$  belonging to the  $\ell^{\text{th}}$  ring (subscript "0" in symbol  $\xi$  is omitted here):

$$\begin{aligned}
 -\frac{4\pi q}{\epsilon_1 |\mathbf{r}_q - \xi'|} = & -\frac{1}{2}\varphi_{I_0}(\xi') - \sum_{k=1}^K \varphi_{I_k} \int_{\Gamma_k} \frac{\partial}{\partial z} G(\mathbf{r}, \xi') dS_1 - \sum_{k=N+1}^P \varphi_{I_k} \int_{\Gamma_k} \frac{\partial}{\partial \rho} G(\mathbf{r}, \xi') dS_2 + \\
 & \sum_{k=p-1}^S \varphi_k \int_{\Gamma_k} \frac{\partial}{\partial z} G(\mathbf{r}, \xi') dS_3 + \sum_{k=1}^N \left( \frac{\partial \varphi_k}{\partial z} \right) \int_{\Gamma_k} G(\mathbf{r}, \xi') dS_1 + \\
 & \sum_{k=N+1}^P \left( \frac{\partial \varphi_k}{\partial z} \right) \int_{\Gamma_k} G(\mathbf{r}, \xi') dS_2 - \sum_{k=p-1}^S \left( \frac{\partial \varphi_k}{\partial z} \right) \int_{\Gamma_k} G(\mathbf{r}, \xi') dS_3
 \end{aligned} \quad (5.4)$$

Fig. 5.3 shows the example of location of points  $\xi$  and  $r$  on the surface.

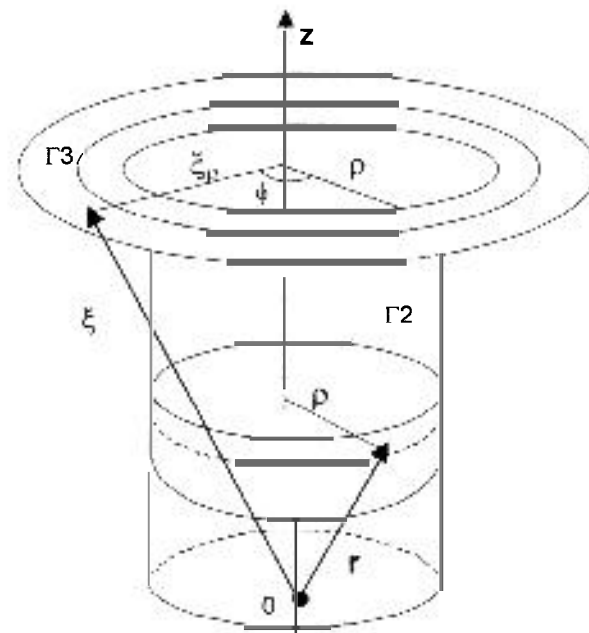


**Figure 5.3.** An example of local position of points  $\xi$  and  $r$  on the surface: the figure shows the case of  $r \in \Gamma_2, \xi \in \Gamma_3$ . Other configurations are possible.

With the following relations (see Fig. 5.3 for definition of angle  $\phi$ )

$$\frac{\partial}{\partial z} G(\mathbf{r}, \xi) = \frac{(-1)(z - \xi_z)}{4\pi |\mathbf{r} - \xi|^3} = \frac{(-1)(z - \xi_z)}{4\pi ((z - \xi_z)^2 + \rho^2 + \xi^2_\rho - 2\rho\xi_\rho \cos\phi)^{3/2}}$$

$$\frac{\partial}{\partial \rho} G(\mathbf{r}, \xi) = \frac{(-1)(\rho - \xi_\rho \cos\phi)}{4\pi ((z - \xi_z)^2 + \rho^2 + \xi^2_\rho - 2\rho\xi_\rho \cos\phi)^{3/2}}$$

$$\mathbf{r} \in \Gamma_1, \quad \mathbf{r} = (0, \rho) \tag{5.5}$$

$$\mathbf{r} \in \Gamma_2, \quad \mathbf{r} = (a, z)$$

$$\mathbf{r} \in \Gamma_3, \quad \mathbf{r} = (h, \rho)$$

integrals in the equation (46), i.e. coefficients K and M that we are looking for, take the form:

$$\mathbf{r} \in \Gamma_1, \quad \mathbf{r} = (0, \rho)$$

$$\int_{\Gamma_1} \frac{\partial}{\partial z} G(\mathbf{r}, \xi) dS_1 = \frac{(-1)}{4\pi} \int_0^{2\pi} d\phi \int_{\rho_c}^{\rho_s} \frac{\rho(h - \xi_z) d\rho}{((\xi_z)^2 + \rho^2 + \xi^2_\rho - 2\rho\xi_\rho \cos\phi)^{3/2}}$$

$$\mathbf{r} \in \Gamma_2, \quad \mathbf{r} = (a, z)$$

$$\int_{\Gamma_2} \frac{\partial}{\partial \rho} G(\mathbf{r}, \xi) dS_2 = \frac{(-1)}{4\pi} \int_0^{2\pi} d\phi \int_{z_1}^{z_2} \frac{(a - \xi_\rho \cos\phi) dz}{((z - \xi_z)^2 + a^2 + \xi^2_\rho - 2a\xi_\rho \cos\phi)^{3/2}}$$

$$\mathbf{r} \in \Gamma_3, \quad \mathbf{r} = (h, \rho)$$

$$\int_{\Gamma_3} \frac{\partial}{\partial z} G(\mathbf{r}, \xi) dS_3 = \frac{(-1)}{4\pi} \int_0^{2\pi} d\phi \int_{\rho_c}^{\rho_s} \frac{\rho(h - \xi_z) d\rho}{((h - \xi_z)^2 + \rho^2 + \xi^2_\rho - 2\rho\xi_\rho \cos\phi)^{3/2}}$$

$$\mathbf{r} \in \Gamma 1, \quad \mathbf{r} = (0, \rho)$$

$$\int_{\Gamma 1_k} G(\mathbf{r}, \xi) dS_1 = \frac{(-1)^{2k}}{4\pi} \int_0^{2\pi} d\phi \int_{\rho_k}^{\rho_{k+1}} \frac{\rho d\rho}{((\xi_z)^2 + \rho^2 + \xi_\rho^2 - 2\rho\xi_\rho \cos\phi)^2}$$

$$\mathbf{r} \in \Gamma 2, \quad \mathbf{r} = (a, z)$$

$$\int_{\Gamma 2_k} G(\mathbf{r}, \xi) dS_2 = \frac{(-1)^{2k}}{4\pi} \int_0^{2\pi} d\phi \int_{z_k}^{z_{k+1}} \frac{a dz}{((z - \xi_z)^2 + a^2 + \xi_\rho^2 - 2a\xi_\rho \cos\phi)^2} \quad (5.6)$$

$$\mathbf{r} \in \Gamma 3, \quad \mathbf{r} = (h, \rho)$$

$$\int_{\Gamma 3_k} G(\mathbf{r}, \xi) dS_3 = \frac{(-1)^{2k}}{4\pi} \int_0^{2\pi} d\phi \int_{\rho_k}^{\rho_{k+1}} \frac{\rho d\rho}{((h - \xi_z)^2 + \rho^2 + \xi_\rho^2 - 2\rho\xi_\rho \cos\phi)^2}$$

Calculating the value of these integrals for each ring and for each fixed point ( $\ell=1, 2, \dots, N+P+S$ ) we fill the matrix of linear system (4.32a)-(4.32b) and solve the system. i.e. get  $\varphi_k$  and  $\left(\frac{\partial\varphi}{\partial n}\right)_k$  on the  $k$ th ring ( $k=1, 2, \dots, N+P+S$ ). We see that all integrals with respect to  $\phi$  are expressed through elliptic integrals. The second integrations with respect to  $\rho$  or  $z$  have to be done numerically.

## 5.2. Point charge near membrane with finite cylindrical channel in the presence of ionic solution in the surrounding space ( $k \neq 0$ )

We now consider a system whose geometry is the same as in previous case (see Fig.5.1). The difference from the first model is that region I surrounding the membrane is filled with an ionic solution with dielectric constant  $\epsilon_1$  and Debye radius  $\lambda = 1/k$  ( $k \neq 0$ ). To find the potential in all space we will apply BEM for Laplace and Poisson-Boltzmann equations, as described in section 4.2.

The basic equations for the potentials and Green functions are (see Section 4.2):

$$\text{For region } I. \quad -\nabla^2 \varphi_I + k^2 \varphi_I = \frac{4\pi q}{\epsilon_1 |r - r_q|}, \quad -\nabla^2 G_I + k^2 G_I = \delta(\mathbf{r} - \xi) \quad (5.7)$$

$$\text{For region II. } -\nabla^2 \varphi_{II} = 0, \quad -\nabla^2 G_{II}(\mathbf{r}, \xi) = \delta(\mathbf{r} - \xi), \quad (5.8)$$

$$G_I(\mathbf{r}, \xi) = \frac{e^{-k|\mathbf{r}-\xi|}}{4\pi|\mathbf{r}-\xi|}, \quad G_{II}(\mathbf{r}, \xi) = \frac{1}{4\pi|\mathbf{r}-\xi|}, \quad (5.9)$$

The general procedure of solving this problem is the same as in the case with  $k=0$ . Therefore we will write only equations analogous to (4.31a) and (4.31b) for  $\varphi_I$  and  $\varphi_{II}$  at some point belonging to the  $\ell$ th ring:

$$\begin{aligned} & -\frac{4\pi q}{\varepsilon_1 |\mathbf{r}_\ell - \xi'|} = \\ & -\frac{1}{2}\varphi_I(\xi') - \sum_{k=1}^N \varphi_k \int_{\Gamma_{1k}} \frac{\partial}{\partial z} G_I(\mathbf{r}, \xi') dS_1 - \sum_{k=N+1}^p \varphi_k \int_{\Gamma_{2k}} \frac{\partial}{\partial \rho} G_I(\mathbf{r}, \xi') dS_2 + \\ & \sum_{k=p+1}^S \varphi_k \int_{\Gamma_{3k}} \frac{\partial}{\partial z} G_I(\mathbf{r}, \xi') dS_3 + \sum_{k=1}^N \left( \frac{\partial \varphi_I}{\partial z} \right)_{k \Gamma_{1k}} \int G_I(\mathbf{r}, \xi') dS_1 + \end{aligned} \quad (5.10a)$$

$$\sum_{k=N+1}^p \left( \frac{\partial \varphi_I}{\partial z} \right)_{k \Gamma_{2k}} \int G_I(\mathbf{r}, \xi') dS_2 - \sum_{k=p+1}^S \left( \frac{\partial \varphi_I}{\partial z} \right)_{k \Gamma_{3k}} \int G_I(\mathbf{r}, \xi') dS_3$$

$$\begin{aligned} 0 = & -\frac{1}{2}\varphi_{II}(\xi') - \sum_{k=1}^N \varphi_k \int_{\Gamma_{1k}} \frac{\partial}{\partial z} G_{II}(\mathbf{r}, \xi') dS_1 - \sum_{k=N+1}^p \varphi_k \int_{\Gamma_{2k}} \frac{\partial}{\partial \rho} G_{II}(\mathbf{r}, \xi') dS_2 + \\ & \sum_{k=p+1}^S \varphi_k \int_{\Gamma_{3k}} \frac{\partial}{\partial z} G_{II}(\mathbf{r}, \xi') dS_3 + \sum_{k=1}^N \left( \frac{\partial \varphi_{II}}{\partial z} \right)_{k \Gamma_{1k}} \int G_{II}(\mathbf{r}, \xi') dS_1 + \end{aligned} \quad (5.10b)$$

$$\sum_{k=N+1}^p \left( \frac{\partial \varphi_{II}}{\partial z} \right)_{k \Gamma_{2k}} \int G_{II}(\mathbf{r}, \xi') dS_2 - \sum_{k=p+1}^S \left( \frac{\partial \varphi_{II}}{\partial z} \right)_{k \Gamma_{3k}} \int G_{II}(\mathbf{r}, \xi') dS_3$$

To illustrate the type of integrals arrived at in the first equation we will write the explicit expression for one of them:

$\mathbf{r} \in \Gamma_2$ ,  $\mathbf{r} = (a, z)$

$$\int_{\Gamma_2} \frac{\partial}{\partial \rho} G_l(\mathbf{r}, \xi) dS_2 = \frac{(-1)^{2\pi}}{4\pi} \int_0^{2\pi} d\phi \int_{z_1}^{z_2} \frac{e^{i((z-z_1)^2 + a^2 + \xi^2 - 2a\xi \cos \phi)} (a - \xi \cos \phi) a dz}{((z - \xi \cos \phi)^2 + a^2 + \xi^2 - 2a\xi \cos \phi)^{3/2}} +$$

$$\frac{(-1)^{2\pi}}{4\pi} \int_0^{2\pi} d\phi \int_{z_1}^{z_2} e^{i((z-z_1)^2 + a^2 + \xi^2 - 2a\xi \cos \phi)} \frac{(a - \xi \cos \phi) a k \sqrt{(z - \xi \cos \phi)^2 + a^2 + \xi^2 - 2a\xi \cos \phi} dz}{((z - \xi \cos \phi)^2 + a^2 + \xi^2 - 2a\xi \cos \phi)^{3/2}}$$

(5.11)

One can see that integration with respect to both variables has to be done numerically, unlike the previous case. Integrals in the second equation (5.10b) are similar to integrals (5.6).

### 5.3. Charged sphere near membrane with finite cylindrical channel in the presence of ionic solution in the surrounding space ( $k \neq 0$ )

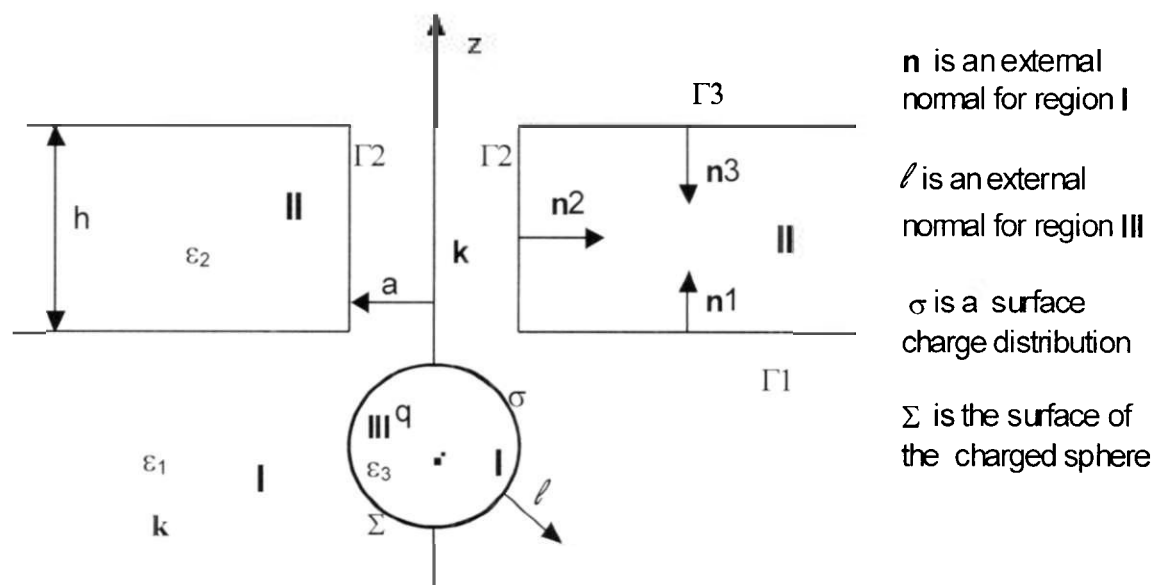


Figure 5.4. Charged sphere (with surface charge distribution  $\sigma$ ) near membrane with finite cylindrical channel in the presence of ionic solution in the channel and surrounding space ( $k \neq 0$ )

A sphere with some cylindrically symmetrical surface charge distribution and dielectric constant  $\epsilon_3$  is placed near the channel, as in Fig. 5.2. There are three different regions in this problem and none of them contains space charge. The external surface charge of the sphere is taken into account by the boundary condition expressed below in (5.18).

This problem is governed by the following equations for potentials and Green functions :

$$\text{For region I.} \quad -\nabla^2 \varphi_I + k^2 \varphi_I = 0, \quad -\nabla^2 G_I + k^2 G_I = \delta(\mathbf{r} - \xi) \quad (5.12)$$

$$\text{For region II.} \quad -\nabla^2 \varphi_{II} = 0, \quad -\nabla^2 G_{II}(\mathbf{r}, \xi) = \delta(\mathbf{r} - \xi), \quad (5.13)$$

$$\text{For region III.} \quad -\nabla^2 \varphi_{III} = 0, \quad -\nabla^2 G_{III}(\mathbf{r}, \xi) = \delta(\mathbf{r} - \xi), \quad (5.14)$$

$$G_I(\mathbf{r}, \xi) = \frac{e^{-k|\mathbf{r}-\xi|}}{4\pi|\mathbf{r}-\xi|}, \quad G_{II}(\mathbf{r}, \xi) = G_{III}(\mathbf{r}, \xi) \frac{1}{4\pi|\mathbf{r}-\xi|}. \quad (5.15)$$

The boundary conditions on the surface  $\Gamma$  and  $\Sigma$  are:

$$\varphi_I|_{\Gamma} = \varphi_{II}|_{\Gamma}, \quad \epsilon (\mathbf{n} \cdot \nabla) \varphi_I|_{\Gamma} = \epsilon_2 (\mathbf{n} \cdot \nabla) \varphi_{II}|_{\Gamma} \quad (5.16)$$

$$\varphi_I|_{\Sigma} = \varphi_{III}|_{\Sigma}, \quad \epsilon_3 (\mathbf{l} \cdot \nabla) \varphi_{III}|_{\Sigma} - \epsilon_1 (\mathbf{l} \cdot \nabla) \varphi_I|_{\Sigma} = 4\pi\sigma$$

where  $(\mathbf{n} \cdot \nabla)$  and  $(\mathbf{l} \cdot \nabla)$  are the derivatives along the normals to the surfaces  $\Gamma$  and  $\Sigma$  respectively.

Equations for potential and its normal derivative on the boundaries take the form:

$$\frac{1}{2} \varphi_I(\xi_0) = - \int_{\Gamma \cup \Sigma} \varphi_I(\mathbf{r}) \nabla G_I(\mathbf{r}, \xi_0) \cdot d\vec{S}_r + \int_{\Gamma \cup \Sigma} G_I(\mathbf{r}, \xi_0) \nabla \varphi_I(\mathbf{r}) \cdot d\vec{S}_r \quad (5.17a)$$

$$\frac{1}{2} \varphi_{II}(\xi_0) = - \int_{\Gamma} \varphi_{II}(\mathbf{r}) \nabla G(\mathbf{r}, \xi_0) \cdot d\vec{S}_r + \int_{\Gamma} \nabla G(\mathbf{r}, \xi_0) \varphi_{II}(\mathbf{r}) \cdot \vec{S}_r \quad (5.17b)$$

$$\frac{1}{2} \varphi_{III}(\xi_0) = - \int_{\Sigma} \varphi_{III}(\mathbf{r}) \nabla G(\mathbf{r}, \xi_0) \cdot d\vec{S}_r + \int_{\Sigma} \nabla G(\mathbf{r}, \xi_0) \varphi_{III}(\mathbf{r}) \cdot \vec{S}_r \quad (5.17c)$$

With boundary condition (5.16) from (5.17a, 5.17b, 5.17c) we obtain pairs of equations for each point of the two surfaces,  $\Gamma$  and  $\Sigma$ :

For  $\forall \xi_0 \in \Gamma$

$$\begin{aligned} \frac{1}{2} \varphi_I(\xi_0^\Gamma) &= - \int_{\Gamma+\Sigma} \varphi_I(\mathbf{r}) \bar{\nabla} G_I(\mathbf{r}, \xi_0^\Gamma) \cdot d\bar{S}_{rI} + \int_{\Gamma+\Sigma} G_I(\mathbf{r}, \xi_0^\Gamma) \bar{\nabla} \varphi_I(\mathbf{r}) \cdot d\bar{S}_{rI} \\ \frac{1}{2} \varphi_I(\xi_0^\Gamma) &= - \int_{\Gamma} \varphi_I(\mathbf{r}) \nabla G(\mathbf{r}, \xi_0^\Gamma) \cdot dS_{rII} + \frac{\varepsilon_1}{\varepsilon_2} \int_{\Gamma} G_I(\mathbf{r}, \xi_0^\Gamma) \nabla \varphi_I(\mathbf{r}) \cdot dS_{rII} \end{aligned} \quad (5.18)$$

For  $\forall \xi_0 \in \Sigma$

$$\begin{aligned} \frac{1}{2} \varphi_I(\xi_0^\Sigma) &= - \int_{\Sigma} \varphi_I(\mathbf{r}) \bar{\nabla} G_I(\mathbf{r}, \xi_0^\Sigma) \cdot d\bar{S}_{rI} + \int_{\Sigma} G_I(\mathbf{r}, \xi_0^\Sigma) \bar{\nabla} \varphi_I(\mathbf{r}) \cdot d\bar{S}_{rI} \\ \frac{1}{2} \varphi_I(\xi_0^\Sigma) &= - \int_{\Sigma} \varphi_I(\mathbf{r}) \bar{\nabla} G(\mathbf{r}, \xi_0^\Sigma) \cdot d\bar{S}_{rIII} + \frac{1}{\varepsilon_2} \int_{\Sigma} G(\mathbf{r}, \xi_0^\Sigma) (4\pi\sigma(\mathbf{r}) + \varepsilon_1(\mathbf{1} \cdot \bar{\nabla})\varphi_I(\mathbf{r})) dS_r \end{aligned}$$

After dividing the surface  $\Gamma$  into  $L$  cylindrical rings and spherical surface  $\Sigma$  into  $P$  spherical rings symmetrical relative to the  $z$  axis, and treating the values of potential and its normal derivative as constant on these rings, a consistent linear system of  $2(L+P)$  equations for  $2(L+P)$  unknowns can be written in a way similar to equations (5.10a)-(5.10b).

Notation  $\bar{S}_I, \bar{S}_{II}, \bar{S}_{III}$  means that an external normal to the appropriate region is taken. One can prove that this linear system has a unique solution.

The inhomogeneous part of this linear system contains terms related to the surface charge of the sphere. In the case of uniform charge distribution the integral in the last equation of (5.18),  $\frac{1}{\varepsilon_2} \int_{\Sigma} G(\mathbf{r}, \xi_0^\Sigma) 4\pi\sigma(\mathbf{r}) dS_r = \frac{4\pi\sigma R}{\varepsilon_2}$ , and is independent of  $\xi_0^\Sigma$ . For some arbitrary charge distribution, the integral  $\int_{\Sigma} G(\mathbf{r}, \xi_0^\Sigma) 4\pi\sigma(\mathbf{r}) dS_r$  depends on point  $\xi_0^\Sigma$  and is to be calculated for each spherical ring.

## CHAPTER 6. TESTING THE PROGRAM

In order to be able to check the results obtained by numerical methods for the problem with a finite channel we would like to have analytical solutions for some limiting cases. This is also important for understanding the physical meaning of the finite channel solutions. Such limiting cases are the infinite cylindrical channel and the infinite membrane without the channel. Solution of the latter problem for the case  $k=0$  can be found in [Grechko, 1984]; for the case when  $k \neq 0$  see Appendix A.

Both cases have been used for testing the numerical solution. Since the problem of interest is the finite channel, the limiting case of the infinite channel is most important. We give the analytical solution of this problem, analyze the physical properties of the solution and compare them with the physical properties of the finite channel solution.

### 6.1. Infinite Cylindrical Hole.

#### 6.1.1. Formulation and solution of the problem

Let us consider the following system. A cylindrical hole of radius  $R$  and infinite length (see Fig.6.1) is filled with ionic solution with dielectric constant  $\epsilon_1$  and Debye radius  $\lambda = 1/k$ . The surrounding space is filled with dielectric that has dielectric constant  $\epsilon_2$ . A positive point electric charge  $q$  is placed on the axis of symmetry at the origin of the coordinate system. The electric potential is to be found.

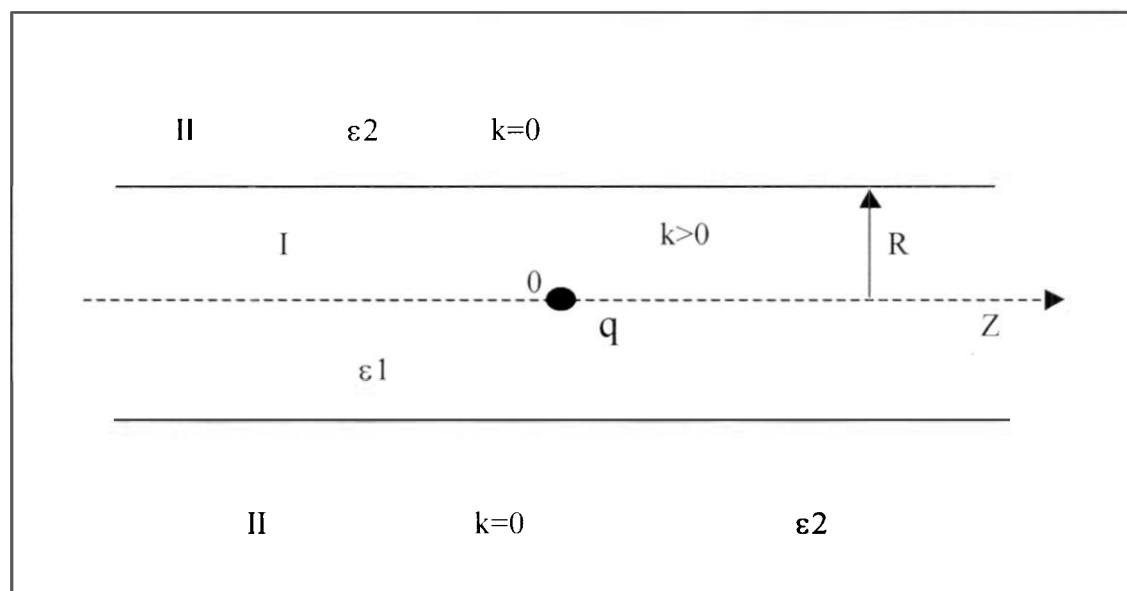


Figure 6.1. A cylindrical hole of radius  $R$  and infinite length is filled with ionic solution with dielectric constant  $\epsilon_1$  and Debye radius  $\lambda=1/k$ . The principal axes of symmetry of the hole coincide with the  $z$  axes. The surrounding space is filled with dielectric that has dielectric constant  $\epsilon_2$ . A positive point charge  $q$  is placed on the axis of symmetry at the origin of the coordinate system

The electric potential  $\varphi_{II}$  in region II is governed by the Laplace equation (5.8), and the potential  $\varphi_I$  in region I satisfies the Poisson equation (5.7). These equations are subject to the following boundary conditions:

$$\begin{aligned} \varphi_I(z, R) &= \varphi_{II}(z, R) \\ \epsilon_1 \frac{\partial \varphi_I}{\partial \rho} \Big|_{\rho=R} &= \epsilon_2 \frac{\partial \varphi_{II}}{\partial \rho} \Big|_{\rho=R} \end{aligned} \quad (6.3)$$

where  $R$  is the radius of the channel. An additional physically obvious condition is that both potentials,  $\varphi_I$  and  $\varphi_{II}$ , vanish at infinity.

The solution of the analogous problem with  $k=0$  can be found in [Smyth, 1968]. The solution for the case when  $k \neq 0$  is given in Appendix B.

### 6.1.2. Results and analysis

We would like to point out two important features of the potential inside the infinite cylinder: (a) the change of sign of polarized charges on the surface of the cylinder in the presence of ionic solution inside the hole and (b) an essential dependence of the

potential on the ratio of Debye length  $\lambda$  to channel radius  $R$ .

In Fig. 6.2 the normal derivative of the potential at the cylindrical surface vs.  $z$  is presented. The two curves correspond to different dielectric constants. The radius of the channel is equal to Debye length ( $R = \lambda = 7 \text{ \AA}$ )

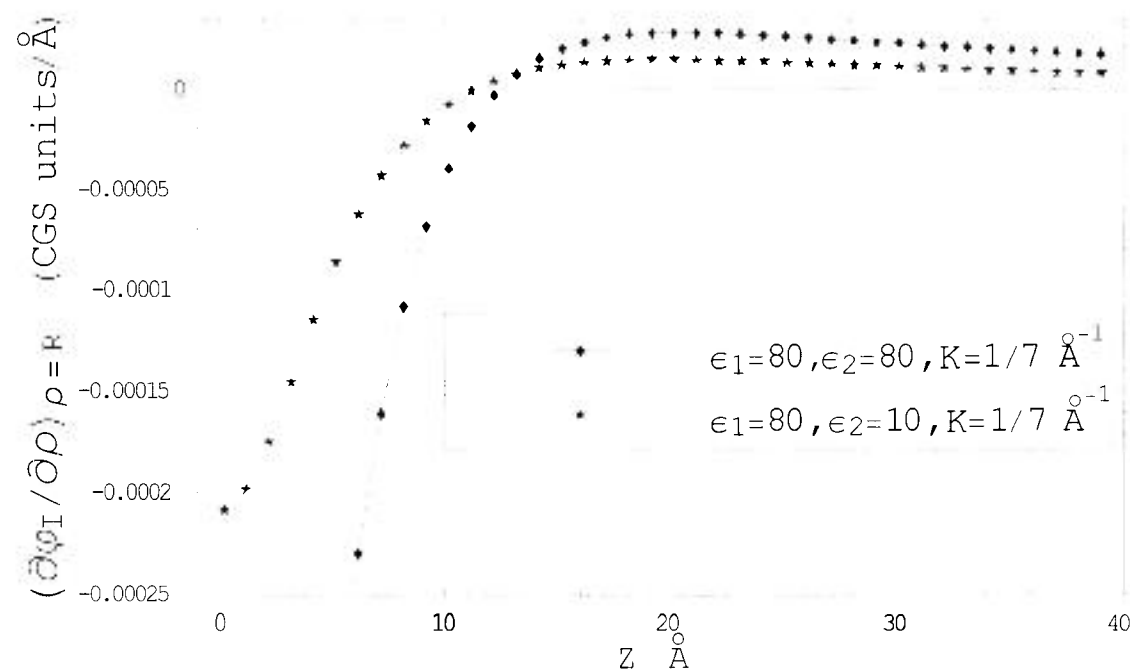


**Figure 6.2.** The normal derivative of the potential in region I on the channel surface as a function of coordinate  $z$  for the case shown in Fig.6.1. Different curves correspond to different sets of dielectric constants: upper curve— for  $\epsilon_1 = 80, \epsilon_2 = 10$ , lower curve— for  $\epsilon_1 = \epsilon_2 = 80$ . Radius  $R$  of the channel is  $7 \text{ \AA}$ ;  $k = 1/7 \text{ \AA}^{-1}$

One can see that the normal component of the electric field at the boundary and, therefore, the density of the induced surface charge, change sign at some value of  $z$  (induced charge is positive near the external point charge  $q$  and becomes negative further away). This effect is observed even in the case of equal dielectric constants ( $\epsilon_1 = \epsilon_2$ ), when there is no induced surface charge; i.e. it is caused by the space charge of free ions in the channel.

Below a similar graph (see Fig 6.3) is presented for the case when there is no ionic solution in the channel ( $k=0$ ).

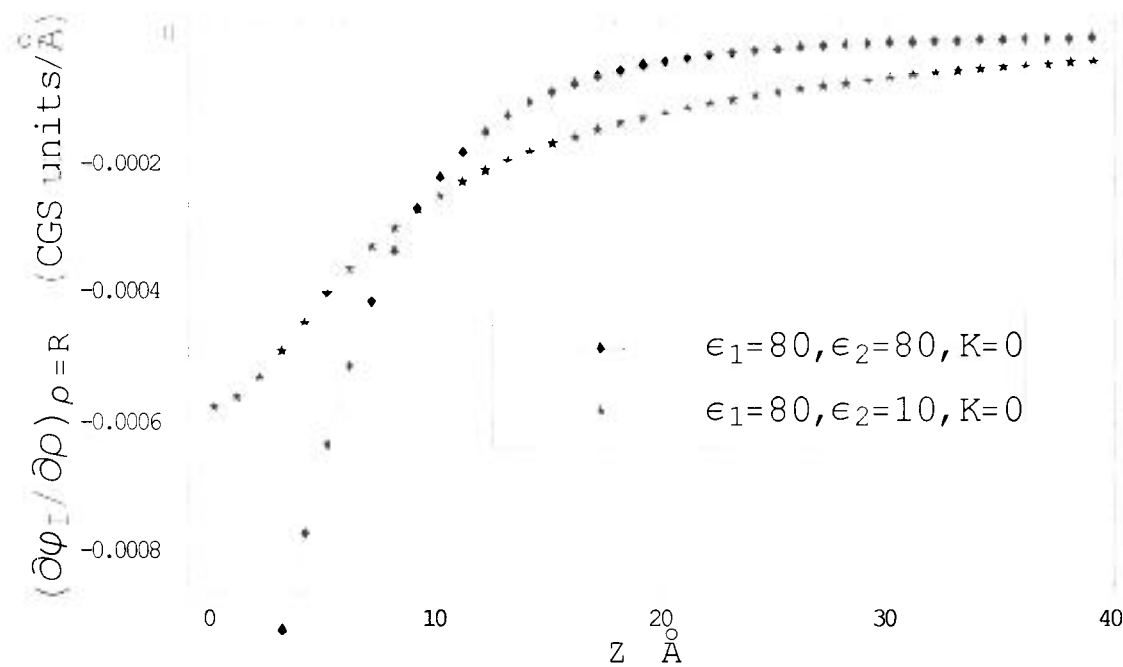


Figure 6.3. Same as Fig 6.2, but for the case  $k=0$  (no ionic solution in channel).

This graph shows once again that the effect of the sign change of the normal component of the electric field on the surface of the cylinder is totally due to the space charge of free ions in the solution. We will discuss this effect qualitatively later.

Now we will examine the influence of the important parameter  $\lambda/R$  on the properties of the system.

Fig. 6.4 represents the potential inside the cylinder at a point with fixed  $z$  coordinate ( $z=5 \text{ \AA}$ ) as a function of  $\rho$  for four different channel radii:  $R=3\lambda$ ,  $\lambda$ ,  $\lambda/3$  and  $\lambda/7$  with  $\lambda=7 \text{ \AA}$ , when the two dielectric constants are the same ( $\epsilon=\epsilon_1=\epsilon_2$ ). For comparison two limiting functions of the potential  $\varphi$  are shown: the bottom one corresponds to the point charge in uniform infinite space (infinite channel radius,  $R \rightarrow \infty$ )  $\varphi = q \exp(-kr)/(\epsilon r)$ , the top one corresponds to vanishing channel radius,  $R \rightarrow 0$ ,  $\varphi = q/(\epsilon r)$ .

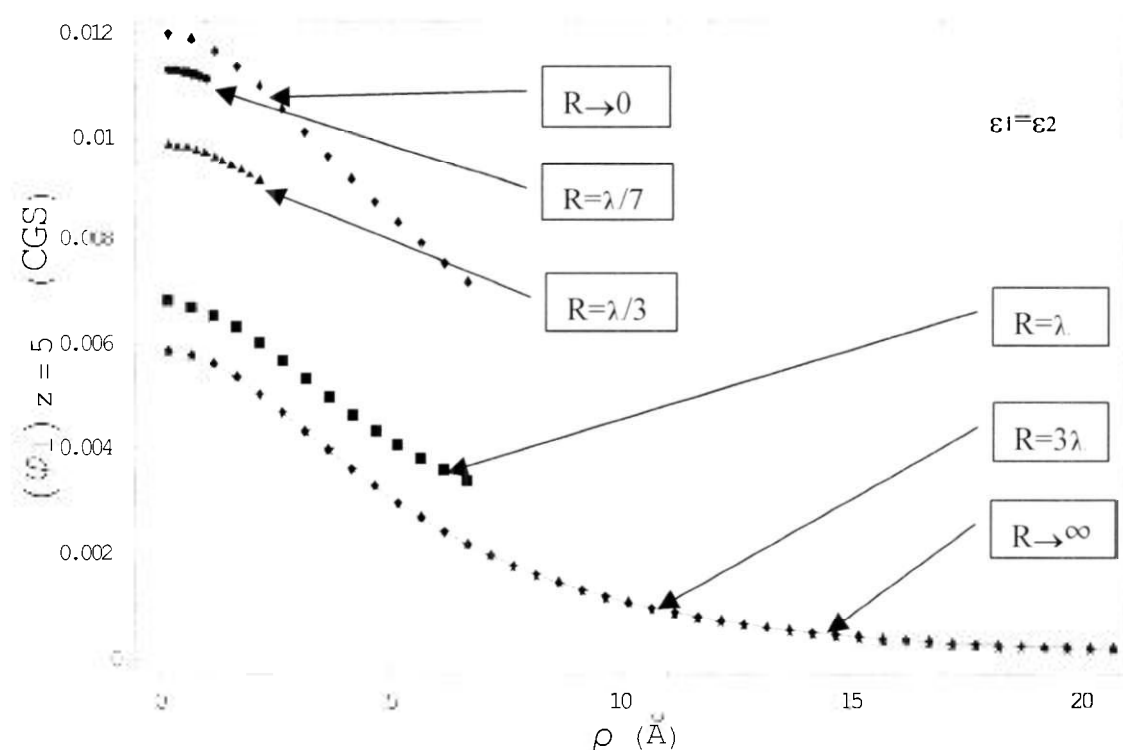


Figure 6.4. The potential inside the cylinder at a point with fixed  $z=5\text{\AA}$  as a function of radial coordinate  $\rho$  for four different channel radii,  $R=3\lambda$ ,  $R=\lambda$ ,  $R=\lambda/3$  and  $R=\lambda/7$  for  $\lambda=7\text{\AA}$  when the two dielectric constants are the same ( $\epsilon_1 = \epsilon_2$ ). Upper and lower curves correspond to limiting functions,  $\varphi = q/(\epsilon_1 r)$  and  $\varphi = q \exp(-kr)/(\epsilon_1 r)$  respectively.

The two lowest curves, corresponding to the potential in the uniform infinite space and potential in the cylinder with radius  $R=3\lambda$  coincide. One sees that for  $R \gg \lambda$  (actually  $R \geq 3\lambda$ ) the potential does not depend on the channel radius, i.e., the charge does not feel the channel boundary and the potential behaves as that of a point charge in the infinite volume filled with ionic solution,  $\varphi = q \exp(-kr)/(\epsilon_1 r)$ . As can be seen from the graph, for  $R \leq \lambda$ , when the screening effect is small, the potential inside the channel approaches the potential of a point charge in the infinite volume without ionic solution ( $\varphi = q/(\epsilon_1 r)$ ).

This conclusion is also illustrated by Fig.6.5, which shows the dependence of the potential at a fixed point on the channel radius for different values of  $\lambda$ :  $\lambda \rightarrow \infty$ ,  $\lambda=2\lambda^*$ ,  $\lambda=\lambda^*$ ,  $\lambda=\lambda^*/2$ , where  $\lambda^*=7\text{\AA}$ . Here both dielectric constants of channel and surrounding medium are the same.

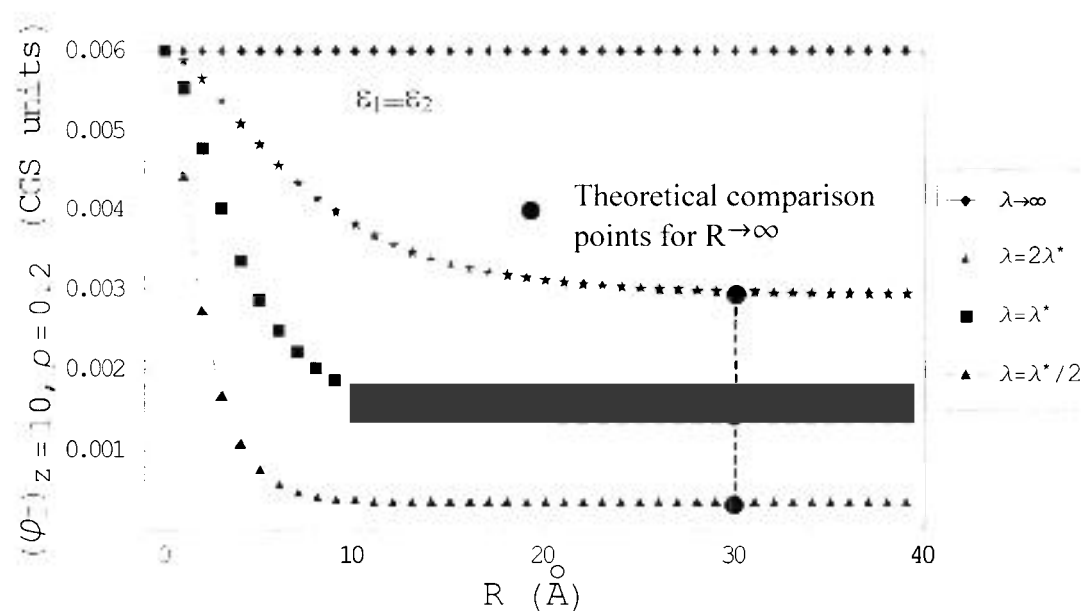


Figure 6.5. Graph representing the potential at a fixed point ( $z=5 \text{ \AA}$ ,  $\rho=0.2 \text{ \AA}$ ) inside the channel as a function of the channel radius  $R$  for four different values of  $\lambda$ :  $\lambda \rightarrow \infty$  (upper curve),  $\lambda=2\lambda^*$ ,  $\lambda=\lambda^*$ ,  $\lambda=\lambda^*/2$  (lower curve), where  $\lambda^*=7 \text{ \AA}$ . The three points plotted at  $R=30 \text{ \AA}$  are analytical solution points for the case  $R \rightarrow \infty$ .

Limiting case points corresponding to the potential in the infinite volume with ionic solution ( $\varphi = q \exp(-kr)/(\epsilon_1 r)$ ), shown connected by a vertical line, are on the asymptotes at very big channel radii. These asymptotes are reached when  $R \gg \lambda$  and the walls of the channel do not influence the potential. When  $R \ll \lambda$  there is no screening effect and, hence, no dependence on the value of  $\lambda$  (in the  $\epsilon_1 = \epsilon_2$  case, of course). This can be seen as the curves for different  $\lambda$  converge to the same value when the channel radius tends to zero. For the curve with  $\lambda \rightarrow \infty$  any value of  $R$ , so there is no screening and there is no dependence on  $R$ .

Fig. 6.6 shows the influence of the parameter  $\lambda/R$  on the distribution and the magnitude of the polarized surface charge on the boundary of the cylindrical channel. The polarized surface charge is represented as a function of coordinate  $z$  for the case when  $R=7 \text{ \AA}$ ,  $\epsilon_1=80$ ,  $\epsilon_2=10$ . One can observe that the width of the region of positive charge is of the order of  $\lambda$  and becomes smaller as  $\lambda/R$  decreases. For  $R \ll \lambda$  the surface charge distribution is similar to the case when  $k=0$  (not shown on the graph), although it changes sign at  $|z| \sim \lambda$ .

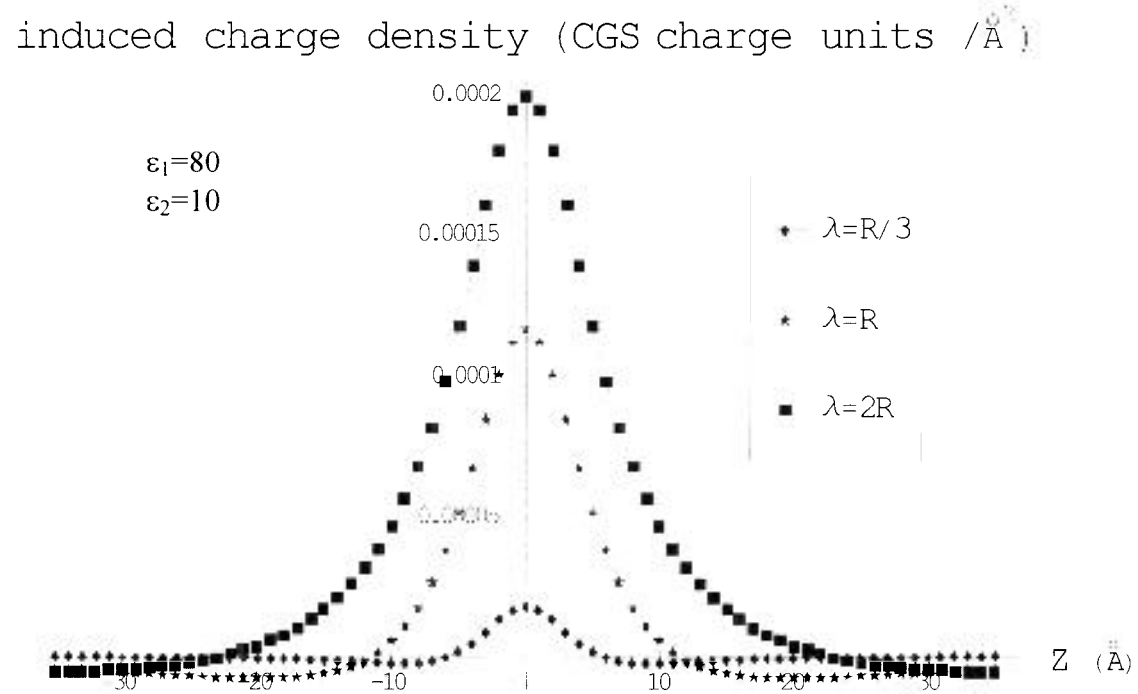
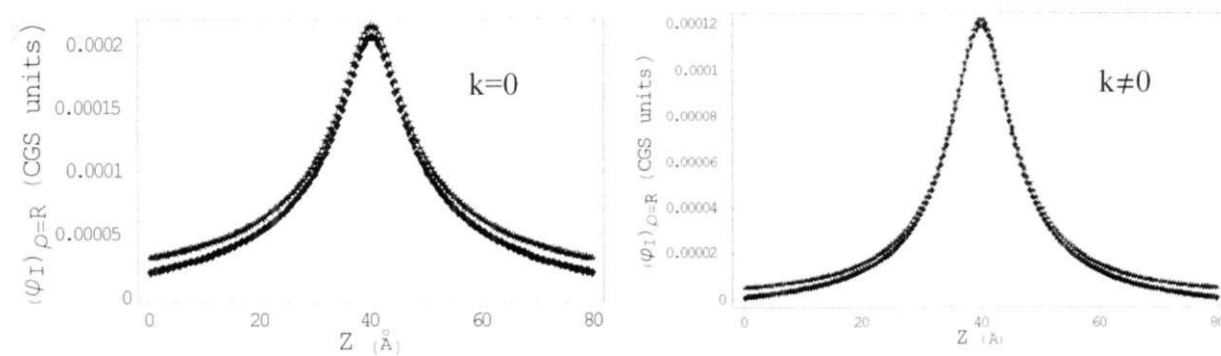


Figure 6.6. Polarized surface charge as a function of coordinate  $z$  for the case when  $R=7$  Å,  $\epsilon_1=80$ ,  $\epsilon_2=10$ .

### 6.1.3. Comparison with results obtained by numerical method

The BEM calculations performed for a very thick membrane should be very close to the analytical result for the infinite cylinder (see Section 6.1.2). These are compared in Fig. 6.7, which shows the dependence on  $z$  of the potential on the surface of the cylindrical channel for infinite and finite membrane for two cases:  $k=0$  and  $k \neq 0$ . One can see a good agreement. The discrepancy can be explained by the finite width of the membrane, within which the potential is lower due to the high dielectric constant of the ionic solution.



**Figure 6.7.** Potential at the channel surface as a function of  $z$  coordinate (both graphs). Point charge is placed at  $z=40$  Å. Upper curve corresponds to the infinite cylinder (analytical solution), lower – finite cylinder (BEM calculations). The curves nearly coincide For both graphs  $R=5$  Å,  $\epsilon_1=80$ ,  $\epsilon_2=40$ . The length of membrane  $L$  is 80 Å.

Fig. 6.8 represents the normal derivative of the potential on the surface of the cylindrical hall as a function of  $z$  coordinate ( $k=0$ ,  $k\neq 0$ ). Curves for finite membrane (BEM calculations) and infinite membrane (analytical solution) almost coincide. The effect of changing sign of the surface charge density of the channel (positive close to the point charge and negative further away) observed for the infinite cylinder is also present in the case of the very thick membrane.

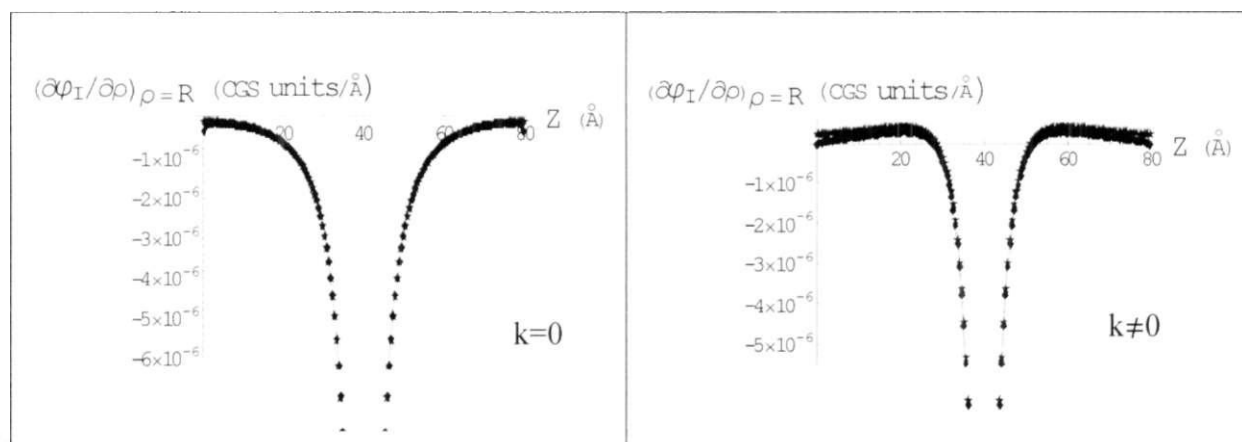


**Figure 6.8.** Normal derivative of the potential on the surface of the cylindrical channel as a function of  $z$  coordinate ( $k=0$ ,  $k\neq 0$ ). Point charge is placed at  $z=40$  Å. Upper curve corresponds to the infinite cylinder (analytical solution), lower – to the finite cylinder (BEM calculation). The curves nearly coincide. For both graphs  $R=5$  Å,  $\epsilon_1=80$ ,  $\epsilon_2=40$ . The length of membrane  $L$  is 80 Å.

Calculations were performed for various values of  $k$ , from  $(1/2)k^*$  to  $3k^*$ , where  $k^* = 1/7 \text{ \AA}^{-1}$ . They show also a very good agreement with the results obtained for the infinite cylinder.

## 6.2 Behavior of the potential and the electric field in the membrane with the finite channel. Comparison with the infinite cylinder

It is interesting to examine the behavior of potential and electric field for the finite membrane in all space. This also demonstrates the ability of BEM to calculate potentials at any point of the space. In the following we will consider two cases: 1) the point charge is in the middle of the finite channel and 2) the point charge is near the finite channel.

1). **Point charge is in the middle of the channel.** Fig. 6.9 shows the equipotential maps inside the membrane and the channel of radius  $R=5 \text{ \AA}$  for three cases  $\lambda=21 \text{ \AA}$  ( $\lambda \gg R$ ),  $\lambda=7 \text{ \AA}$  ( $R \approx \lambda$ ),  $\lambda=2.3 \text{ \AA}$  ( $\lambda \ll R$ ). Equipotential lines are drawn in the plan containing  $z$  axes.

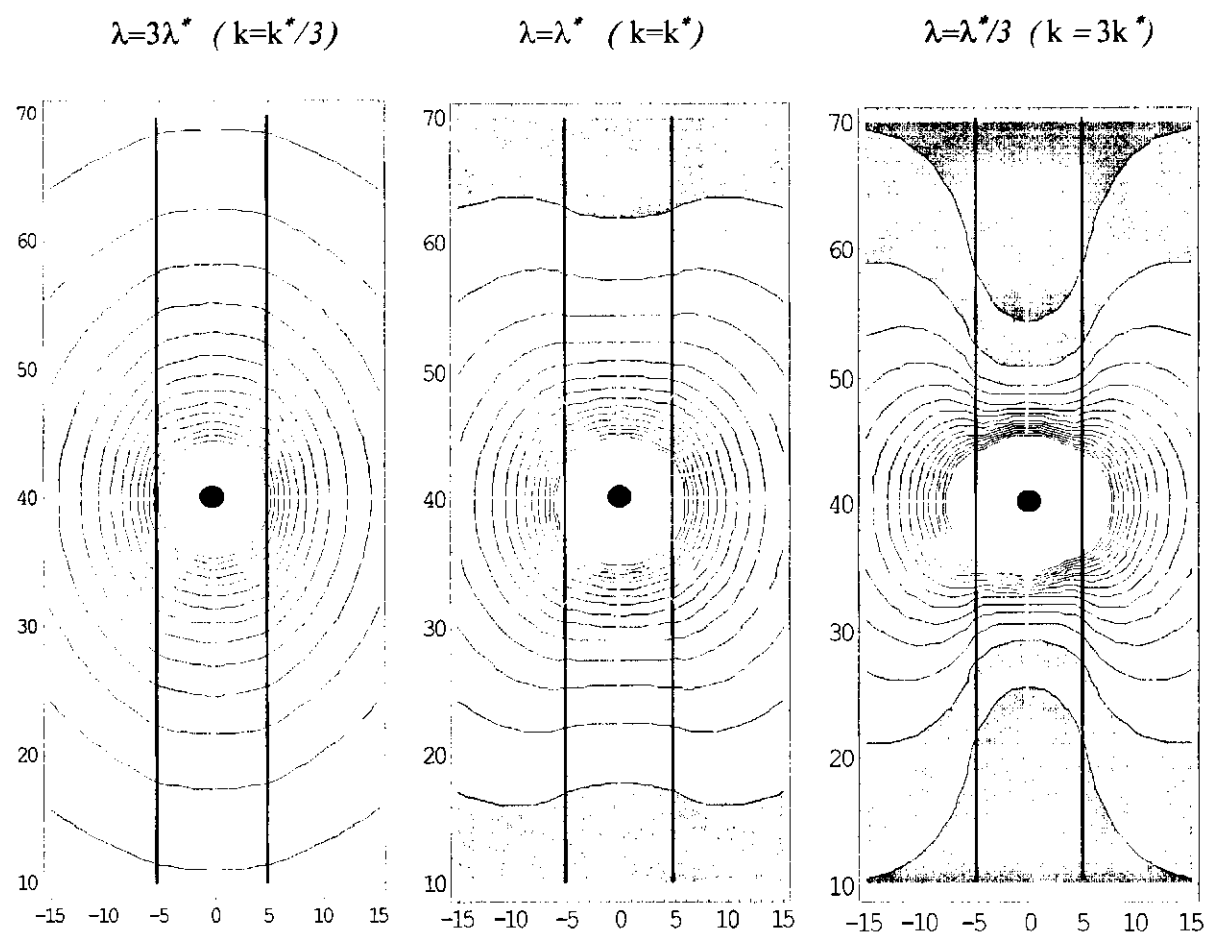


**Figure 6.9.** Equipotential maps inside the channel ( $R = 5 \text{ \AA}$ ) and membrane for three cases:  $\lambda = 21 \text{ \AA}$  ( $\lambda \gg R$ ),  $\lambda = 7 \text{ \AA}$  ( $R \approx \lambda$ ),  $\lambda = 2.3 \text{ \AA}$  ( $\lambda \ll R$ ). Equipotential lines are drawn in the plane containing  $z$  axes. As one moves from one equipotential contour to the next, the potential changes by a fixed step,  $\Delta\Phi$ . Point charge is placed in the middle of the channel. Vertical axis shows  $z$  coordinate in Angstroms, The length of membrane is  $70 \text{ \AA}$ . Horizontal axis shows radial coordinate in Angstroms. Electric field lines are drawn in white. Black lines shows the boundary of the channel.

As the value of  $k$  increases (or, equivalently,  $\lambda$  decreases), Inside the channel with increasing  $k$  (or, equivalently,  $\lambda$  decreases), the electric potential inside the channel along the  $z$  axis inside the channel falls off faster (density of the equipotential lines becomes higher). The rate of change of the electric potential inside the membrane does not vary much (as  $k$  is changed) since there is no screening effect due to free charges there. As a consequence, the electric field lines (drawn in white) for  $\lambda < R$  at some distance from the point charge converge towards the channel and reenter the channel.

One can see that the point at the channel boundary where the normal component of the electric field changes sign is closer to the point charge for large  $k$ , in agreement with what was observed in the case of an infinite cylinder (see Fig. 6.6)

2) **Point charge is near the channel.** When the point charge is not inside the channel, but near the channel (we do not have an analytical solution for this case), we expect to observe the properties of the potential analogous to those in the infinite channel and in the thick membrane. Fig. 6.10 shows the equipotential lines for the case, when the distance of the charge from the surface is equal to  $7 \text{ \AA}$ . (As before, equipotential lines are drawn in the plane containing  $z$  axes). One can see that the electric field on the surface of the channel also changes sign at some distance from the charge.

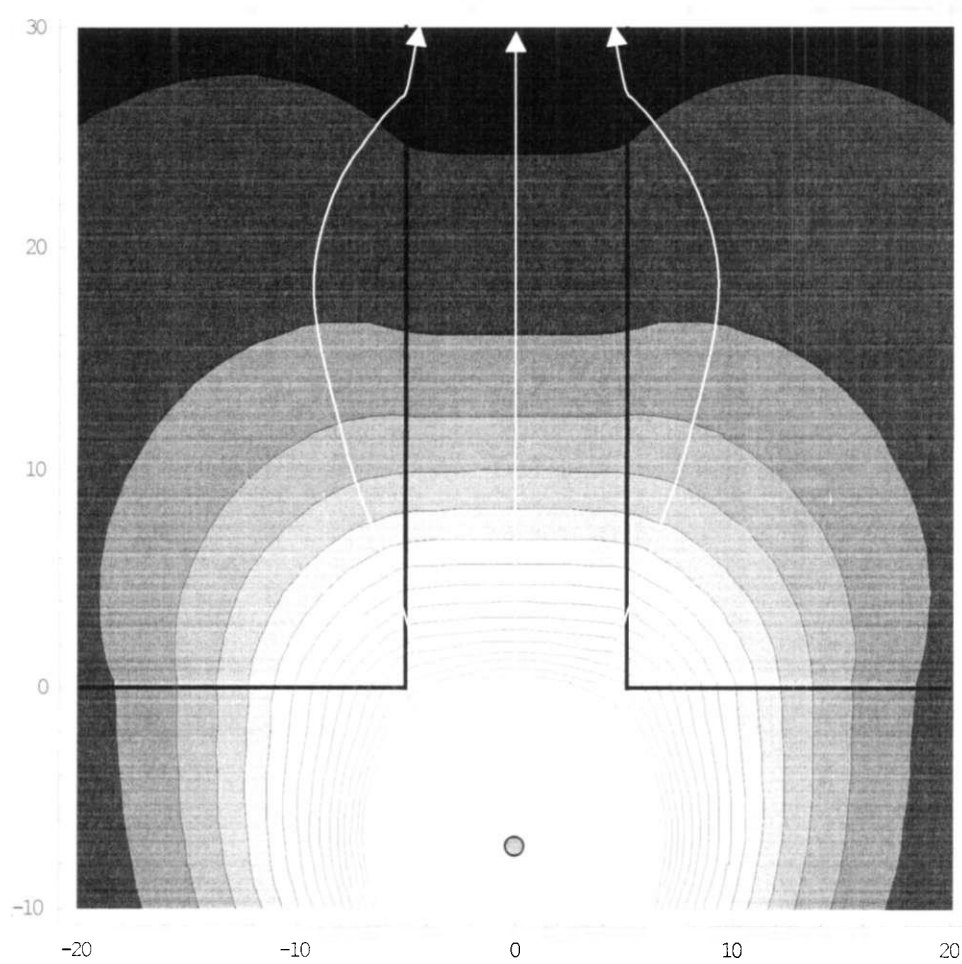


Figure 6.10. Equipotential lines (in the plane containing  $z$  axes) inside the channel ( $R=5 \text{ \AA}$ ) and membrane for the case:  $\lambda=7 \text{ \AA}$ , ( $R \approx \lambda$ ),  $d=7 \text{ \AA}$ ,  $\epsilon_1=80$ ,  $\epsilon_2=10$ .). As one moves from one equipotential contour to the next, the potential changes by a fixed step. Point charge is placed outside the channel ( $d=7 \text{ \AA}$ ). Vertical axes shows  $z$  coordinate in Angstroms. The length of membrane is  $70 \text{ \AA}$ . Horizontal axes shows radial coordinate in Angstroms. Electric field lines are drawn in white. Black lines shows the boundary of the channel and the membrane.

Results of calculations (not presented here) show that the distance at which the electric field changes sign increases with decreasing  $k$ . For  $k=0$  the convergence of electric field lines towards the channel is not observed. We noted the same effects in the infinite cylinder and in the finite cylinder with the charge placed in the middle of the channel.

Finally, we compare the numerical calculation for the potential inside the channel of small radius due to the point charge near the membrane channel with another limiting case, when this point charge is placed near the membrane without the channel. We expect that when the channel radius approaches zero, the solution should approach the analytical solution of the above limiting case. Fig. 6.11 shows the potential as a function of  $z$  coordinate for three different channel radii,  $R=15 \text{ \AA}$  (bottom),  $R=3 \text{ \AA}$ ,  $R=1 \text{ \AA}$ . One can see that the BEM-calculated curves span the space between the two analytical curves representing the free space solution ( $\varphi = q \exp(-kr)/(\epsilon_1 r)$ , bottom curve) and the above-mentioned solution for a charge near the membrane without the channel (top curve). We also see here that for  $R \gg \lambda$  the potential doesn't feel the channel: curves for free space solution and for  $R=15 \text{ \AA}$  coincide. This is in agreement with what was observed in the case of an infinite cylinder (see Fig. 6.3, Fig. 6.4).

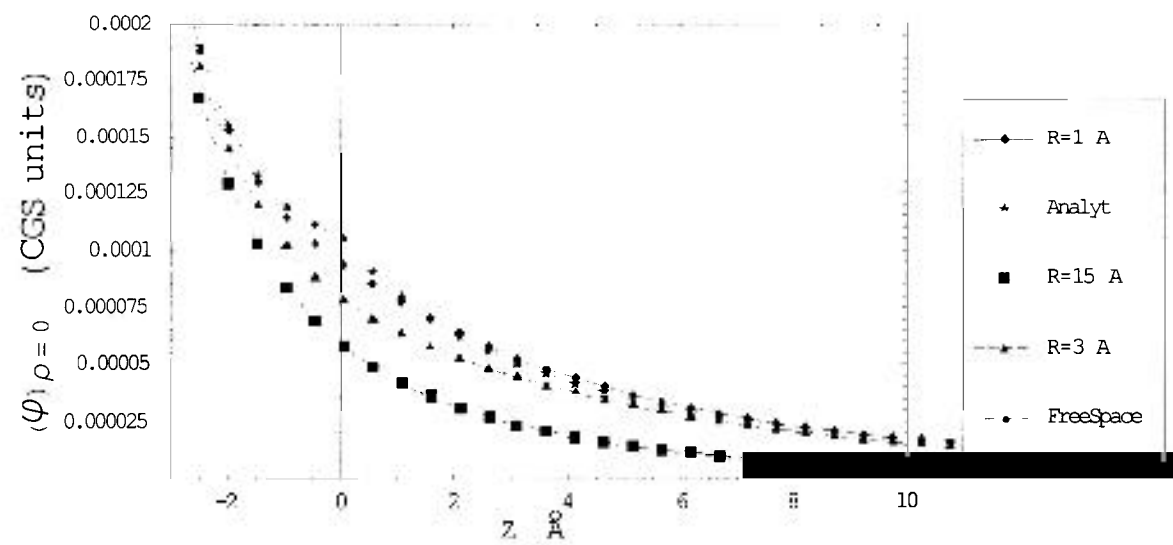


Figure 6.11. Potential as a function of  $z$  coordinate for three different radii of the channel:  $R=15 \text{ \AA}$  (bottom),  $R=3 \text{ \AA}$ ,  $R=1 \text{ \AA}$ , Upper curve (Analyt) is for the potential due to point charge near membrane without the channel. Free Space curve ( $\varphi = q \exp(-kr) / (\epsilon_1 r)$ ) coincide with the curve for  $R=15 \text{ \AA}$ . For all cases  $\epsilon_1=80$ ,  $\epsilon_2=10$ .

So, after the above analysis we can conclude that numerical results obtained with BEM are accurate.

## CHAPTER 7. RESULTS AND DISCUSSION

### 7.1. Influence of parameters of the basic model on the behaviour of the potential inside the channel

In Chapter 6 we considered the problem of the potential due to a point charge inside an infinite cylinder filled with ionic solution. We discussed the importance of the parameter  $\lambda/A$  ( $\lambda$  is the Debye length, and, in the current chapter,  $A$  stands for the radius of the channel) for the potential behaviour. In particular, when  $\lambda/A \ll 1$  the screening effect is essential and the field around the charge is almost unaffected by the presence of the channel. In the same chapter we discussed the screening of the potential of a point charge within or near the channel of a finite membrane. The importance of the parameter  $\lambda/A$  holds true for this system as well, although in this case additional governing dimensionless geometrical parameters become important. They are the distance of the charge from the membrane  $d/\lambda$  and the thickness of the membrane  $H/\lambda$ . Calculations show that for  $d/\lambda > 1$  (when the potential of the charge is almost screened) the field in the channel does not feel the membrane. For our model with a charged sphere of radius  $R$  near the finite channel another physical parameter appears due to the finite size of the sphere,  $R/\lambda$ . The importance of this parameter can be seen from formula (3.11) which describes the potential of a charged sphere placed in an infinite ionic solution. When  $R/\lambda \ll 1$  the potential is close to the potential of a point charge. When  $R/\lambda \gg 1$  the potential differs from the point charge potential by a constant factor at each point in space. For the typical parameters of our system,  $R=10 \text{ \AA}$  and  $\lambda=7 \text{ \AA}$ , this factor is 1.7. This factor grows exponentially with  $R$  and is due to the fact that screening takes place outside the sphere only.

So, the number of important parameters in our system is substantial. Under such circumstances a complete analysis of all the dependencies is not realistic. We will study the sensitivity of the potential to different parameters within the realistic range. This study is important, because there is uncertainty in the values of major physical parameters of the system such as the radius of the channel, its length and dielectric constants in the

system. Also the shape of the toxin molecule and charge distribution in it used in the model is only approximation of the real shape and charge distribution of the R13Q.

Fig. 7.1 shows the potential along the  $z$  axis (the axis of symmetry of the system) for three models: point charge near the membrane of finite width without the channel, point charge near the membrane of finite width with channel, and uniform charged sphere near the membrane of finite width with channel. In all three cases  $\lambda=7 \text{ \AA}$ ,  $H=30 \text{ \AA}$ , and distance  $d$  from the centre of the charge to the membrane is  $11 \text{ \AA}$ . The radius of the sphere  $R$  is  $10 \text{ \AA}$  and the channel radius  $A$  is  $3 \text{ \AA}$ .

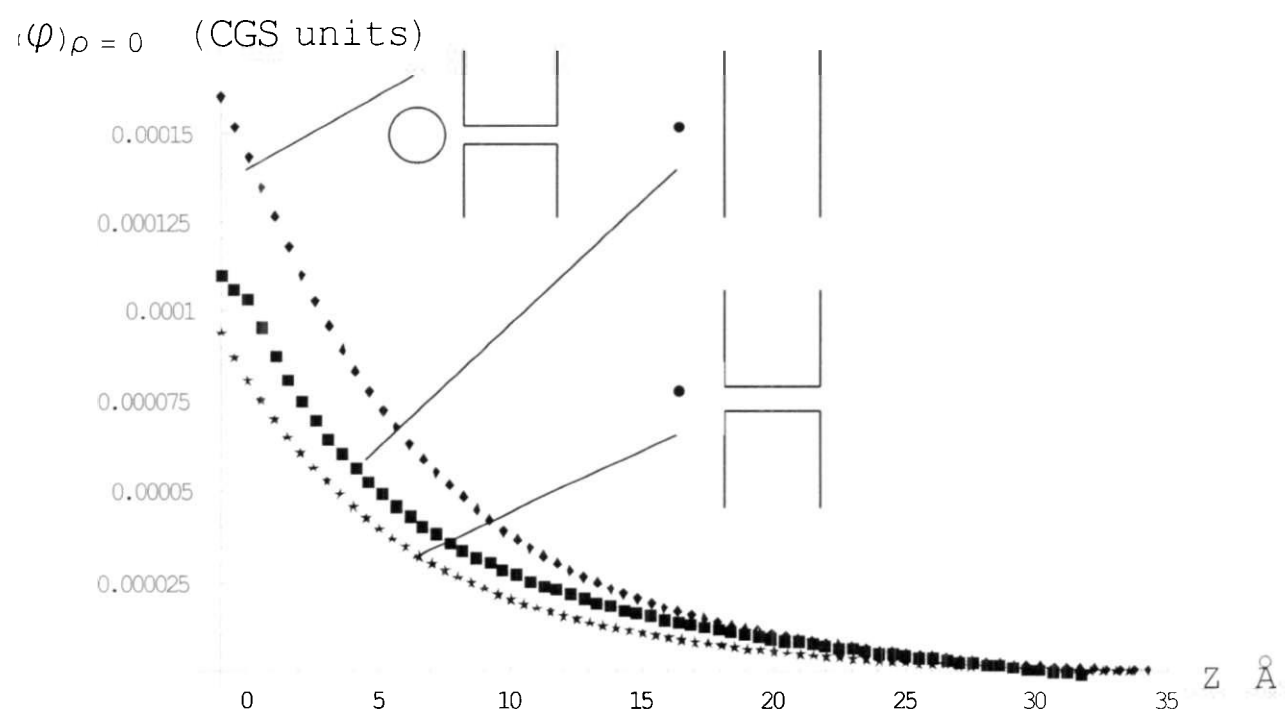


**Figure 7.1.** Potential as a function of  $z$  coordinate ( $\rho=0$ ) for different models. Models top to bottom are: spherical charge near the membrane with a channel; point charge near the membrane without the channel; point charge near the membrane with the channel.  $z=0$  corresponds to the left side of the membrane. In all three cases  $\lambda=7 \text{ \AA}$ ,  $H=30 \text{ \AA}$ , and distance  $d$  from the centre of the charge to the membrane is  $11 \text{ \AA}$ . The radius of the sphere  $R$  is  $10 \text{ \AA}$  and the channel radius  $A$  is  $3 \text{ \AA}$ .

This graph shows that both the finite size of the charge and the presence of the channel noticeably influence the behaviour of the potential.

Fig. 7.2 demonstrates the influence of the membrane thickness on the potential distribution. Variation of this parameter within the realistic range from  $H=30 \text{ \AA}$  to  $H=50 \text{ \AA}$  ( $R=3 \text{ \AA}$ ) leads to a hardly noticeable change of the potential. For  $H=10 \text{ \AA}$  the

potential changes substantially. On the outer side of the membrane this potential is close to the potential of the sphere in free space. For  $H=3 \text{ \AA}$  the potential becomes closer to the potential of the sphere in free space even within the membrane. This is due to the fact that the length of the membrane is much less than the Debye length ( $\lambda=7 \text{ \AA}$ ) and the effect of the membrane is small.

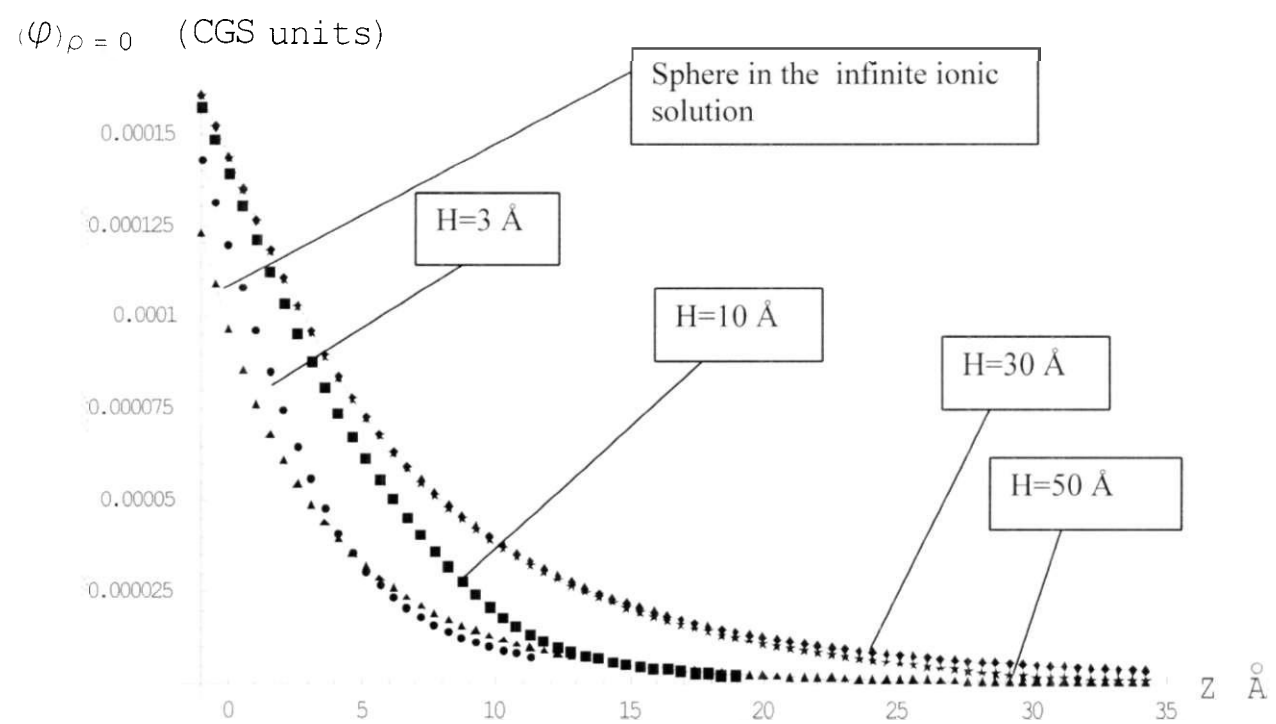


**Fig. 7.2.** Potential as a function of  $z$  coordinate ( $\rho=0$ ) for different width of the channel. For all cases  $\lambda=7 \text{ \AA}$ ,  $R=10 \text{ \AA}$ ,  $A=3 \text{ \AA}$ ,  $d=11 \text{ \AA}$ . Potential due to charged sphere in the infinite ionic solution is presented as well.

Calculations for a wider channel (radius  $R=5 \text{ \AA}$ ) were performed for realistic values of  $H$  between  $30 \text{ \AA}$  and  $50 \text{ \AA}$  and they have shown the similar results. We may therefore conclude that the uncertainty in the membrane width will not greatly influence the results.

There is some uncertainty in the values of dielectric constants of the membrane and of the charged toxin molecule. Fig. 7.3 shows the influence of these parameters on the potential inside the channel.

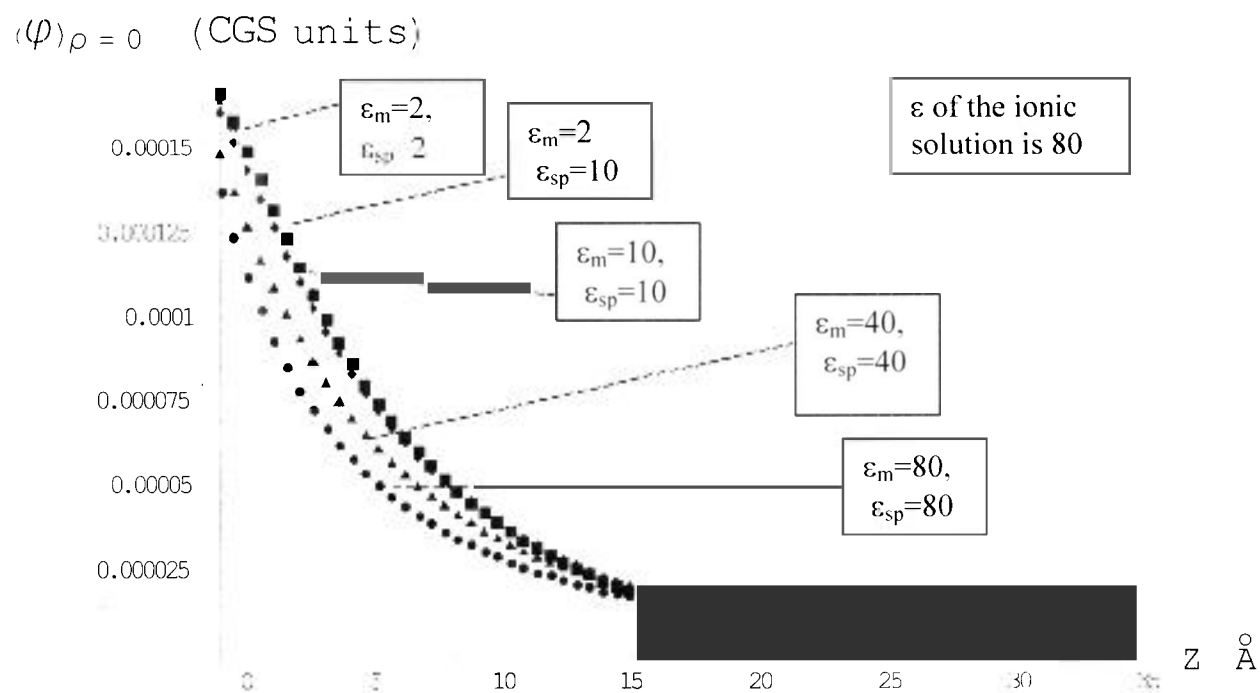


Fig.7.3. Potential as a function of  $z$  coordinate ( $\rho=0$ ) for different values of dielectric constants.  $\epsilon_m, \epsilon_{sp}$  are dielectric constants of membrane and sphere respectively. For all cases  $\lambda=7$  Å,  $R=10$  Å,  $A=3$  Å,  $d=11$  Å,  $H=30$  Å.

The bottom curve represents calculations for the model with the same dielectric constant throughout the whole system ( $\epsilon=80$ ). The next one was calculated with the membrane and R13Q-molecule dielectric constants changed to 40. The last three curves were obtained with the dielectric constant of the membrane  $\epsilon_m$  and R13Q-molecule  $\epsilon_{sp}$  being  $\epsilon_m=10$  and  $\epsilon_{sp}=2$ , and  $\epsilon_m=2$  and  $\epsilon_{sp}=10$ . These three cases are almost indistinguishable, which shows that in the realistic range of 2 to 10 for the dielectric constants of the membrane and the toxin the uncertainty in these values is not very important for calculations, as the final result is not sensitive to these parameters. This type of conclusion may change with different system geometry. In this particular case we used the most realistic values of geometric parameters, namely:  $H=30$  Å,  $A=3$  Å,  $R=10$  Å,  $d=11$  Å. When the value of  $A$  (width of the membrane) is 5 Å this influence diminishes even more and for  $A=1$  Å the difference is a little more pronounced.

Fig. 7.4. illustrates calculations of the potential along the  $z$  axis for various channel radii from 1 Å to 10 Å. The last value was found to produce a potential distribution that is very close to that around a sphere in a infinite ionic solution without the membrane (lower curve on this graph). This is understandable, because in this case the distance from the sphere to different parts of the membrane is more then the Debye length. So, the electric potential on the  $z$  axis almost does not feel the presence of the membrane. The real channel itself is not a cylinder with constant radius. A reasonable estimate of its radius variation is of 1.5 to 6 Å. Assuming that the potential distribution for a non-cylindrical channel is somewhere between the potential distributions for the cylindrical channels with the maximum and minimum possible channel radii we can make an estimate of the uncertainty in the modeling of the potential.

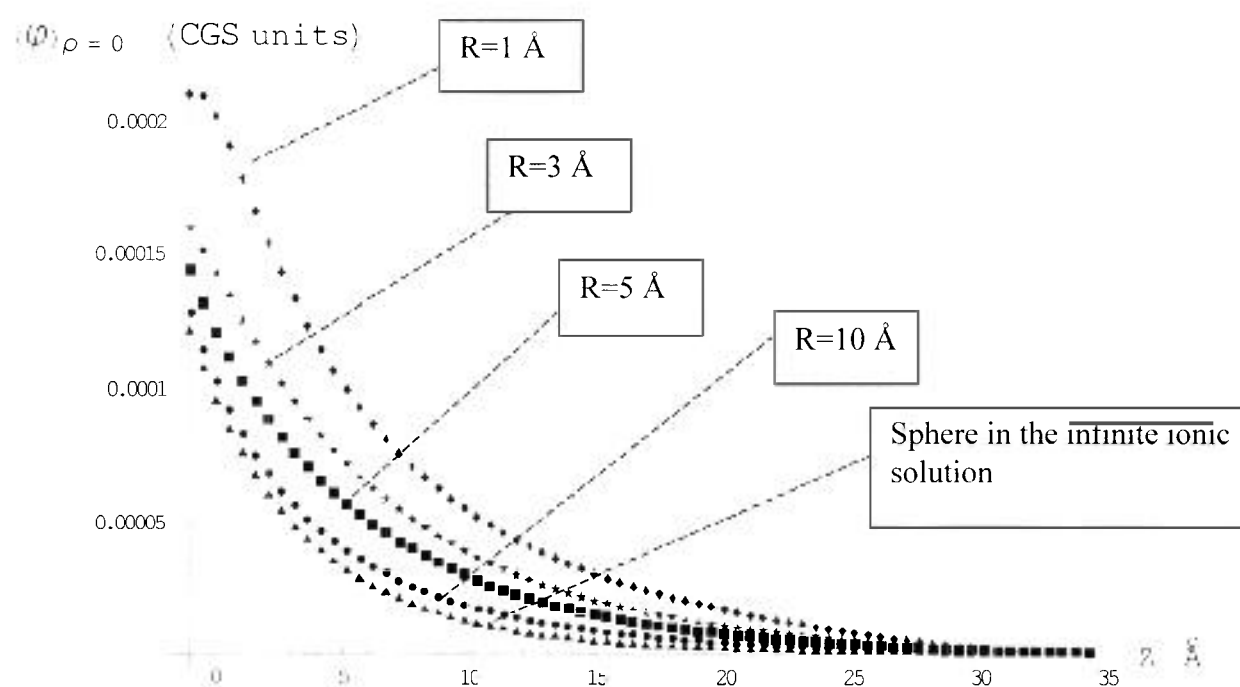
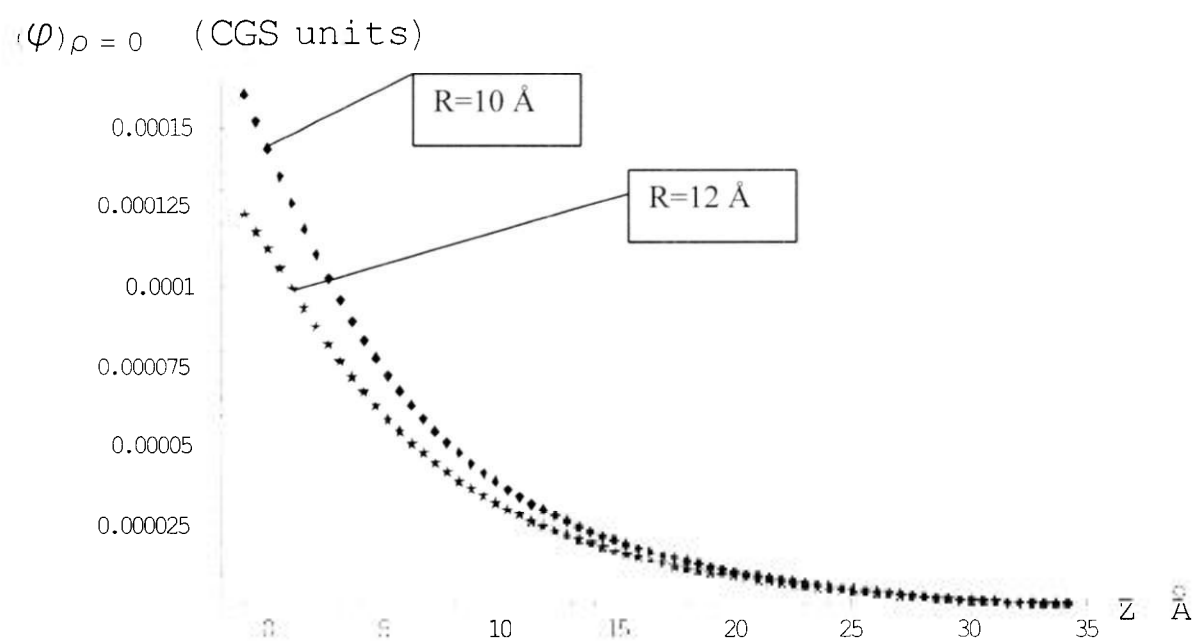


Fig. 7.4. Potential as a function of  $z$  coordinate ( $\rho=0$ ) for different radii of the channel. From the top to the bottom:  $R=1$  Å,  $R=3$  Å,  $R=5$  Å,  $R=10$  Å. For all four cases  $R=10$  Å,  $d=11$  Å. Lower curve represents the potential of the sphere in the infinite ionic solution.

The real toxin molecule is not a sphere (Fig.2.1). Based on the examination of its structure, we assume that it could be reasonably represented by a sphere of radii from 10 Å to 12 Å. Fig.7.5 shows the influence of the sphere radius on the behaviour of the

potential inside the channel. The surface of the sphere is at a distance of  $1\text{ \AA}$  from the membrane surface in both cases. The difference in the potentials is not large. Naturally, the potential of the larger sphere is lower here due to a larger distance between some parts of the larger sphere and the point of observation.



**Fig. 7.5.** Potential as a function of  $z$  coordinate ( $\rho=0$ ) for different radii  $R$  of the charged sphere. Upper curve corresponds to  $R=10\text{ \AA}$ , lower to  $R=12\text{ \AA}$ . For each case  $d=11\text{ \AA}$ ,  $A=3\text{ \AA}$ .  $z=0$  corresponds to the beginning of the membrane.

In all the previous calculations the charge of R13Q was assumed evenly distributed over the surface of this molecule. Now we want to consider non-uniformities in the charge distribution. Biochemical data suggest that the neutral Q13-residue of this molecule is the closest to the channel (indeed enters the channel). We will try to take this fact into account by a slightly changed model of the R13Q, in which the charged sphere has a neutral cap of some diameter  $s$  (see Fig.7.6).

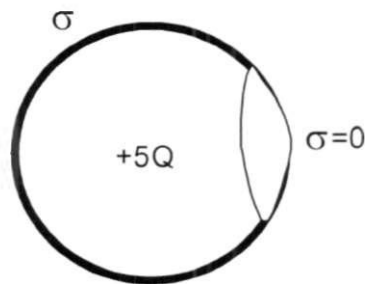


Fig. 7.6. Simple modeling of nonuniform charge distribution in R13Q-molecule.  $\sigma$  is the surface charge density. The residue of R13Q closest to the channel is represented by a neutral hat.

In Fig.7.7 we present the result of calculation of the potential inside the channel for such a nonuniform surface charge density distribution of the R13Q molecule. From top to bottom the curves on this graph correspond to the following cases: no cap, cap with diameter 2.8 Å (0.5% of the sphere area), cap with diameter 5 Å (1.6% of the sphere area), and cap with diameter 8.7 Å (5% of the sphere area). In all four cases  $R=10$  Å.

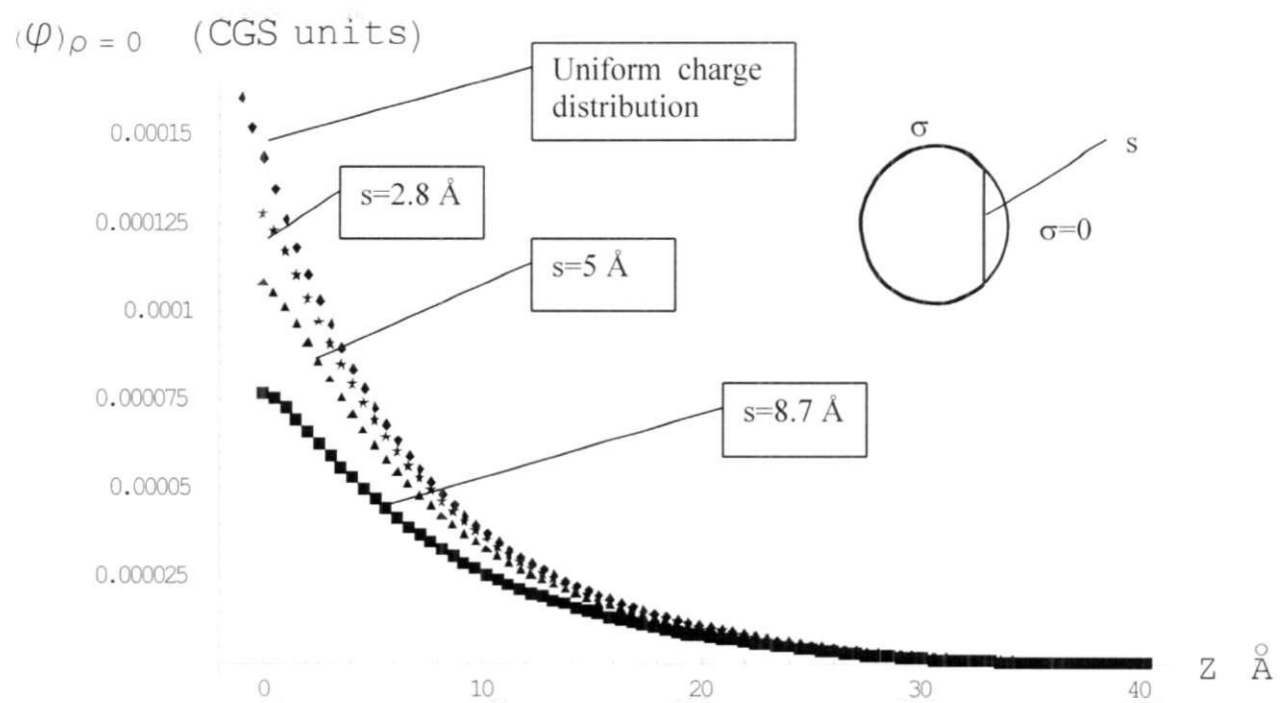


Fig. 7.7. Potential as a function of  $z$  coordinate ( $\rho=0$ ) for different diameters of surface charge nonuniformity of the sphere.  $s$  is the diameter of the neutral cap. Radius of the sphere  $R$  is 10 Å.  $z=0$  corresponds to the beginning of the membrane.  $d=11$  Å.

One can see that the distribution of the charge on the sphere is important, but further improvement of accuracy might be attained by using realistic structure for the charge distribution in this molecule. Within our model the estimate with cap diameter 5 Å looks reasonable to us as a measure of the influence of nonuniformity of the charge.

Based on the above analysis we can conclude that, within a realistic range of parameters of our system, radius of the channel, radius of the sphere and surface charge distribution of the sphere influence the potential distribution most strongly. The uncertainty in the width of membrane and dielectric constants of membrane and sphere can be neglected.

## 7.2. Estimation of location of DEA binding site

As was described in Chapter 2, the presence of R13Q causes a shift of the energy level  $\Delta\epsilon_{R13Q}$  for the DEA at the adsorption site. From the experimental data (see Chapter 2) we have obtained the numerical value for this shift:  $\Delta\epsilon_{R13Q} = (14.6 \pm 1.5)$  meV. The shift (expressed in terms of potential) and the potential on the z axes for different essential parameters of the system are presented in Fig. 7.8. Based on this graph we can make an estimation of not only the adsorption site location, but also (within our basic model) its uncertainty due to the uncertainty in the channel radius, R13Q radius and the nonuniformity of the charge distribution of R13Q.

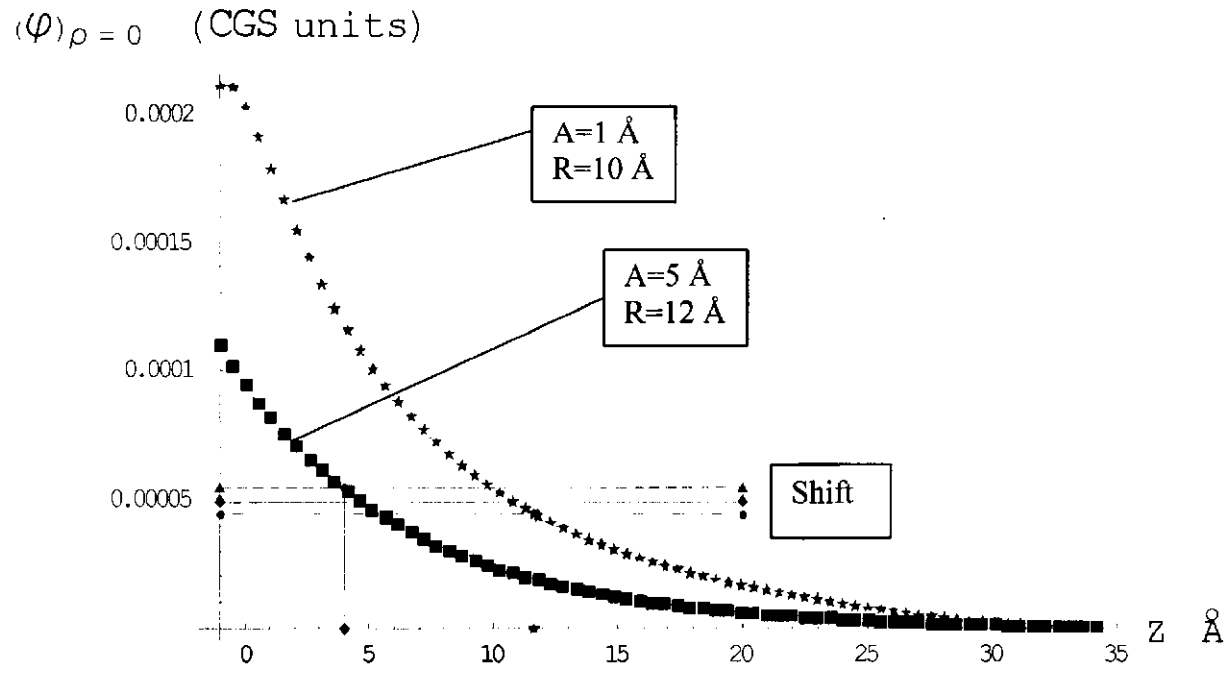


**Fig. 7.8.** Final graph for estimation of location of DEA binding site. Potential as a function of  $z$  coordinate ( $\rho=0$ ) for limiting realistic parameters of the system is shown. Upper curve corresponds to  $R=10 \text{ \AA}$ ,  $A=1 \text{ \AA}$ . Lower curve corresponds to  $R=12 \text{ \AA}$ ,  $A=5 \text{ \AA}$ . For both cases  $d=11 \text{ \AA}$ ,  $H=30 \text{ \AA}$ ,  $\epsilon_m=10$ ,  $\epsilon_{sp}=10$ ,  $\epsilon$  of ionic solution is 80. Horizontal lines represent the shift in DEA energy level (with the error), expressed in units of potential. Location of DEA binding site is  $4 \text{ \AA}$ - $11.5 \text{ \AA}$  from the front wall of the membrane.

The upper curve corresponds to  $1 \text{ \AA}$  channel radius and R13Q radius  $10 \text{ \AA}$ . The lower one corresponds to  $A = 5 \text{ \AA}$  and  $R = 12 \text{ \AA}$ . All the intermediate cases lie between these curves. Based on our previous results, the curves representing realistic variations in the charge distribution are also covered by the presented range. This gives an estimate of the maximum possible difference in calculated potential for a realistic range of main parameters. Based on the above estimates and on the experimentally measured energy shift (with its error) we can estimate the position within the channel of the adsorption site of DEA to be somewhere from  $4 \text{ \AA}$  to  $11.5 \text{ \AA}$  as measured from the front membrane surface.

### 7.3. Conclusion

The range 4 Å–11.5 Å for location of DEA adsorption site obtained for our basic model of a sodium channel seems realistic. Biochemical data [Lipkind and Fozzand, 2000] for sodium channel suggest that the distance between the outer end of the vestibule of the channel protein and selectivity filter could be approximately 14-17 Å, and the length of the selectivity filter is probably 2 Å–4 Å. If we equate the front surface of the simplified membrane geometry in our model to the outer surface of the vestibule of the real channel protein (See Fig. 3.2) and take into account that DEA cannot go through the selectivity filter, then our result would imply that the selectivity filter is located <11.5 Å from the outer end of the vestibule. This value is somewhat smaller than that implied by the Lipkind-Fozzand model. The discrepancy can be qualitatively explained as resulting from simplification made in our geometrical model. In the real channel, part of the R13Q-molecule is surrounded by the channel protein. If the model were to include this effect, the potential inside the channel due to R13Q would be larger because of the lower dielectric constant of the protein and the decrease of the screening effect of the ionic solution. Calculations with a point charge placed inside a uniform solid membrane without the channel (results are not presented here) qualitatively support this conclusion. Also, the narrowest part of the pore of the real channel does not contain the ionic solution. If this effect were to be included in our model, this would likewise increase the potential in the channel. In addition, the space between the outer end of the vestibule and the selectivity filter of the real channel probably does not contain negative ions from the surrounding ionic solution; this should also increase the potential. Any effect that tends to increase the potential in our model channel will increase our estimate of the distance between the outer end of the vestibule and the DEA adsorption site. On the other hand, the charges of the R13Q-molecule are located at the ends of the residues, which are 2 Å - 5 Å from the main body of the molecule. This factor will decrease the potential. Although it is hard to say how far the channel protein extends into the ionic solution and how deep the R13Q-molecule is immersed into the protein, it is possible to perform BEM calculations for a more realistic channel boundary shape and for more realistic geometry of the R13Q, and examine the influence of uncertain parameters on the behaviour of the potential.

To sum up then, our model, given the simplifications employed, has produced reasonably realistic estimates of the DEA adsorption site. Future calculations could easily be enhanced to give improved fits to experimental data.

## BIBLIOGRAPHY

Becker, S., Prusak-Sochaczewski, E., Zamponi, G., Beck-Sickinger, A.G., Gordon, R.D., and French, R.J. 1992. Action of derivatives of  $\mu$ -Conotoxin GVIA on sodium channels. Single amino-acid substitutions in the toxin separately affect association and dissociation rates. *Biochemistry* 31:8229-8238.

Cai, M. and Jordan, P.C. 1990. How does vestibule surface charge affect ion conduction and toxin binding in a sodium channel? *Biophys. J.* 57:883-891.

Corry, B., Kuyucak, and Chung, S. Tests of continuum theories as models of ion channels. II. Poisson—Nernst-Planck Theory versus Brownian dynamics. *Biophys. J.* 78:2364-2381.

Doyle, D. A., Cabral, J.M., Pfuetzner, R.A., Kuo, A., Gulbis, J. M. Cohen, S.L., Chait, B.T., and MacKinnon, R. 1998. The Structure of the potassium channel: molecular basis of K<sup>+</sup> conduction and selectivity. *Science* 280:69-74.

French, R.J., Worley III, J.F., Blaustein, M.B., Romine, W.O., Jr., Tam, K.K., and Krueger, B.K. 1986. Gating of batrachotoxin-activated sodium channels in lipid bilayers. From Ion Channel Reconstitution. Ed. Miller, K. Plenum.

French, R.J., Prusak-Sochaczewski, E., Zamponi, G.W., Becker, S., Kularatna, A. S, and Horn, R. 1996. Interactions between a pore-blocking peptide and the voltage sensor of the sodium channel: an electrostatic approach to channel geometry. *Neuron* 16:407-413.

French, R.J., Zamponi, G.W., Sierralta, I.E. 1998. Molecular and kinetic determinants of local anaesthetic action on sodium channels. *Toxicology Letters* 100-101:247-254

Grechko, L.G., Sudakov, V.I., Tomasevich, O.F., Fedorchenko, A.M. 1984. Problems of Theoretical Physics. Vysshaya Shkola, Moscow.

Hille, B. 1992. Ionic Channels in Excitable Membrane. Sinauer, Sunderland, MA

Horn, R., Vanderberg, C.A., and Lange, K. 1984. Statistical analysis of single sodium channels. Effects of N-bromoacetamide. *Biophys. J.* 45:323-325.

Hoyles, M., Kuyucak, S., Chung, Shin-Ho. 1996. Energy barrier presented to ions by the vestibule of the biological membrane channel. *Biophys. J.* 70:1628-1642.

Jackson, J.D., 1999. Classical Electrodynamics. John Wiley and Sons, New-York.

Jordan, P.C. 1983. Electrostatic modeling of ion pores. II. Effects attributable to the membrane dipole potential. *Biophys. J.* 41:189-195.

Juffer, A.H., Argos, P., and Vogel H.J. 1997. Calculating acid-dissociation constants of proteins using the Boundary Element Method. *J.Phys.Chem.* 101:7664-7673.

Kuyucak, S., Hoyles, M., and Chung, S. 1998. Analytical solutions of Poisson's equation for realistic geometrical shapes of membrane ion channels. *Biophys. J.* 74:22-36.

Li, S.C., Hoyles, M., Kuyucak, S., and Chung, S. 1998. Brownian dynamics study of ion transport in the vestibule of membrane channels. *Biophys. J.* 74:37-47.

Lipkind, G., and Fozzard, H. 2000. KcsA crystal structure as framework for a molecular model of the Na channel pore. *Biochemistry.* 39:8161-8170.

Mathias, R.T., Baldo, G.J., Manivannan, K., and McLaughlin, S. Discrete charges on biological membranes. From R.Guidelli (ed). *Electri.. Interfaces in Physics, Chemistry and Biology.*1992. 473-490. Kluwer Academic, Netherlands.

Mayer, J.E., and Goeppert Mayer, M. 1977. *Statistical Mechanics*. John Wiley and Sons, New York.

Mikhlin, S.G. 1970. *Mathematical Physics, an Advanced Course*. North-Holland, Amsterdam.

Morse, P.M., and Feshbach. 1953. *Methods of Theoretical Physics, vol.II*. McGraw-Hill, New York.

Moy, G., Corry, B., Kuyucak, S., and Chung S. Tests of continuum theories as models of ion channels. I. Poisson-Boltzmann theory versus Brownian dynamics. *Biophys. J.* 78:2349-2363.

Nonner, W., Catacuzzeno, L., and Eisenberg, B. Binding and selectivity in L-type Calcium channels: a mean spherical approximation. *Biophys. J.* 79:1976-1992

Paris, F., Canas, J. 1997. *Boundary Element Method. Fundamentals and Applications*. Oxford University Press, Oxford.

Partenskii, M.B., and Jordan, P.C. 1992. Theoretical perspectives on ion-channel electrostatics – continuum and microscopic approaches. *Quart. Rev. Biophys.* 25:477-510.

Sigworth, F., and Neher, E. 1980. Single Na channel currents observed in cultured rat muscle cells. *Nature* 287:447-449.

Smyth, W. R. 1968. *Static And Dynamic Electricity*. McGraw-Hill, New York.

Stakgold, I.S. 1979. *Green's Functions and Boundary Value Problems*. Wiley and Sons, New York.

Stillinger, F.H., Jr. 1961. Interfacial solutions of the Poisson-Boltzmann equation. *J. of Chem. Phys.* 35:1584-1589.

Stühmer, W., Conti F., Suzuki, H., and Wang, X., Noda M., Yahagi, Nn., Kubo, H., and Numa S. 1989. Structural parts involved in activation and inactivation of the sodium channel. *Nature* 339:597-603.

Van Kampen, N.G. 1984. *Stochastic Processes in Physics And Chemistry*. North-Holland, Amsterdam.

Zamponi, G.W. and French, R.J. 1993. Dissecting lidocaine action: diethylamide and phenol mimic separate modes of lidocaine block of sodium channels from heart and skeletal muscle. *Biophys. J.* 65:2335-2347.

Zamponi, G.W., Sui X., Coddling, P.W., and French, R.J. 1993. Dual actions of procainamide on batrachotoxin-activated sodium channels: open channel block and prevention of inactivation. 1993. 65:2324-2334.

## APPENDIX A

### INFINITE CYLINDRICAL HOLE.

For formulation of the problem see Section 6.1.1. The radius of the channel here will be denoted by  $a$ .

The electric potential in region II (see Fig. 6.1) is governed by Laplace equation:

$$\nabla^2 \varphi_{II} = 0 \quad (1)$$

The potential in region I satisfies the equation

$$\nabla^2 \varphi_I - k^2 \varphi_I = -\frac{4\pi q}{\epsilon_1} \delta(\bar{r} - \bar{r}_0) \quad (2)$$

These equations are subject to the following boundary conditions:

$$\begin{aligned} \varphi_I(z, a) &= \varphi_{II}(z, a) \\ \epsilon_1 \left. \frac{\partial \varphi_I}{\partial \rho} \right|_{\rho=a} &= \epsilon_2 \left. \frac{\partial \varphi_{II}}{\partial \rho} \right|_{\rho=a} \end{aligned} \quad (3)$$

where  $a$  is the radius of the channel. An additional physically obvious condition is that both potentials vanish at infinity.

The first step is to find the potential in region II. In cylindrical coordinates  $(\rho, \phi)$  equation (1) takes the form:

$$\frac{1}{\rho} \frac{\partial}{\partial \rho} \left( \rho \frac{\partial \varphi_{II}}{\partial \rho} \right) + \frac{1}{\rho^2} \frac{\partial^2 \varphi_{II}}{\partial \phi^2} + \frac{\partial^2 \varphi_{II}}{\partial z^2} = 0 \quad (4)$$

Because of symmetry the second term in this equation vanishes and the equation can be written in the following form:

$$\frac{1}{\rho} \frac{\partial}{\partial \rho} \left( \rho \frac{\partial \varphi_{II}}{\partial \rho} \right) + \frac{\partial^2 \varphi_{II}}{\partial z^2} = 0 \quad (5)$$

Equation (5) is subject to variable separation. Let

$$\varphi_{II} = R(\rho)Z(z) \quad (6)$$

After substitution (6) into (5) and simple transformations we get:

$$\frac{1}{\rho R} \frac{\partial}{\partial \rho} \left( \rho \frac{\partial R}{\partial \rho} \right) + \frac{1}{Z} \frac{\partial^2 Z}{\partial z^2} = 0 \quad (7)$$

Introducing a separation constant we can write:

$$\frac{1}{Z} \frac{d^2 Z}{dz^2} = -\alpha^2 \quad (8)$$

and

$$\frac{\rho}{R} \frac{d}{d\rho} \left( \rho \frac{dR}{d\rho} \right) = \alpha^2 \rho^2 \quad (9)$$

General solution of equation (8) is of the following form:

$$Z(z) = Ae^{-i\alpha z} + Be^{i\alpha z}, \quad (10)$$

Solutions with imaginary  $\alpha$  do not meet the boundary condition  $V \rightarrow 0$  as  $z \rightarrow \pm\infty$ . Consequently, the solution can be rewritten in real form  $Z(z) = A(\alpha)\sin(\alpha z) + B(\alpha)\cos(\alpha z)$ , where  $\alpha$  is a real number. Without limiting generality we can consider  $\alpha \geq 0$ . Because of the symmetry of the problem the potential is an even function of  $z$  and the term with  $\sin(\alpha z)$  will be absent in the solution. So,

$$Z(z) = B(\alpha)\cos(\alpha z) \quad (10a).$$

By applying substitution  $v = \alpha \cdot \rho$  we transform equation (9) to the form:

$$\frac{d^2 R}{dv^2} + \frac{1}{v} \frac{dR}{dv} - R = 0 \quad (11)$$

This is the modified Bessel equation. Its general solution is of the form:

$$R(v) = C \cdot I_0(v) + D \cdot K_0(v) \quad (12)$$

or

$$R(v) = C \cdot I_0(\alpha \rho) + D \cdot K_0(\alpha \rho) \quad (13)$$

where  $I_0(v)$  and  $K_0(v)$  are the modified Bessel functions. The function  $I_0(v)$  grows to infinity at infinite  $v$ , which violates the boundary condition at infinity.

Finally, the general solution of Laplace equation in region II can be presented in the following form:

$$\varphi_{II}(\rho, z) = \int_0^{\infty} A(\alpha) K_0(\alpha \rho) \cos(\alpha z) d\alpha \quad (14)$$

Now let us consider the solution in region I. First we find the solution of the homogeneous equation

$$\nabla^2 \varphi_I - k^2 \varphi_I = 0 \quad (15)$$

This equation, similar to equation (1), admits variable separation. Let  $V = R(\rho)Z(z)$ . After transformations this equation is reduced to two equations, which are similar to equations (8) and (9).

$$\frac{1}{Z} \frac{d^2 Z}{dz^2} = -\alpha^2 \quad (16)$$

$$\frac{\rho}{R} \frac{d}{d\rho} \left( \rho \frac{dR}{d\rho} \right) = \rho^2 (k^2 + \alpha^2) \quad (17)$$

Because of the similarity of the boundary conditions for equations (8) and (16) along the  $z$  axis the solution of equation (16) is  $Z(z) = A(\alpha) \cos(\alpha z)$ .

The substitution  $v = \sqrt{k^2 + \alpha^2}$  reduces (17) to the modified Bessel's equation (11) with general solution of the form (12). So, general solution  $\varphi_{I,0}$  of homogeneous equation (15) can be presented in the form:

$$\varphi_{I,0}(\rho, z) = \int_0^{\infty} \left[ B(\alpha) K_0(\rho \sqrt{k^2 + \alpha^2}) + C(\alpha) I_0(\rho \sqrt{k^2 + \alpha^2}) \right] \cos(\alpha z) d\alpha \quad (18)$$

A particular solution  $\varphi_{I,p}$  of inhomogeneous equation (2) is

$$\varphi_{I,p}(\rho, z) = \frac{qe^{-kz}}{\epsilon_1 r} \quad (19)$$

The integral representation of this solution is:

$$\varphi_p(\rho, z) = \frac{2q}{\pi \epsilon_1} \int_0^{\infty} K_0(\rho \sqrt{k^2 + \alpha^2}) \cos(\alpha z) d\alpha \quad (20)$$

General solution of equation (2) can be written as a sum of a particular solution of this equation and general solution of homogeneous equation:

$$\varphi_l(\rho, z) = \int_0^{\tau} \left[ B(\alpha) K_0(\rho\sqrt{k^2 + \alpha^2}) + C(\alpha) I_0(\rho\sqrt{k^2 + \alpha^2}) \right] \cos(\alpha z) d\alpha + \frac{2q}{\pi\epsilon_1} \int_0^{\tau} K_0(\rho\sqrt{k^2 + \alpha^2}) \cos(\alpha z) d\alpha \quad (21)$$

Since the last term in this formula represents singular part of the potential associated with the charge there should be no other singularity in the solution and we have to let  $B=0$  to eliminate  $K_0$ , which is singular at  $\rho = 0$ . Instead of a rigorous proof of this assumption we will obtain the solution that satisfies equations and boundary condition of the problem at hand. Based on the theorem of uniqueness of the solution we will be able to conclude that this assumption is valid.

Finally, for general solution of inhomogeneous equation (14) we get:

$$\varphi_l(\rho, z) = \int_0^{\tau} B(\alpha) I_0(\rho\sqrt{k^2 + \alpha^2}) \cos(\alpha z) dz + \frac{2q}{\pi\epsilon_1} \int_0^{\tau} K_0(\rho\sqrt{k^2 + \alpha^2}) \cos(\alpha z) d\alpha \quad (22)$$

Using boundary conditions (3) we come up with two integral equations, which can be solved for coefficient functions  $A(\alpha)$  and  $B(\alpha)$ , which appear in general solutions  $\varphi_l$  and  $\varphi_u$ . Finally, the solution of the initial problem is the following:

$$\varphi_l(\rho, z) = \frac{2q}{\pi\epsilon_1} \int_0^{\tau} (K_0(\rho\sqrt{k^2 + u^2}) + F(u) I_0(\rho\sqrt{k^2 + u^2}) \cos(zu)) du \quad (23)$$

where

$$F(u) = \frac{-u\epsilon_2 K_0(R\sqrt{k^2 + u^2}) K_1(Ru) + \epsilon_1 \sqrt{k^2 + u^2} K_0(Ru) K_1(R\sqrt{k^2 + u^2})}{\epsilon_1 \sqrt{k^2 + u^2} I_1(R\sqrt{k^2 + u^2}) K_0(Ru) + u\epsilon_2 \sqrt{k^2 + u^2} I_0(R\sqrt{k^2 + u^2}) K_1(Ru)}$$

$$\varphi_u(\rho, z) = \frac{2q}{\pi\epsilon_1} \int_0^{\tau} K_0(Ru) \frac{(I_1(R\sqrt{k^2 + u^2}) K_0(R\sqrt{k^2 + u^2}) + I_0(R\sqrt{k^2 + u^2}) K_1(R\sqrt{k^2 + u^2}))}{I_1(R\sqrt{k^2 + u^2}) K_0(Ru) + (u\epsilon_2 / \epsilon_1 \sqrt{k^2 + u^2}) I_0(R\sqrt{k^2 + u^2}) K_1(Ru)} \cos(zu) du \quad (24)$$

**APPENDIX B**

**POINT CHARGE NEAR MEMBRANE OF THE  
FINITE WIDTH SURROUNDED BY IONIC SOLUTION**

Fig. A1 shows the geometry of the system under consideration.

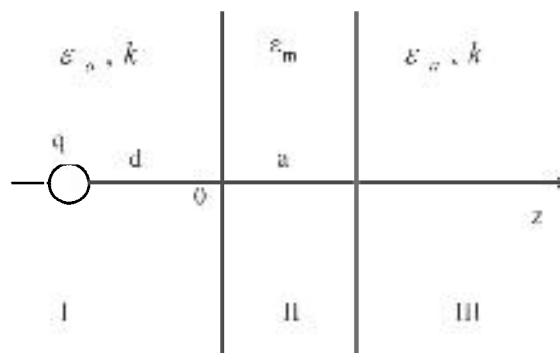


**Fig A1. Geometry of the system: point charge near membrane with finite width surrounded by ionic solution**

The membrane of width  $a$  and dielectric constant  $\epsilon_m$  is in the salt solution with dielectric constant  $\epsilon_a$  and Debye length  $\lambda=1/k$ . The charge  $q$  is at the distance  $d$  from the membrane. It is convenient to place the origin of the cylindrical coordinate system ( $z=0$ ,  $\rho=0$ ) on the left surface. The space is divided into three regions. Region I contains the solution and the charge, region II corresponds to membrane, and region III contains the solution on the other side of the membrane.

Usually this type of the problem is solved by adjusting the general solutions of every region to the boundary conditions of the problem.

The electric potential  $\varphi$  is governed by the following equations:

$$\text{in region III} \quad \Delta\varphi_{III} - \kappa^2\varphi_{III} = 0 \quad (1)$$

$$\text{in region II} \quad \Delta\varphi_{II} = 0 \quad (2)$$

$$\text{in region I} \quad \Delta\varphi_{III} - \kappa^2\varphi_{III} = \frac{4\pi q}{\epsilon_0} \delta(\mathbf{r} - \mathbf{r}_0) \quad (3)$$

where vector  $\mathbf{r}_0$  corresponds to the position of the charge.

The problem is clearly axisymmetric and solution  $\varphi$  will be independent of the polar angle. The general solutions of (1) - (3) vanishing at the infinity and represented in cylindrical coordinates  $(z, \rho)$  become:

$$\varphi_{III} = \int_0^\infty A_3(\alpha) J_0(\alpha\rho) e^{-\sqrt{\alpha^2+k^2}z} d\alpha \quad (4)$$

$$\varphi_{II} = \int_0^\infty B_2(\alpha) J_0(\alpha\rho) e^{\alpha z} d\alpha + \int_0^\infty D_2(\alpha) J_0(\alpha\rho) e^{-\alpha z} d\alpha \quad (5)$$

$$\varphi_I = \frac{q}{\epsilon_0} \frac{e^{-k\sqrt{\rho^2+z^2}}}{\sqrt{\rho^2+z^2}} + \int_0^\infty C_1(\alpha) J_0(\alpha\rho) e^{-\sqrt{\alpha^2+k^2}z} d\alpha \quad (6)$$

where  $J_0$  is the Bessel function of the first kind, and  $A_3$ ,  $B_2$ ,  $D_2$ ,  $C_1$  are arbitrary coefficients.

In expression (6) for  $\varphi_I$  the first term is a particular solution of inhomogeneous equation, which represents the screened potential of the point charge. It can also be written as an integral from the Bessel function with the use of the following relation:

$$\frac{e^{-k\sqrt{\rho^2+z^2}}}{\sqrt{\rho^2+z^2}} = \int_0^\infty \alpha J_0(\alpha\rho) \frac{e^{-\sqrt{\alpha^2+k^2}z}}{\sqrt{\alpha^2+k^2}} d\alpha \quad (7)$$

In order to specify the arbitrary coefficients of the general solution boundary conditions must be satisfied. In cylindrical coordinates we have:

at the interface between regions I and II ( $z=0$ )

$$\varphi_I(\rho, 0) = \varphi_{II}(\rho, 0) \quad (10)$$

$$\varepsilon_a \frac{\partial \varphi_I(\rho, z)}{\partial z} \Big|_{z=0} = \varepsilon_b \frac{\partial \varphi_{II}(\rho, z)}{\partial z} \Big|_{z=0} \quad (11)$$

at the interface between regions II -III ( $z=a$ )

$$\varphi_{II}(\rho, a) = \varphi_{III}(\rho, a) \quad (12)$$

$$\varepsilon_m \frac{\partial \varphi_{II}(\rho, z)}{\partial z} \Big|_{z=a} = \varepsilon_a \frac{\partial \varphi_{III}(\rho, z)}{\partial z} \Big|_{z=a} \quad (13)$$

Solutions (4) - (6) and a system of equations (10) - (13) completely determine the potential in all space. After simplification, system (10) - (13) is reduced to a linear system of equations with the arbitrary coefficients of the general solution as unknowns.

Solution of this system determines the exact solution of the problem. The potentials are presented below:

$$\varphi_I(\rho, z) = \frac{q}{\varepsilon_a} k \frac{e^{-\sqrt{1+p^2}(z+d)}}{\sqrt{1+p^2}} + \frac{q}{\varepsilon_a} k \int_0^\infty \frac{p}{\sqrt{1+p^2}} \frac{\beta(p)(1-e^{-2pa})}{1-\beta^2(p)e^{-2pa}} J_0(p\rho) e^{-\sqrt{1+p^2}(z-d)} dp \quad (14)$$

$$\begin{aligned} \varphi_{II}(\rho, z) = & -\frac{2q}{\varepsilon_a} k \int_0^\infty \frac{p}{\sqrt{1+p^2}} \frac{\beta^2(p)e^{-2pa}}{\varepsilon_m p (1-\beta^2(p)e^{-2pa})} J_0(p\rho) e^{-\sqrt{1+p^2}d} e^{pz} dp \\ & + \frac{2q}{\varepsilon_a} k \int_0^\infty \frac{p}{\sqrt{1+p^2}} \frac{1}{\varepsilon_m p (1-\beta^2(p)e^{-2pa})} J_0(p\rho) e^{-\sqrt{1+p^2}d} e^{-pz} dp \end{aligned} \quad (15)$$

$$\varphi_{III}(\rho, z) = \frac{4q}{\varepsilon_a} \frac{\varepsilon_m}{\varepsilon_a} k \int_0^\infty \frac{p^2}{(\sqrt{1+p^2} + \varepsilon_m p)^2} \frac{e^{-\sqrt{1+p^2}d}}{1-\beta^2(p)e^{-2pa}} J_0(p\rho) e^{-\sqrt{1+p^2}d} e^{-pz} dp \quad (16)$$

$$\text{where } \beta(p) = \frac{\varepsilon_a \sqrt{1+p^2} - \varepsilon_m p}{\varepsilon_a \sqrt{1+p^2} + \varepsilon_m p} \quad (17)$$

All distances here are normalized by the length  $\lambda=1/\kappa$ .